Biodiesel and ULSD Fueled Compression Ignition Engines Operating with Multiple Fuel Injections

By

Tyler Jeffrey Simpson

Submitted to the graduate degree program in Mechanical Engineering and the Graduate Faculty of the University of Kansas in partial fulfillment of the requirements for the degree of Master of Science.

Chair: Dr. Christopher Depcik

Dr. Xianglin Li

Dr. Edward Peltier

Date Defended: September 30, 2020

The thesis committee for Tyler Jeffrey Simpson certifies that this is the approved version of the following thesis:

Biodiesel and ULSD Fueled Compression Ignition Engines Operating with Multiple Fuel Injections

Chair: Dr. Christopher Depcik

Date Approved: October 7, 2020

Abstract

Biodiesel offers an inherent life-cycle carbon dioxide emissions reduction compared to conventional diesel, along with renewability, making it an attractive alternative fuel from the prospective of greenhouse gas emissions and dependence on foreign oil. However, biodiesel comes with an economic disadvantage due to its high upfront cost and higher fuel consumption. In addition, a misconception exists that biodiesel produces higher emission of nitrogen oxides than conventional diesel. As a result, biodiesel has struggled to gain mainstream acceptance, thus, denying its potential contributions to the fight against climate change.

Multiple fuel injections have had great success at providing benefits in both emissions and fuel consumption with conventional diesel fueled compression ignition engines. Moreover, biodiesel fueled compression ignition engines employing multiple injections have shown to be just as affective, if not more so, than conventional diesel. To contribute to the limited amount of literature on multiple fuel injections with biodiesel and gain a fundamental understanding of multiple injections overall, experimentation was conducted to compare combustion between soybean biodiesel and ULSD when a single pilot injection is employed. The results of testing showed that soybean biodiesel largely produced reduced amounts of partial products of combustion, nitrogen oxides, and particulate matter relative to ULSD, with further potential benefits to be had with more complex injection strategies. This effort lays the groundwork for additional work with biodiesel and multiple fuel injections that will hopefully play a part in the proliferation of biodiesel use in the future.

Acknowledgments

I want to start by thanking my advisor, Dr. Christopher Depcik, for his guidance and dedication he has provided throughout both my graduate and undergraduate careers at the University of Kansas. I have had the opportunity to work with Dr. Depcik as a student, teaching assistant, and research assistant, during which he has truly served as a role model who demonstrates the highest extents of hard work and integrity. It is his research and notoriously high expectations that inspired me to pursue a Master of Science in the first place. Throughout the process of conducting this research, he has reciprocated all my own effort with unrivaled availability and support, especially during the writing process, and for that I am truly grateful. I also want to thank my peers in the lab, Charu Srivatsa, Shah Saud Alam, and Dr. Jon Mattson for their immense help with conducting the experimentation in this work and providing me with great examples of what it means to be a student in academia.

Table of Contents

Figures

Tables

Nomenclature

Abbreviations

0-D	Zero-Dimension
AC	Alternating Current
ATDC	After Top Dead Center
BMEP	Brake Mean Effective Pressure
BSFC	Brake Specific Fuel Consumption
$BSFC_g$	Gross Brake Specific Fuel Consumption
BTDC	Before Top Dead Center
CFD	Computational Fluid Dynamics
CI	Compression Ignition
CO	Carbon Monoxide
cRIO	Compact-Reconfigurable I/O
DC	Direct Current
DOC	Diesel Oxidation Catalyst
DOE	Design of Experiment
DPF	Diesel Particulate Filter
ECU	Engine Control Unit
EGR	Exhaust Gas Recirculation
EOC	End of Combustion
EOI	End of Injection
EPA	Environmental Protection Agency
ESC	European Stationary Drive Cycle
FID	Flame Ionization Detector
FPGA	Field Programmable Gate Array
FSN	Filter Smoke Number
FTIR	Fourier Transform Infrared Spectroscopy
FTP	Federal Test Procedure
GUI	Graphical User Interface
HC	Hydrocarbon

HCCI	Homogeneous Charge Compression Ignition
HiMICS	Homogeneous Charge Intelligent Multiple Injection Combustion System
HPC	Highly Remixed Combustion
HSDI	High Speed Direct Injection
IF	Inorganic Fraction
IMEP	Indicated Mean Effective Pressure
$IMEP_g$	Gross Indicated Mean Effective Pressure
$IMEP_n$	Net Indicated Mean Effective Pressure
ISFC	Indicated Specific Fuel Consumption
LII	Laser Induced Incandescence
LNT	Lean NO_x Trap
LTC	Low Temperature Combustion
MBT	Maximum Brake Torque
MFB	Mass Fraction Burned
NI	National Instruments
NO_x	Nitrogen Oxides
OEM	Original Equipment Manufacturer
PCCI	Premixed Charge Compression Ignition
PCI	Peripheral Component Interconnect
PM	Particulate Matter
PPCI	Partially Premixed Charge Compression Ignition
RHR	Rate of Heat Release
RMS	Root Mean Square
rpm	Revolutions Per Minute
RSM	Response Surface Method
SCR	Selective Catalytic Reduction
SOC	Start of Combustion
SOF	Soluble Organic Fraction
SOI	Start of Injection
SOV	Start of Vaporization

TCA	Test Cell Analysis
TDC	Top Dead Center
THC	Total Hydrocarbon
TICS	Timing and Injection Rate Control System
ULSD	Ultra-Low Sulfur Diesel
U.S.	United States
WCO	Waste Cooking Oil
YDAQ-p	Yanmar Performance Data Acquisition Program

Chapter 1 – Introduction

Interest in using biodiesel as an alternative fuel for compression ignition (CI) engines has greatly risen over the past few decades. Since biodiesel can be produced from many different plant feedstocks and animal byproducts, it is considered a renewable fuel that can also reduce dependency on foreign oil. Furthermore, biodiesel is seen as a "carbon neutral" fuel; i.e., while carbon dioxide (CO_2) is still the main product of combustion from these hydrocarbon-based fuels, the carbon within the oil or fat used to create biodiesel is derived mostly from CO_2 in the air [1]. Although biodiesel is often stated as tailpipe carbon neutral, there are still carbon emissions associated with the life cycle of biodiesel (e.g., the production process, transportation, etc.). However, the literature has shown that these lifecycle emissions are still far less than petroleum diesel. One such effort by Sheenhan et al. [2], studied a fleet of urban buses fueled with neat soybean biodiesel and it was found that its lifecycle CO_2 emissions were 78% less than petroleum diesel. Conversely, there are drawbacks pertaining to biodiesel use that have kept it from gaining mainstream acceptance, such as its lower energy content that incurs a fuel economy penalty along with its high cost and perceived greater nitrogen oxides (NO_x) production potential. The latter will be of particular interest in this effort, as the fuel injection strategies studied here are known to greatly influence engine out emissions such as NO_x. The remainder of this chapter will detail the use of biodiesel in CI engines, along with its advantages and drawbacks, followed by an introduction to the advanced fuel injection strategies employed in CI engines, and lastly, the scope of work covered in this thesis.

1.1. Biodiesel Use in Compression Ignition Engines

Biodiesels are defined as the monoalkyl esters derived from plant oils or animal fats [3]. There are two classifications of plant oils viable for biodiesel production, the first is vegetable

oil, of which the most commonly used feedstocks include rapeseed, soybean, coconut, and waste cooking oils. Second, is the non-edible class of plant oils, of which jatropha oil is popular. As for animal fats, biodiesel can be made from tallow, lard, and yellow grease. However, these raw oils have viscosities that range from 10 to 17 times higher than petroleum diesel [3]. This necessitates a transesterification process that lowers viscosity to a level acceptable for use in a CI engine (though still higher than conventional diesel). In addition to the higher viscosity of biodiesel compared to petroleum diesel, biodiesel generally has a higher cetane number, greater density, lower energy content, higher flash point, and larger oxygen content (about 10% compared to 0%), which all contribute to differences in combustion when a CI engine is fueled with biodiesel.

While the main advantages of biodiesel use are its renewability and carbon neutral qualities, there are other advantages including its non-toxicity and respectively fast biodegradability (approximately four times faster than petroleum diesel [3]). Moreover, there are tailpipe emissions advantages inherent to biodiesel use. For instance, its higher combustion efficiency [3] brought on by its oxygen content and greater adiabatic flame temperature [4] result in lower emissions of partial products of combustion, specifically, carbon monoxide (CO) and hydrocarbons, or total hydrocarbons (THCs) [5]. Furthermore, Mangus et al. has found potential reductions in NO_x emissions with neat biodiesel as compared to ultra-low sulfur diesel (ULSD) when injection timing is modified to account for the fuel's higher cetane number and other fuel properties. However, this contradicts the general finding in the literature that NO_x emissions increase with biodiesel use. Being that NO_x emissions are a primary concern with CI engines due to regulations, this plays a large roll in biodiesel's consumer and OEM acceptance.

Some minor disadvantages of biodiesel include its higher pour point and cloud point [6]. This becomes important in colder climates where these properties could present issues for

consumers at the pump and hinder the ability of fuel to be pumped from the fuel tank to the engine. Another primary disadvantage is the cost of biodiesel, as the average cost of neat biodiesel in April of 2020 was $3.51/gallon in comparison to ULSD at $2.61/gallon [7]. This higher upfront cost coupled with a degraded fuel economy (due to biodiesel's lower energy content) creates an economic disadvantage for biodiesel. However, advanced fuel injection strategies, such as multiple injections, have resulted in lowering fuel consumption for CI engines [8]. Furthermore, multiple injections have demonstrated widespread success in reducing NO_x and Particulate Matter (PM) emissions concurrently. As a result, the use of multiple injections with biodiesel to lower emissions and fuel consumption simultaneously could help facilitate a broader acceptance of biodiesel.

1.2. Multiple Injections with Compression Ignition Engines

Until the early 1990s the predominant method of fuel delivery for CI engines was the mechanical pump-line-nozzle system. These systems typically consisted of a cam-driven pump that would send pressurized fuel to the fuel injectors where injection timing was fixed according to the pressure required to overcome the spring pressure of the injector needle. These configurations were robust and relatively simple; however, they were limited to a single fuel injection event per thermodynamic cycle and respectively low injection pressures of 200-300 bar [9]. Due to their limited flexibility, a poorly mixed and highly stratified air fuel mixture would result and produce relatively high levels of both NO_x and PM. Subsequently, the onset of stringent emissions standards pertaining to NO_x and PM necessitated the advancement of fuel injection technology and eventually led to the proliferation of the high-pressure common rail electronic fuel injection system developed by Bosch. This system brought about two major advantages, the first being the high-pressure fuel pump that can operate at fuel pressure of up to

2500 bar [10]. This increase in fuel pressure allowed better atomization and fuel spray penetration that improves mixing and homogeneity of the air fuel mixture that can positively influence emissions, as well as fuel economy. While there are advantages inherent to higher fuel pressures alone, the second feature of this new generation of fuel injection system, the electronic fuel injector, is what facilitated widespread use of this new technology. The electronic fuel injector allows for flexible and precise injection timing and quantity to better control emissions and engine operation in general. Furthermore, these injectors allowed for multiple fuel injection events per thermodynamic cycle, which can have a significant impact on the performance and emissions of a CI engine.

The topic of multiple fuel injections within CI engines has been well researched for conventional diesel fuel and is a standard practice for automotive CI engines today, with OEM's employing up to 10 fuel injections per combustion cycle [11]. Multiple fuel injections have been shown to potentially decrease fuel consumption and all major CI engine out emissions including partial products of combustion, NO_x, and PM. However, due to differences in fuel properties between biodiesel fuels and conventional diesel, coupled with the absence of widespread biodiesel use with CI engines, understanding the influence of multiple injections on biodiesel combustion pales in comparison to conventional diesel. Hence, the primary goal of this work is to gain a fundamental understanding of biodiesel-fueled CI engine operation while employing multiple fuel injections.

1.3. Scope of Work

The first step towards gaining this understanding of multiple injection use with biodiesel is to perform a literature review, which will be the second chapter of this thesis. This chapter will describe the different multiple injection strategies and how they affect engine performance and

emissions. Moreover, the literature review will recount multiple injection investigations of CI engines fueled with both biodiesel and petroleum diesel (i.e., conventional diesel). This is because petroleum diesel is the primary fuel used in CI engine equipped passenger cars/trucks and heavy-duty trucks, all of which must meet the emissions standards that drive this research. Here, most efforts in the literature employ multiple injections while using petroleum diesel, and there is much to be gained from understanding this research. Furthermore, a review of biodiesel research will involve studies of neat biodiesel and biodiesel/conventional diesel blends, although neat biodiesel is the primary fuel of interest in this work.

Proceeding the literature review of multiple injection strategies, the third chapter of this work will present the experimentation carried out in the single-cylinder test cell at the University of Kansas. A single biodiesel fuel type and single injection strategy was chosen to begin understanding the fundamental influences of biodiesel and fuel injection on combustion and emissions. Here, single injection experiments spanning the entire load range of the Yanmar L100V were conducted to compare biodiesel and ULSD and to provide a baseline to which the multiple injection experiments could then be compared. Subsequent post-processing of these data through analyses of performance, heat release, emissions, and combustion noise were utilized to provide a holistic view of how combustion differs between the two fuels. Following the single injection experiments, a single pilot injection strategy was employed (totaling two injection events) to be compared between the two fuels. The pilot injection was chosen because it is relatively simple and if often the starting point for multiple injection research in the literature. Moreover, the pilot injection is known to influence all aspects of combustion (emissions, fuel economy, and combustion noise). Whereas, the next basic multiple fuel injection strategy, the post injection, is typically only employed to reduce PM emissions or for catalyst heating. Hence,

there is more information to be gained from this initial pilot injection testing. Furthermore, the pilot injection experiments swept timing of the pilot injection event from 15°-25° before top dead center (BTDC) while also varying the pilot quantity from 10-20% of the total fuel injected. In addition, the tested load range was shortened, to 4.5, 9.0, and 13.5 N-m in order to limit the number of experiments and still maintain low, medium, and high load points (i.e. premixed dominated to diffusion-burn dominated combustion). Finally, the same methods of post-processing used for the single injection experiments were utilized for the pilot injection tests, providing the holistic and fundamental understanding of combustion between the two fuels and their injection strategies this effort set out to accomplish.

The concluding chapter ties together the trends seen from the experiments conducted to the literature review. Here, the most important comparisons will involve how biodiesel emissions and fuel consumption react to the chosen multiple injection strategy. Moreover, the testing results are discussed to highlight specific aspects important for this effort (e.g., biodiesel fuel type, engine specs, etc.) and to contribute novel information for the literature. Lastly, the effects of multiple injection testing were summarized to understand how and why additional multiple injection strategies could be implemented in future efforts.

Chapter 2 – Literature Review of Multiple Injections with Compression Ignition Engines

2.1. Multiple Injections Overview

As a preface to a literature review involving multiple injection strategies employed in CI engines, it is necessary to understand the various parameters controlled during these multiple injection events and the associated language. Moreover, the fundamental mechanisms at play regarding the formation and abatement of exhaust emissions constituents must be understood. This understanding will aid in the analysis of engine performance and emissions resulting from these injection schemes, as well as provide the ability to assess the similarities and differences seen when comparing conventional diesel and biodiesel fuels under multiple injection operation.

In the literature, there are three primary groups of exhaust emissions constituents of interest regarding CI engines. These groups can be delineated first by unburned hydrocarbons and carbon monoxide, which are readily controlled through aftertreatment using an oxidation catalyst. The second group includes nitrogen oxides, in which tailpipe emissions reduction requires additional catalytic hardware. Lastly, particulate matter, including soot, is of paramount importance and requires a particulate filter, as well as regenerative engine operation to oxidize built-up PM within the filter. A synopsis of the formation and abatement of these constituents will provide adequate preparation for delving into the literature where these species are the main motivation behind the exploration of multiple fuel injections.

Pollutant emissions make up about 1% of the exhaust constituents in diesel-fueled CI engines [12]. Figure 2.1 illustrates the five groups within the pollutant emissions group: CO, HC, NO_x, SO_x, and PM. Note that since the mandate of ULSD use by the Environmental Protection Agency (EPA) that has been in effect since 2006 [13], SO_x emissions have been greatly reduced.

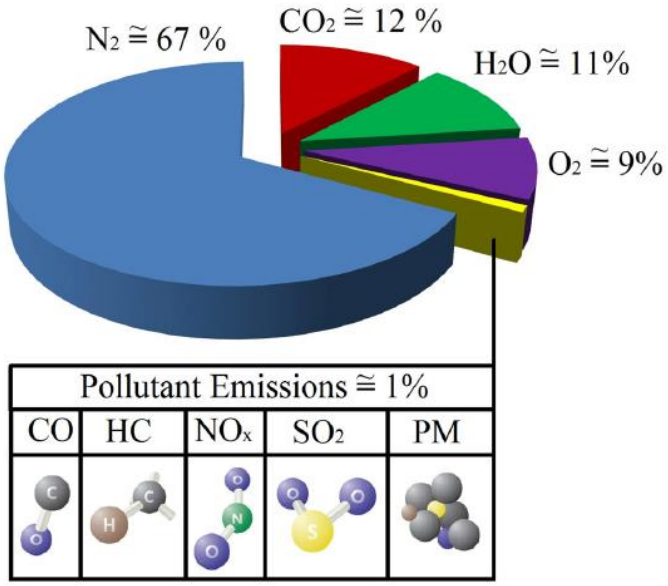

Figure 2.1: Exhaust constituents from diesel-fueled CI engines [12].

Beginning with HCs and CO, both constituents are generally a product of incomplete combustion, stemming from a rich air/fuel mixture or low combustion temperatures. For CI engines specifically, lean operation is predominantly used; hence, HC and CO formation is largely minimal [14], although there are still circumstances where significant amounts of these species can form. For example, HCs can be a problem during light load operation, due to excessively lean mixtures leading to flame speeds too low for complete combustion [15]. Moreover, CO can form due to poor fuel spray characteristics [16] in addition to a small portion of CO emitted due to chemical kinetics [17]. Generally, HCs and CO can be fully oxidized once exhausted from the engine using a diesel oxidation catalyst (DOC) with its effectiveness depending on temperature and the time required for its initial heating under cold-start scenarios.

Next, NO_x, which is primarily comprised of NO and NO_2, is formed at high temperatures in excess of 1,600° Celsius, and is exacerbated by presence of excess air [18, 19]. Thus, it is a significant issue for lean operating CI engines. For CI combustion, NO_x production is

predominantly formed during the premixed combustion stage, when the piston is close to top dead center (TDC) and in-cylinder pressures and temperatures are the highest. The abatement of NO_x includes in-cylinder means such as exhaust gas recirculation (EGR), where combustion products are introduced to the intake stream to dilute the inducted charge with, mostly inert, gases that lower the overall oxygen concentration and reduce combustion temperatures. However, EGR cannot be the only source of NO_x reduction, as the reduced cylinder temperatures associated with EGR can lead to a growth of HC, CO, and PM emissions. In combination, there are aftertreatment methods of NO_x mitigation including lean NO_x traps (LNTs) and selective catalytic reduction (SCR). LNTs store NO_x on the surface of a catalyst washcoat during lean operation, which is then released and reduced to nitrogen catalytically during a rich regeneration phase [20]. In comparison, SCR is seen as more straightforward methodology to LNT technology, where a urea solution is injected into the exhaust stream and forms ammonia, which then reacts with NO_x to form nitrogen and water [20]. Here, SCR systems include an additional bit of complexity, as they require on-board tanks for urea storage and frequent refilling.

Finally, PM, which includes soot along with the soluble organic fraction (SOF) and the inorganic fraction (IF) of HCs, is the product of incomplete combustion and the agglomeration of small particles of partly burned fuel or lubricating oil [16, 21]. Soot typically makes up more than 50% of PM and is seen black smoke in the exhaust [14], while the SOF consists of heavy hydrocarbons adsorbed on the soot [22]. The formation of PM is dependent on many factors, such as the combustion and expansion process, sulfur and ash content of the fuel, lubricating oil quality and consumption, combustion temperature, and the EGR level [23]. The primary source of PM that is of pertinence here involves the diffusion burn phase of CI combustion and the introduction of un-atomized liquid fuel during the combustion process [24]. Moreover, exhausted

soot is said to be the result of a constant soot formation and oxidation battle, where numerous factors can affect either the formation or oxidation of soot; thus, influencing the level of net soot in the exhaust [24]. To note, the terms “PM” and “soot” are used interchangeably in the literature, sometimes being referred to as “smoke”, which also falls within the PM spectrum. Although PM can be oxidized during combustion, once it has been exhausted, the only other means of abatement is by using a diesel particulate filter (DPF). This effective catalytic filtration device traps and oxidizes PM, but develops a pressure drop when saturated and requires regeneration. Not only can this pressure drop decrease performance due to an increased back pressure in the exhaust system, the frequency of regeneration can contribute to a reduced fuel economy [25]. Now that the major constituents of CI combustion and their mechanisms have been discussed, the remainder of this section will examine combustion basics followed by the various injection schemes associated with split, pilot, and post injections along with their purposes.

Before delving into multiple injection strategies, the basics of single fuel injection CI combustion must first be reviewed. For single injection operation, there are three phases of combustion involved. The first is the premixed burn phase, where a portion of the injected fuel reaches autoignition as the atomized fuel jet mixes with the surrounding air. This is followed by the diffusion burn phase, where fuel burns as it mixes with air in an environment where a flame is already present under respectively high pressures and temperatures. Lastly, there might be a third stage where soot will continue to oxidize as the flame is extinguishing [26]. Figure 2.2 uses a plot of injection current and combustion heat release on a crank angle basis to illustrate the different phases of single injection combustion. The start of injection (SOI) will typically take place during the compression stroke somewhere in the range of 15°-5° Before Top Dead Center

(BTDC) and lasts for a few crank angle degrees. Once SOI has been initiated, there will be short period before the premixed burn phase occurs as the fuel atomizes and mixes with the air. This period is referred to as the ignition delay and includes the duration between SOI, start of vaporization (SOV), and start of combustion (SOC), as shown in Figure 2.2.

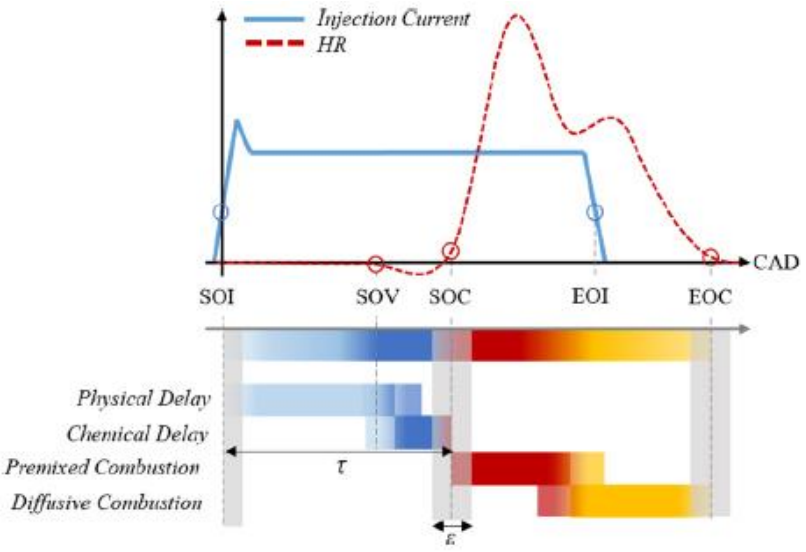

Figure 2.2: Plot of injection current and heat release illustrating the different phases of CI combustion utilizing a single fuel injection [27].

Ignition delay can be separated into two stages: physical delay (SOI to SOV), which is the time required for fuel droplet break-up, air entrainment, and vaporization, and the second stage, chemical delay (SOV to SOC), which is controlled by the fuel's autoignition kinetics. Physical delay is typically much longer than chemical delay, and there is often overlap between the two stages [27]. Following the ignition delay, the SOC takes place that initiates the premixed combustion phase, where the propensity for NO_x creation is higher due to the heat release spike. Subsequently, the diffusion burn phase of combustion with a greater PM production tendency takes place shortly before or after the end of injection (EOI) and lasts until the end of combustion (EOC), potentially containing the late stage soot oxidation phase. With the fundamentals of

single fuel injection CI combustion covered, the potential benefits and different types of multiple fuel injections can be explored.

"Multiple injections" is a general term that describes when more than one fuel injection event per engine cycle is employed. While the terminology used in the literature pertaining to multiple injections is somewhat diverse, there is generally agreed upon language that will be used throughout this work and is described as follows. Three basic strategies can be employed, with the first option being a pilot injection approach. Pilot injection schemes involve breaking up the main fuel injection event into a respectively small quantity (typically around 5-10% of the total fuel mass) that is usually injected during the compression stroke, subsequently followed by a larger main injection event that is injected just before or after TDC. This has two significant effects; the first is a reduction in the peak heat release rate of the main combustion phase through a shortening of the main ignition delay. This dampens the premixed combustion event (shown in Figure 2.3), which lowers maximum cylinder temperatures and NO_x production. The second effect is a subsequent reduction in the cylinder pressure rise rate, which is widely believed to be a source of combustion noise. Furthermore, pilot injections are not limited to a single pilot. Instead, multiple pilot injections can be used before the main injection event [28-33], and they all do not necessarily need to be the same quantity of fuel injected [33].

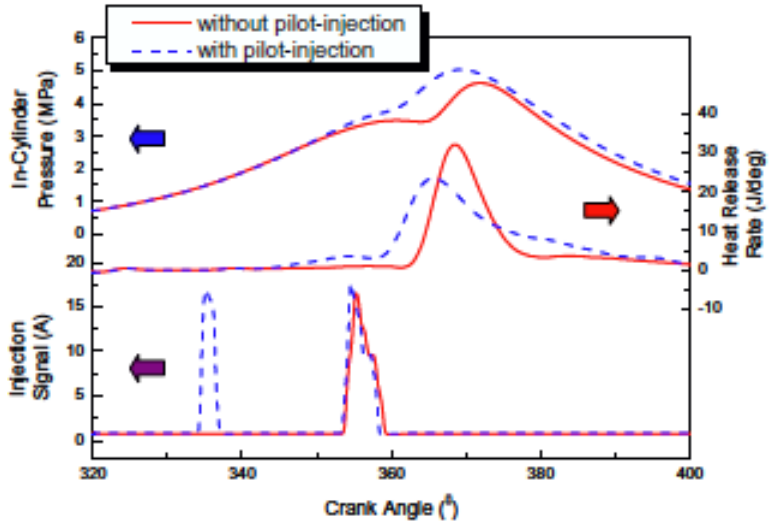

Figure 2.3: Example of the effect pilot injections have on the heat release rate and cylinder pressure rise rate [34].

Some researchers use the term "early injection" to designate an injection event before a pilot injection for combustion strategies employing homogeneous charge compression ignition (HCCI) or premixed charge compression ignition (PCCI) [35, 36]. This may be because this "early" injection heat release event does not interact with the main injection energy release. However, this is where terminology inconsistencies start to appear, as some researchers use "pilot" and "early" injection terms interchangeably. In addition, researchers have used the terms "pre-injection" [37-40] or "boot injection" [41] to describe a pilot injection event. Furthermore, a parameter often discussed involving pilot injections is the "dwell". This designates the time, or crank angle degrees, between the pilot and main injection events. In general, "dwell" can be used to describe phasing between any two injections.

The next type of multiple injection approach is the "split" injection strategy, which designates that the fuel quantity be broken up into two or more equal parts throughout the injection process [42] (e.g., a 50/50 or a 33/33/33 split). This is often used for further NO_x and noise reduction (shown in Figure 2.4). Notation consistency involving this term is especially

loose, as many researchers will refer to any type of multiple injection scheme as a split (e.g., a pilot injection scheme being referred to as a 10/90 split). While splitting of a main injection event is the most common tactic, a split can be applied to any fuel quantity delivered within the cycle. For example, there are examples of pilot splits [28-32], as well as dividing the post injection event [43] that is discussed in the next paragraph.

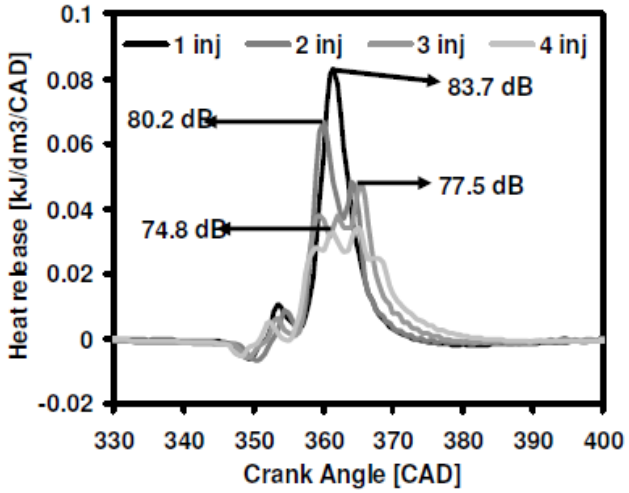

Figure 2.4: Combustion noise reduction brought on by pilot injection and main injection splitting [44].

Lastly, the post injection event, or "after" injection for some researchers, provides a small fraction of the total fuel quantity injected later in the expansion stroke. Post injections have been shown to be effective in reducing soot emissions through improved mixing and enhancing the late soot oxidation phase [24]. In addition, post injections can be used to introduce excess hydrocarbons into the exhaust for catalyst warmup or DPF regeneration [43, 45].

There has also been significant research into employing multiple injections with low temperature combustion (LTC) operation. LTC is a regime for CI engines where an intended homogeneous mixing process is married with low flame temperatures; hence, simultaneously reducing both NO_x and PM [46]. NO_x reduction is a function of the well understood mechanism

of limiting cylinder temperatures below ~2200 K and maintaining low heat release rates. PM reduction is the interesting part of this concept and this works by minimizing the amount of liquid fuel introduced into a respectively hot flame. During normal CI operation, liquid fuel is injected during combustion where a hot flame is present and this leads to thermal decomposition (or thermal cracking) that produces soot [47]. Homogeneous charge compression ignition (HCCI) and premixed charge compression ignition (PCCI) are two types of LTC strategies that utilize a two-stage pre-mixed combustion process necessitating multiple injections. Figure 2.5 shows where both HCCI and PCCI lie within the LTC regime.

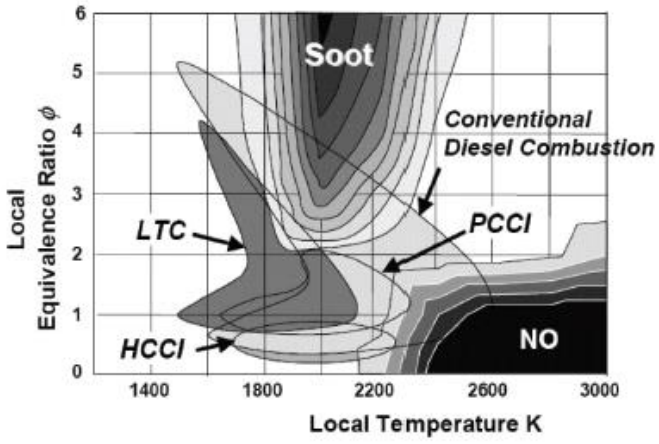

Figure 2.5: Emissions map of different LTC strategies [46].

The first stage is the cold flame chemical reaction with the lowest temperatures, followed by a thermal flame combustion stage [48]. While effective in emissions reduction, this combustion process often requires heavy EGR usage (e.g., 50-60%) and is only suitable for part load situations. Moreover, cold flame combustion introduces reaction kinetics that differ from conventional CI combustion. Due to these facets, LTC efforts will not be covered in this work; however, there might be some overlap between the LTC and conventional CI combustion

regimes in the work discussed. Now that a background in multiple injection strategies for CI engines has been established, a thorough review of the literature can be covered.

2.2. Literature Review

2.2.1. Multiple Injections with Conventional Diesel Fuel

The early 1990's mark the start of the extensive compilation of research seen today regarding CI multiple fuel injection strategies. Here, the proposal of the United States (U.S.) Federal Tier 1 light-duty emissions standards (see Table 2.1) that would go into effect in 1994 [49] was the catalyst that motivated early research in this field.

Table 2.1: Tier 0 and Tier 1 emissions standards for light-duty vehicles and light-duty trucks [49].

	Vehicle Type	Emission Category	Vehicle Useful Life												
			5 Years / 50,000 Miles						10 Years / 100,000 Miles						
			NMHC [a] (g/mi)	NMOG (g/mi)	CO [b, c]	NOx [d] (g/mi)	PM (g/mi)	HCHO (g/mi)	THC [c, e, f] (g/mi)	NMHC [a] (g/mi)	NMOG (g/mi)	CO [g] (g/mi)	NOx (g/mi)	PM (g/mi)	HCHO (g/mi)
Federal [h, i, j]	LDT3	Tier 0	-	-	-	-	-	-	0.8	0.67 [k]	-	10	1.7	0.26 [l]	-
		Tier 1	0.32	-	4.4	0.7	-	-	0.8	0.46	-	6.4	0.98	0.1	-
	LDT4	Tier 0	-	-	-	-	-	-	0.8	0.67 [k]	-	10	1.7	0.13 [l]	-
		Tier 1	0.39	-	5	1.1	-	-	0.8	0.56	-	7.3	1.53	0.12	-

The implementation of stringent NO_x and PM regulations necessitated further means of engine-out emissions reduction, such as injection rate shaping and multiple fuel injection events. To note, multiple injections were not a completely new concept as there are accounts of experimentation with pilot injections as early as 1937 to reduce combustion noise and to combat fuels with low cetane numbers and poor ignition qualities [50].

The first publication that investigates multiple injections in a CI engine dates back to 1984 [51]. This study concluded that combustion noise and emissions could be reduced using a split injection approach. To note, this effort did not utilize common rail or modern high-pressure fuel injection hardware. Instead, they achieved split injections using a "split injection device"

installed on the high-pressure side of the injection system. Furthermore, the literature cites efforts involving the use of pilot injections in the timeframe of 1989 to 1991 [37, 52-55]. While these publications are not readily available, they were the first reported with the goal of reducing ignition delay and rapid pressure rise for the purpose of NO_x emissions abatement in combination with modern fuel injection technology. In addition, Herdin in 1990 [56] experimented both with "modulated" injections (i.e., rate shaping) and pilot injections. They reported advantages in HC, CO, and combustion noise due to the shortened ignition delay, but experienced issues with increased smoke at low load.

The first true record of the promise of a pilot injection occurred in 1992, when Shundoh et al. [57] experimented with different methods of reducing ignition delay. They found that the use of a pilot injection could simultaneously reduce NO_x by 35% and smoke up to 80% without a compromise in fuel economy.

Another promising study by Needham et al. [58] followed in 1993 that employed high-pressure common rail electronic injection and "flexible" injection control. They were able to meet Tier 1 medium duty emissions requirements without an oxidation catalyst. Also in that year, Bower and Foster [59] conducted experiments with split injections in a physically simulated CI combustion chamber. They were the first to highlight fuel distribution differences with split injections and the effect it has on mixing and vaporization. Moreover, this study marks the start of multiple injection research within academia. Prior to this effort, all research had been done by Original Equipment Manufacturers (OEMs) or 3rd party automotive developers.

Overall, 1994 was a significant year in multiple injection research. Starting with Nehmer and Reitz [50], an initial study was conducted using the lab's heavy-duty single cylinder CI

engine. The engine was a modified version of the Caterpillar 3406, having a displacement of 2.44 L and compression ratio of 15:1. It was tested at a constant 80% load and 1600 revolutions per minute (rpm). The effects of injection rate-shaping and pilot injections were investigated. For this work, the injection parameters varied were the pilot quantity, from 10-75%, and the pilot-main dwell, from 3-8°. They successfully implemented pilot injections that produced lower levels of NO_x without growing soot levels. They postulated that an optimal pilot quantity existed somewhere between 10-25%. Moreover, they reported that split injections allow combustion to continue into the expansion stroke without an increase in PM due to the enhanced mixing introduced. This study was also the first to discuss the wave dynamics present when employing multiple injections in a common-rail system due to the injector closing. This phenomenon can either increase or decrease the local rail pressure at a particular injector, causing the delivered fuel mass to vary during subsequent injections.

In parallel within the same laboratory, Tow et al. [60] examined a triple injection event, in addition to expanding test conditions to lower load points. The same engine was used and operated at 1600 rpm; however, this time at 25% and 75% load. The goal of this effort was to study a larger range of dwell times between double injections in addition to the triple injection strategy. They reported that a 50/50 split with a significantly long dwell (10°) could reduce particulates by a factor of three with no increase in NO_x at 75% load. They also stated that a small pilot quantity (13%) was effective in reducing NO_x at both 25% and 75% load. As for the triple injection cases, it was proven that they offer additional control and performance if the parameters are calibrated appropriately. The 7/44/49 injection case, with 2° and 10° dwell times between the respective injections produced simultaneous NO_x and soot reductions of 40% and 50%, respectively, at low load. Furthermore, they observed that a long dwell before the last triple

injection reduced PM. They contributed this effect to an enhanced fuel air mixing provided by the multiple injections, as well as particulate oxidation late into the expansion stroke. This last observation is significant as it is the first indirect mention of the potential of post injections for particulate oxidation. This fact, along with the findings relating to pilot injections by Nehmer and Reitz, is responsible for these two publications being the two most highly cited works within multiple injection research involving CI engines.

Concurrently, Ishida et al. [61] performed experiments with pilot injections at the University of Nagasaki. They experimented on a 3.3 L High Speed Direct Injection (HSDI) Mitsubishi 4D31-T four-cylinder CI engine with a compression ratio of 16:1. A mechanical pilot injector system developed by Yoshizu and Nakayama [62] was used, where pilot quantity was varied by changing the seat diameter of the plunger, and pilot/main dwell could be varied by changing the plunger lift. Operating points at a fixed engine speed of 1750 rpm and low and high load points of 3.97 and 8.30 bar, respectively, were tested at a fuel pressure of 18.5 MPa. The main injection was varied from 5° to -5° BTDC while the pilot/main dwell was held at approximately 5°. It was reported that the maximum heat release rate was greatly reduced at low load; whereas, high load was not significantly affected. Moreover, pilot and main ignition delays are about half of the single injection cases and were more affected by load than pilot quantity. Significant improvements in the NO_x -fuel consumption trade-off were seen at low load with a delayed main injection timing. Furthermore, reductions of 12 g/kW-hr and 6 g/kW-hr were observed at both low and high loads, respectively. This fuel consumption reduction was attributed mainly to a decrease in exhaust energy, as seen via a diminished exhaust gas temperature that was subsequent to an enhanced thermal efficiency due to earlier combustion with the pilot injection. The second explanation for this improvement was a reduction in cooling

losses, as well as an estimated 5% increase in mechanical efficiency. However, a small increase in smoke was observed due to the overlap of the main spray and pilot combustion events.

Contributing to the boom of research in 1994, Yamaki et al. [63] experimented with pilot injections on a 6.9 L six-cylinder turbocharged heavy-duty CI engine. Pilot timing and quantity were investigated, allowing for reduced NO_x and HC at low load, a 50% reduction in PM at low speeds along with increased torque and an improved cold start ability. Concurrently, Ishiwata et al. [64] investigated pilot injections on their single cylinder CI engine through their Timing and Injection Rate Control System (TICS) that was described as a "two spring" mechanical injector used in conjunction with a high fuel pressure. Overall, there were issues regarding the accuracy of their fuel timing and quantity; hence, their tests provided inconclusive results.

That same year, Nakakita et al. [65] set out to optimize pilot injection timing on an optical HSDI 0.9 L CI engine fitted with a high pressure electronic fuel injection system. Engine speed was held at 1800 rpm and two different injector nozzle types (0.26 mm four-hole and 0.18 mm five-hole) were tested at low and medium load at fuel pressures of 95 and 40 MPa, respectively. At each operating point, the main injection event was varied from 0° to 10° After Top Dead Center (ATDC) while utilizing various pilot/main dwell times. Overall, they stated that a delayed main injection timing was necessary for NO_x reduction. In specific, this was due to the advancement of main combustion brought on by the pilot injection that cancels the positive effect of a heat release rate reduction. At light load, they reported significantly decreased HC emissions with a small reduction in NO_x levels without any increase in PM at delayed main injection timings. However, this was only possible with the smaller hole injector nozzle. At medium load, NO_x reduction was respectively smaller and came with an increased level of smoke. Finally, the efforts of 1994 are concluded with Durnholz et al. [38], who investigated

"preinjections" and rate shaping as a means for emissions and combustion noise reduction. Results showed it was possible to reduce combustion noise by as much as 10 dB over the entire load range, along with simultaneous reduction of NO_x and HC levels without a significant increase in smoke. These benefits in emissions and combustion noise were realized using a respectively small pilot injection (~6%) and pilot/main dwell of 15°.

Implementation of the TICS system was researched further by Minami et al. [66] in 1995, when they experimented with a turbocharged 12.1 L six-cylinder CI engine. Initial testing at 1000 rpm and low load yielded up to a 70% reduction in the peak heat release rate and a pilot quantity of 12% was found to be optimal. Thus, the remainder of testing conducted at 1200 rpm and various loads employed a 12% pilot injection amount, while the pilot SOI was varied from approximately 15° to -5° BTDC with a pilot/main dwell of about 9°. The effects of pilot injection were most apparent at low load, where simultaneous reductions in NO_x, HC, and fuel consumption were attained, but with a small growth in the level of smoke while the SOF decreased. This increase in smoke was a function of the entrainment of the pilot burned gas by the atomized main spray that slowed the main combustion event. Emissions effects were less apparent at medium load, as pilot injections helped stabilize combustion in regions where low NO_x levels are typically present. No noticeable effect on heat release or emissions were seen at high load with pilot injections, and only a small penalty in fuel consumption occurred that was postulated to be due to an ineffective usage of the pilot injection.

That same year, Pierpont et al. [67] set out to attain simultaneous NO_x and PM reductions using multiple injections at high load including the presence of EGR; an operating condition notorious for PM production. Using the same engine setup as their previous studies, they tested double and triple injections at 75% load and 1600 rpm. They, again, saw that a smaller injection

proceeding the main injection was effective in reducing PM, this time calling it a “secondary” injection. Overall, they were successful in reducing NO_x and PM well within the Tier 1 standard while employing 6% EGR; however, there was a penalty in the brake specific fuel consumption (BSFC) due to a respectively delayed injection timing.

The same laboratory produced another publication in 1996 by Han et al. [68], digging into the exact mechanism behind NO_x and soot reduction with multiple injections. For this effort, they conducted physical experimentation in conjunction with a KIVA-II combustion model. Regarding NO_x reduction, they concluded that the mechanism was similar to that of a delayed single injection event. In specific, the reduced heat release rate during the first injection diminishes NO_x produced by decreasing the level of pre-mixed combustion; whereas, the second injection event does not contribute further to the generation of NO_x. Their findings with respect to soot reduction were more profound. With help of the KIVA-II code, they were able to visualize the soot reduction with multiple injections as illustrated in Figure 2.6.

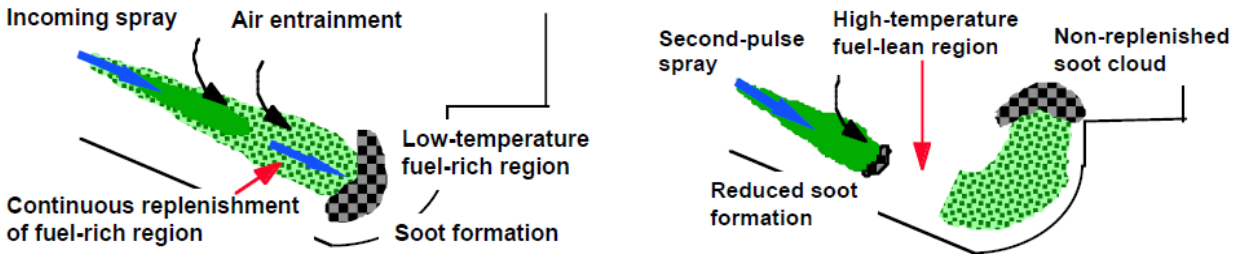

Figure 2.6: Visualization of the multiple injection soot reduction mechanism [68].

This mechanism can be explained as follows: normally, a single injection produces a continuous, high momentum jet with a rich, soot-producing region at the tip of the jet. Conversely, under multiple injections the soot production is discontinued at the termination of the first injection. Then, the injection that follows is introduced into a respectively lean, high

temperature environment resulting from the initial pre-mixed combustion event. This enables prompt and fast combustion. Moreover, the soot produced during the initial injection continues to oxidize, having a favorable effect on the competition between soot formation and oxidation. This confirmed their lab's previous theory that multiple injections enhance fuel mixing and vaporization.

In 1997, Yokota et al. [69] had developed their Homogeneous charge Intelligent Multiple Injection Combustion System (HiMICS) through KIVA-II simulations and set out to validate their results utilizing a single-cylinder research engine. Simulations predicted that improvements in the NO_x -fuel consumption trade-off could be attained by using a pilot injection early in the induction stroke. However, when tested, the results demonstrated worsened trade-offs in both NO_x -fuel consumption, as well was NO_x -smoke. Moreover, there were difficulties involving early autoignition of the fuel and inadequate homogenization. However, improvements in the fuel consumption-smoke tradeoff were seen for respectively delayed pilot injections, albeit with increased HCs and CO emissions.

From 1998-1999, the lab at the University of Wisconsin-Madison published two papers utilizing the Two-Color Imaging method [70] of combustion visualization analysis. The first, by Hampson and Reitz [71], delved further into understanding the soot reducing mechanisms of multiple injections. Using the same engine as a prior study but now modified with an endoscope placed in the cylinder head for imaging, testing was carried out at 75% load and 1600 rpm at 90 MPa of fuel pressure for double and triple injection events. Their conclusions for the soot reduction mechanism of the first two injections validated the results of the previous effort by Han et al. [68]. In essence, the temperature rise associated with the first injection creates an environment for the second injection to burn rapidly and does not form soot fuel rich zones.

Moreover, the increased mixing aids in enhanced oxidation of the already formed soot. Figure 2.7 provides interesting insight to this mechanism, showing that there is an additional heat release spike associated with the termination of the first injection. This "burst" of heat release seen is due to the sudden growth of the flame towards the injector tip once the overly rich fuel region in the jet is discontinued by fresh air and the already developed flame rapidly swallows the newly reactive mixture. As a result, an environment is created for the second injection such that it starts burning immediately, not as a pre-mixed flame, but as a diffusion flame. In addition, the slope of the immediate diffusion burn heat release associated with the second injection is steeper than the diffusion burn heat release seen with single injection events; hence, making it plausible that there is an inherent reduction in soot production related to this type of combustion.

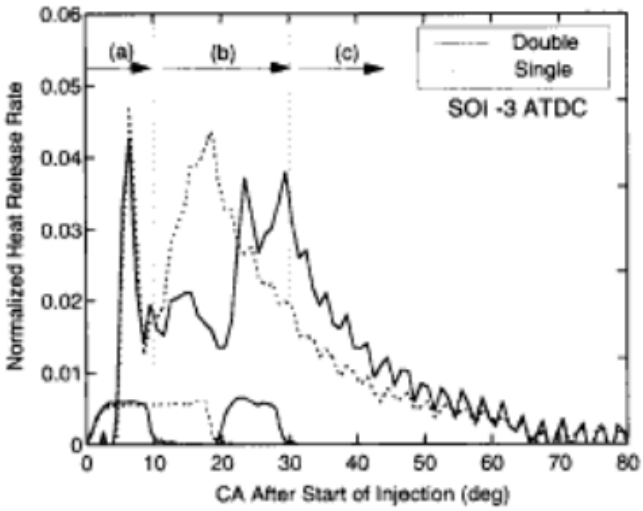

Figure 2.7: Rate of heat release plot comparing multiple injections to a single injection [71].

Results for the triple injections provided additional insight to soot oxidizing "late" or "secondary" injections. They found that the third injection event was helpful for reducing soot if there was still a short ignition delay associated with the termination and resumption between the second and third injections. Furthermore, when SOI was too far delayed they reported a "soot

catastrophe", where soot output rose by an order of magnitude, highlighting the importance of carefully selecting injection timings. The second study, Bakenhus and Reitz [72], was similar in analysis by using Two-Color Imaging to visualize both NO_x and soot reducing mechanisms. Overall, their results mirrored those of the lab's previous studies.

Lastly, in 1999 there was a study by Zhang [73] for Isuzu, another highly cited work within the multiple injection research field. They wanted to understand the effect pilot injections had on NO_x and soot when used for combustion noise reduction. This was done by experimenting with a 0.63 L single-cylinder CI research engine with a compression ratio of 18.5:1 operating at light, medium, and full load at 2200 rpm. Pilot quantities of 12.5%, 25%, and 50% were investigated at identical injection timings and compared to the base single injection case. They were successful in reducing combustion noise and NO_x at light loads but saw little changes in peak heat release at full load. Often, rate of heat release plots are used to analyze the NO_x reduction quality of pilot injections, but Zhang used Figure 2.8 to demonstrate how cylinder pressure rise rates are an equally valid form of analysis. Specifically, explaining that the smallest pilot quantity had the greatest NO_x reduction as a result of having the lowest peak cylinder pressure rise rate as compared to the single injection case. To note, their experiments only demonstrated the NO_x and soot trade-off mechanism, rather than a simultaneous reduction of the two constituents. This is most likely due to using a fixed injection timing.

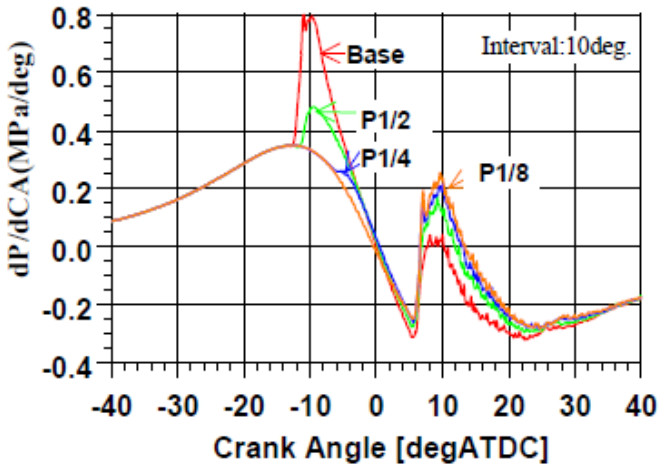

Figure 2.8: Comparison of cylinder pressure rise rate between pilot injection quantities [73].

Moving forward, 1999 was another significant year for CI engine research, as the U.S. Federal Tier 2 emissions standards (see Table 2.2) were adopted in December and scheduled to start going into effect in 2004 [74].

Table 2.2: Tier 2 emissions standards for light-duty vehicles, light-duty trucks, and medium-duty passenger vehicles [49].

	Standard	Emission Limits at 50,000 miles					Emission Limits at Full Useful Life (120,000 miles) [a]				
		NOx (g/mi)	NMOG (g/mi)	CO (g/mi)	PM (g/mi)	HCHO (g/mi)	NOx (g/mi)	NMOG (g/mi)	CO (g/mi)	PM (g/mi)	HCHO (g/mi)
Federal	Bin 1	-	-	-	-	-	0	0	0	0	0
	Bin 2	-	-	-	-	-	0.02	0.01	2.1	0.01	0.004
	Bin 3	-	-	-	-	-	0.03	0.055	2.1	0.01	0.011
	Bin 4	-	-	-	-	-	0.04	0.07	2.1	0.01	0.011
	Bin 5	0.05	0.075	3.4	-	0.015	0.07	0.09	4.2	0.01	0.018
	Bin 6	0.08	0.075	3.4	-	0.015	0.1	0.09	4.2	0.01	0.018
	Bin 7	0.11	0.075	3.4	-	0.015	0.15	0.09	4.2	0.02	0.018
	Bin 8	0.14	0.100 / 0.125 [c]	3.4	-	0.015	0.2	0.125 / 0.156	4.2	0.02	0.018
	Bin 9 [b]	0.2	0.075 / 0.140	3.4	-	0.015	0.3	0.090 / 0.180	4.2	0.06	0.018
	Bin 10 [b]	0.4	0.125 / 0.160	3.4 / 4.4	-	0.015 / 0.018	0.6	0.156 / 0.230	4.2 / 6.4	0.08	0.018 / 0.027
	Bin 11 [b]	0.6	0.195	5	-	0.022	0.9	0.28	7.3	0.12	0.032

Chen [75] published the first effort motivated by Tier 2 standards in 2000, having the goal of achieving simultaneous reduction of NO_x and particulates utilizing pilot and post

injections. They tested a 1.2 L four-cylinder CI engine with a compression ratio of 19.5:1 while employing EGR and a turbocharger. Operating points of 2 and 6 bar brake mean effective pressure (BMEP) at 2000 rpm, and 5 bar BMEP at 1000 rpm were investigated. The pilot injection testing was done by initially fixing a main SOI at TDC and varying the pilot SOI from 10° to 50° BTDC. This resulted in significant NO_x reduction with greater dwells, but this increased HCs along with the BSFC and smoke level. Next, they experimented with fixing the pilot SOI at TDC and varying the main SOI. It was found that a main SOI of 10° ATDC produced simultaneous reductions in NO_x and smoke, and delaying the main injection further continued to reduce NO_x, but at the cost of higher smoke, BSFC, and HCs. Post injections were then explored, by holding a 10% pilot quantity at an SOI of 0° ATDC and the main SOI at 8° ATDC. Here, a 10% post injection quantity was injected while varying the SOI between 17° to 31° ATDC. It was seen that post injections delayed up to 27° ATDC were effective in reducing smoke with little effect on NO_x and BSFC. After 27° ATDC, a rapid increase in HCs and BSFC was seen. Overall, the triple injection strategy (pilot/post combination) was able to attain a 50% reduction in NO_x and 40% reduction in smoke at medium load, 2000 rpm, and 11% EGR as compared to the baseline single injection case; however, this came with a 6% increase in BSFC. At medium load, 1000 rpm, and 19% EGR, simultaneous NO_x and smoke reduction was also achieved, but with only a 3% increase in BSFC.

In 2001, Beatrice et al. [76] experimented with multiple injections for the purpose of meeting Euro 4 emissions standards (see Appendix). Their setup consisted of a 1.9 L four-cylinder Fiat JTD-F3 CI engine with a compression ratio of 17.5:1 while running with a turbocharger and cooled EGR. Testing was done in-vehicle on a chassis dynamometer and different injection strategies were evaluated at 1500 rpm and 5 bar BMEP. These results (see

Figure 4 in ref [76]) were significant because they demonstrated how the Euro 4 emissions standards could be approached without the use of a complex aftertreatment system.

Also in 2001, Montgomery and Reitz [8] explored multiple injections with their heavy-duty single-cylinder CI engine in conjunction with flexible control of EGR and boost while utilizing optimization techniques. Using injection pressure, boost pressure, combustion phasing, dwell, fuel percentage in each injection, and EGR rate as optimization factors for mathematical objective functions, a response surface method (RSM) [77] was employed to influence calibration points to attain desired emissions and fuel consumption levels. They tested the engine at three operating points used in the U.S. Federal Test Procedure (FTP) cycle: Mode 3 took place at 993 rpm and 75% load, while Mode 5 was at 1737 rpm and 57% load, and Mode 6 was at 1789 rpm and 20% load. The optimized schedule for Mode 3 was a 60/40 split with a 9° dwell and a SOI of 3° BTDC. This resulted in a 1.4% reduction in BSFC, 56% reduction in NO_x, and 36% reduction in PM as compared to the optimized single injection case. The optimized Mode 5 injection scheme had a 55/45 split, 9.2° dwell, and 2.5° BTDC SOI with simultaneous reductions in BSFC, NO_x, and PM of 7.1%, 54.2%, and 29.7%, respectively. Lastly, Mode 6 ended up with a 70/30 split at 7.7° dwell and 5.5° BTDC SOI along with respective reductions in BSFC, NO_x, and PM of 9.8%, 67.6%, 59.8%, respectively.

Concurrently, Benajes et al. [39] explored pre and post injection events for emissions reductions in preparation of meeting Euro 4 emissions standards. They experimented with a heavy duty 1.75 L single-cylinder CI engine with a compression ratio of 16.3:1. Operating points at four modes of the European Stationary Drive Cycle (ESC) [78] (see Appendix) were used while testing the pre and post injection strategies separately. Equating to engine speeds ranging from 1200 to 1800 rpm and loads varying from 50-100%, pilot/post injection quantities varying

from 5.6-20% at main injection timings alternating from 2°-6° were tested. The pre injection strategy showed improvements in BSFC due to advanced combustion phasing that resulted in more efficient combustion; however, this increased NO_x and soot emissions. They reported that post injections were effective in reducing soot with no change in NO_x and a small penalty in BSFC. Moreover, a growth in BSFC observed was exacerbated as post injection quantity and dwell increased. Overall, they attributed the increases in NO_x seen with the pre injection event to the higher maximum cylinder temperatures encountered, while soot reduction was correlated with greater combustion temperatures during the final stages of combustion after 75% of the total fuel mass had been burnt.

Lastly in 2001, Badami et al. [79] explored soot and NO_x formation when using pilot injections. They conducted their tests with a 1.9 L four-cylinder CI engine and a compression ratio of 17.2:1. Operating points of 1500 rpm and 5 bar indicated mean effective pressure (IMEP), 2000 rpm and 2 bar IMEP, and lastly, 2500 rpm and 8 bar IMEP were studied at EGR rates of 14%, 40%, and 16%, respectively. They reported increases in NO_x as pilot quantity rose that was said to be a result of higher cylinder temperatures, although combustion noise decreased. In addition, soot grew due to the reduction in premixed combustion and subsequent growth of the diffusion burn phase. Similar results (i.e., NOx and soot increased) were observed with decreasing dwell.

In 2002, Corcione [40] investigated multiple injections with a 0.44 L single-cylinder CI engine with a compression ratio of 18:1. They experimented with a pilot/main strategy, as well as a pilot/pre/main strategy, both at 1800 rpm. They found for both injection schemes an SOC of 0° BTDC offered the best NO_x and combustion noise characteristics without penalties in engine

performance, but the pilot/pre/main injection scheme could achieve a lower peak heat release rate and subsequent rate of heat release.

Concurrently, Yamane and Shimamoto [80] tested both early pilot injection and two stage split injections in an HSDI single-cylinder CI engine and proved that reductions in formaldehyde, NO_x, and smoke were possible with these strategies. An improvement in BSFC was seen with the two-stage split strategy that was attributed to efficiency gains as a result of a growth in constant volume combustion. Conversely, the early pilot injection experiments showed an increase in BSFC but with a reduction in NO_x.

That same year, a lab at the Polytechnic University of Turin in Italy published two papers experimenting with multiple injections. Badami et al. [81] produced the first effort while utilizing their 1.9 L four-cylinder CI engine with a compression ratio of 17.2:1. This effort initially tested a pilot/pilot/main injection at 2000 rpm and 2 bar BMEP, with the first two injections having injection quantities of 10% and 7%, respectively. Two variations of this strategy were then explored. Strategy 1 involved fixing the second pilot injection and main injections at an SOI of 7° and 3° BTDC, respectively, while the first pilot injection SOI was varied from 39° to 9° BTDC. Strategy 2 held the first pilot and main injections at SOIs of 35° and 3°, respectively, while the second pilot SOI was varied from 29° to 4° BTDC. Results of both these experiments showed increased NO_x and soot as compared to their previous tests with only a single pilot injection; however, gains in BSFC and combustion noise were seen. Then, they investigated pilot/main/post schemes using four different tests, with the 1500 rpm experiments having pilot and post injection quantities of 8-15% and 12%, respectively, and the 2500 rpm experiments having pilot and main injection quantities of 3-6% and 4-6%, respectively. The first two strategies focused on short dwell times between the pilot and main

injections, while varying the SOI of the post injection. Strategy 3a was carried out at 1500 rpm and 5 bar BMEP and it involved fixed pilot and main SOIs at 5° and 1° BTDC, correspondingly, while varying post SOI from 6° to 17° ATDC. Strategy 3b was then carried out at 2500 rpm and 8 bar BMEP, with pilot and main SOIs fixed at 8° and 3° BTDC, respectively, while post SOI was varied from 10° to 37° ATDC. The last two strategies then focused on post injection in conjunction with a wide pilot/main separation, with Strategy 4a operating at 1500 rpm and 5 bar BMEP and having fixed pilot and main SOIs of 13° and 1° BTDC, respectively, while post SOI was varied from 6° to 17° ATDC. Lastly, Strategy 4b was held at 2500 rpm and 8 bar BMEP, having fixed pilot and main SOIs at 38° and 3° BTDC, respectively, and a variable post SOI from 10° to 37° ATDC. They found that all post injection strategies were effective in reducing soot, but injection parameters had to be carefully selected so the best trade-off between NO_x, soot, and BSFC could be achieved.

Mallamo et al. [82] then published the second paper based on experiments employing their 0.95 L non-road two-cylinder CI engine with a compression ratio of 19:1. They tested similar injection parameters as the previous effort by Badami et al., this time adding a pilot/pilot/main/post schedule to the mix. Their best results were attained at 3600 rpm and 100% load, where NO_x reductions of 10% and PM reductions of 15% were seen, simultaneously, with no penalty in BSFC.

That same year, Payri et al. [83] delivered an effort studying the effects of post injection on the emissions and performance of a 1.85 L heavy-duty single-cylinder CI engine with a compression ratio of 16.3:1. Five operating points were selected from the ESC to employ post injection quantities ranging from 5-20% while varying the main/post dwell. Here, the main injection timing and EGR rates were identical to respective cases employing single injections at

the same operating point. Post injections were reported to be an effective means for soot reduction without an increase in NO_x; e.g., soot reductions of 40-45% at low loads with post injection quantities of 15-20% and a decrease of 25-45% at full load with quantities ranging from 7-10%.

Beatrice et al. [84] then published another paper in 2003, this time experimenting with two different engines and their optical variants to investigate pilot and post injection strategies while also validating their Computational Fluid Dynamics (CFD) combustion models. The first engine was the same 1.9 L four-cylinder used previously, and the second was a 1.3 L variant with a higher compression ratio of 18:1. Both had duplicate engines modified for optical access. With the 1.9 L engine, they experimented with both a 10%(20°)90% pilot/main strategy, as well as a pilot/main/post strategy where the 10% pilot was held at an SOI of 1.4° BTDC with a 2° dwell leading to the main injection followed by a 27% post injection with a varied SOI from 5° to 12.5° ATDC. The 1.3 L engine tested two 10%/90% pilot/main strategies where the main injection event was held at an SOI of 4° BTDC and the pilot SOI was tested at 18° and 7° BTDC. They claimed the tests were successful in controlling NO_x and soot emissions, although there were no detailed emission results.

Concurrently, Carlucci et al. [85] investigated the effects of pilot injections on a turbocharged 1.93 L four-cylinder CI engine with a 19.8:1 compression ratio. The engine was operated at 1400 rpm at a range of loads from 23 to 45.5 N-m, as well as at 2000 rpm from 25 to 79 N-m. The main injection timing was held at 3.4° BTDC for the 1400 rpm points, while the pilot SOI was varied from 16° to 32.7° BTDC. At 2000 rpm, the main SOI was held at 4.8° BTDC and the pilot SOI was varied from 22.8° to 46.8° BTDC. They concluded that the timing of the pilot injection has a greater effect on the main injection ignition delay in comparison to

pilot quantity; however, the influence of either parameter on main injection ignition delay is dependent on load. Moreover, NO_x was shaped primarily by pilot quantity with the effect of pilot timing more apparent at low speed and low load. Finally, both pilot quantity and timing affected smoke emissions, particularly at medium to high loads.

Also in 2003, Badami et al. [86] investigated the effects of pilot/pilot/main and pilot/main/post injection schemes and their effects on NO_x, soot, noise, and BSFC as compared to their previous pilot injection effort in 2001. The same operating points were tested as the prior effort, employing pilot/pilot/main strategies for the 2000 rpm (2 bar BMEP) condition, and pilot/main/post strategies for the 1500 rpm (5 bar BMEP) and 2500 rpm (8 bar BMEP) conditions. Injection strategies 1 and 2 involved pilot/pilot/main schemes, with strategy 1 utilizing pilot quantities of 10% and 7% for the first and second pilot quantities, respectively, in addition to varying the first pilot SOI from 37° to 12° BTDC while holding the second pilot SOI at 7° BTDC and main SOI at 2° BTDC. Strategy 2 employed the same injection quantities as strategy 1; however, the first pilot SOI was held at 33° BTDC and the second pilot SOI was varied from 28° to 7° BTDC while the main SOI was fixed at 2° BTDC. For the pilot/main/post strategies, strategy 3 was tested at the 1500 rpm (5 bar BMEP) condition while varying pilot and post injection quantities from 8-15% and 11-12%, correspondingly, along with fixed respective pilot and main SOIs of 5° and 0° BTDC, respectively, with a varied post SOI from 5°-16° ATDC. Strategy 4 tested pilot and post injection quantities of 3-6% and 4-8%, respectively, with a set pilot SOI of 7° BTDC, main SOI of 3° BTDC, and the post SOI varied from 10°-37°. Strategies 1 and 2 experienced increased NO_x and soot compared to the previous pilot injection study, although reductions in CO and HC emissions were seen, as well as lowered combustion noise and BSFC. Strategies 3 and 4 were observed to produce the same low NO_x levels, if not

slightly less than the previous study, in addition to soot reductions of up to 40% due to the post injection. Finally, the lowest soot levels were attained with the close-coupled post injections; however, if the post injection was too delayed, a substantial increase in soot and CO was seen.

In 2004, Park et al. [34] conducted experiments involving pilot and post injections with varying fuel pressures. They used a single-cylinder optical research engine with a displacement of 0.49 L and an 18.9:1 compression ratio. All injection parameters were tested during an 800 rpm idling condition, with 13% pilot and post injections being individually tested at fuel pressures varying from 30 to120 MPa. First, the effects of varying fuel pressure were explored for a single injection event while varying the SOI from 17° to -3° BTDC. Results showed a downward trend in HCs, CO, and opacity with increasing fuel pressure; however, this did raise NO_x emissions while lowering the IMEP. This result was explained by a greater mixing effect with the air and smaller fuel droplet size associated with high injection pressures contributing to more pre-mixed combustion and an advanced phasing towards TDC. Moreover, another benefit of the higher injection pressure is the mitigation of unburned HC emissions associated with excess fuel left in the sac volume of the injector. This fuel eventually makes its way through the nozzle at low speeds during combustion and expansion and exits with the exhaust as emitted HC. Pilot injections were then explored at low and high injection pressures (30 and 120 MPa) by varying the main SOI from 16.4° to -5.6° BTDC while also adjusting the pilot/main dwell from 10° to 60°. The results demonstrated that pilot injection with a low injection pressure was more effective in reducing the peak heat release rate and subsequent NO_x emissions. In contrast, utilizing a high injection pressure achieved a greater IMEP while maintaining smoke and fuel consumption levels. Furthermore, high injection pressures during early pilot injections could cause lean misfires due to overmixing of the fuel. Post injections were then explored at low and

high fuel pressures by varying the main SOI event from 18.6° to -1.7° BTDC, as well as the main/post dwell from 0° to 40°. It was seen that the high fuel pressure injection case was effective in reducing soot, producing almost zero soot emissions for all tests; whereas, the lower injection pressure case was still effective for soot reduction with respectively delayed post injections. To conclude the study, pilot and post injections were used simultaneously in a triple injection scheme tested at high and low fuel pressures with respective pilot, main, and post SOIs of 35°, 5°, and -15° BTDC, respectively. The high fuel pressure case produced minimal decreases in NO_x and increased opacity, while the low pressure case achieved simultaneous reduction of NO_x and smoke of 30% and 40%, respectively, with a 4% decrease in IMEP.

The lab at the University of Wisconsin-Madison published another work in 2005 where Liu and Reitz [87] used a HSDI single cylinder engine to test optimized injection parameters produced from their KIVA-3V code. The engine was a single cylinder version of a 2.4 L five-cylinder CI engine with a compression ratio of 18.8:1. They employed EGR and boost while testing it at 2000 rpm and part load for two and five injection events. They were able to achieve the best BSFC and emissions results with widely spaced double split injection schemes employing SOIs of ~50° and -13° BTDC.

Also that year, researchers at Brunel University in the UK investigated multiple injections motivated by the goal of meeting Euro 4 emissions. Gill et al. [28] tested up to four injections per cycle with pilot and post injections, having up to three pilot injections per cycle. Experiments were carried out on a Ricardo Hydra single cylinder CI engine modified with a prototype Ford Puma cylinder head and optical access. This engine had a swept volume of 0.5 L and a compression ratio of 15.9:1. All operating points within the test matrix were held at 1500 rpm, 40% load and tested at 80, 100, and 120 MPa of fuel pressure. The pilot/main strategy was

first explored by varying the number of pilot injections from one to three. The main SOI was held at 10° BTDC, and the 18% pilot quantities had SOIs varying from 30° to 70° BTDC. Overall, two pilot injections resulted in a heat release rate reduction for the 80 and 100 MPa fuel pressure cases, although with a decreased IMEP as compared to the single pilot injection case. Conversely, the 120 MPa injection pressure case with two pilot injections caused a large spike in heat release and a greater IMEP; however, both less than the single pilot injection baseline. Three pilot injections showed similar results to the 80 and 100 MPa two pilot fuel pressure cases, albeit with slightly lower heat release peaks and IMEP. The 120 MPa fuel pressure case with three pilot injections caused a heat release spike as large as the single injection case, as well as a lower IMEP. These results indicated there might not be any additional benefit to using three pilot injections over two; therefore, only up to two pilot injections were implemented in the remaining experiments with post injections. Two injection strategies with post injection were studied, both with main and post SOIs of 10° and 0° BTDC, respectively, while the pilot SOIs were 30° BTDC for the single pilot case, and 50° and 30° BTDC for the double pilot injection case. Pilot fuel quantities remained at 18% and post injection quantities were 41% for the single pilot case and 23% for the double pilot case. The results for one and two pilot injections with the addition of a post injection were like the previous results at the respective fuel pressures without a post injection. Nevertheless, there were gains in IMEP without an increase in the heat release rate, implying a pilot/pilot/main/post strategy could be effective for both NO_x and soot reduction.

Concurrently, Carlucci et al. [88] investigated the effects of using both early and pilot injection events. The tests that were carried out included early/main, pilot/main, and early/pilot/main schemes. This was done while varying the injection quantities of the early and pilot injections, as well as the injection timing. Simultaneous NO_x and soot reduction was

reported at low loads and speeds with early injections, and further reductions in NO_x were attained with the addition of the pilot injection, albeit with increased HC emissions.

The final publication of 2005 was produced by Toyota. Here, Hotta et al. [29] used a 0.5 L single-cylinder research CI engine with a compression ratio of 17:1 to investigate the effects of early pilot, late pilot, and post injections. Testing was carried out at full, medium, and light load conditions at 1200, 2000, and 1380 rpm, respectively. This was accomplished with corresponding fuel pressures of 90, 80, and 55 MPa. At full load, an early pilot injection having an SOI of 55° BTDC was observed to have a 6% increase in IMEP along with a 4 dB decrease in combustion noise and a subsequent NO_x reduction. However, this came with an increase in HCs and a slight increase in smoke, though still within the allowable limit. Interestingly, the equivalence ratio under this condition was nearly 1.0, implying complete utilization of air in the cylinder; hence, improving the smoke limit of the engine. At part load and respectively low speed, the early 32% pilot injection event caused a further increase in HC emissions and fuel consumption. This was remedied by implementing a second pilot injection with an additional 19% fuel quantity that also reduced combustion noise. In general, the low load condition presented a challenge for the early injection strategy. Here, the combination of the reduced fuel pressure and turbulence caused cylinder wall impingement issues and a subsequent rise in HC emissions. Thus, the low load condition necessitated a small pilot quantity close to the main injection event (~10% pilot quantity and 4° BTDC SOI) which decreased NO_x, fuel consumption, HCs, and noise as compared to the single injection case with an acceptable increase in smoke as well. In addition, a post injection event was evaluated at the low load condition having a quantity of 17% and SOI shortly after the main injection pulse. This attained reductions in HCs, smoke, and fuel consumption, albeit with an increase in NO_x emissions.

Adding EGR was effective in maintaining the low NO_x levels achieved by the pilot injection while still benefitting from post injection, concluding with a desirable effect on the NO_x -smoke trade-off.

Another effort motivated by the upcoming Euro 4 emissions regulations was published in 2007 by Ehleskog et al. [42], where optimal injection scheduling was explored for a main injection split of up to four injections while also using a pilot injection. This effort is significant because the authors bring to light an important distinction between heavy-duty CI and HSDI operation. Unlike heavy-duty CI engines with relatively quiescent conditions, the increased swirl in HSDI engines results in combustion products from the first injection (of a multiple injection event) potentially being carried away by the swirl and not interacting with subsequent injections. This can have important implications regarding soot emissions [89]. Their subsequent testing was done on a 0.48 L Ricardo Hydra single-cylinder research CI engine with a Volvo NED5 cylinder head, bringing the compression ratio to 16.8:1. The test matrix consisted of four 2000 rpm operating points with 8% pilot injections, the first three being at 6.5 bar IMEP and 64 MPa rail pressure, except the third point which was raised to 96 MPa. The first three points also had fixed pilot and main SOIs of 20° and 4° BTDC, respectively, and an EGR rate 16.3%, except for the second point with a rate of 24.5%. The final operating point was at an IMEP of 9.5 bar, rail pressure of 87.3 MPa, 13.8% EGR, and respective pilot and main SOIs of 46° and 3° BTDC. Split main injections varying from one to four injections were tested at each operating point and the dwell times between main injections were chosen by finding the mechanical limit for the shortest dwell possible and adding 1°. Results showed torque increased with the double main injection due to the relatively high heat release for the longest time, subsequently giving the greatest thermal efficiency. As three and four injections were added, combustion duration

increased while heat release decreased, overall causing torque to decrease. With respect to emissions, two main injections created the most NO_x while the three and four main injection schemes had lower NO_x, but more PM due to a slower and less efficient combustion process.

An additional study was done in 2007 by Okude et al. [30], this time a single main injection event was studied with up to three pilot injections. Testing was done using a 0.74 L single cylinder CI engine with a compression ratio of 15.7:1 at a constant 1620 rpm and 8.2 bar IMEP. For all tests, the main SOI was fixed at -2.5° BTDC, along with a constant 140 MPa of rail pressure, 24% EGR, and 47 kPa of boost. Additionally, the authors provided some interesting insight by comparing the case of a normal single pilot (one pilot injection followed by a main injection) to only a single pilot injection (no main injection). Since the pilot injection fuel amount is usually much smaller than the main injection event, one might assume that the emissions contributed by the pilot injection are lesser than that of the main injection; however, this is not always the case. Figure 2.9 shows the relationship between the NOx formed by the pilot and main injections at different pilot injection times. It is seen that the more advanced the pilot injection, the less NO_x that is produced by the pilot injection.

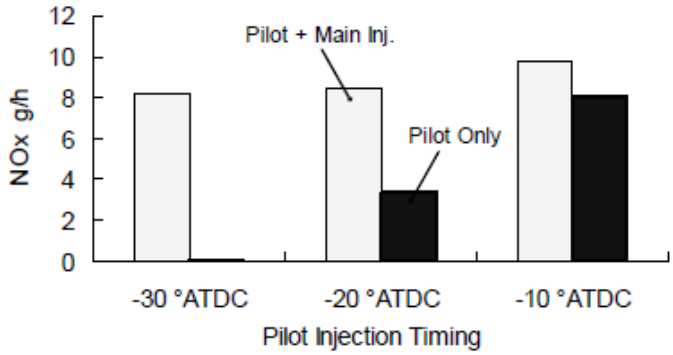

Figure 2.9: NO_x emissions contribution of a pilot injection [30].

As for the results of the remaining experiments, the main takeaway was that multiple pilot injections were useful for emissions reduction This is because smaller quantity injections avoid cylinder wall impingement and a subsequent growth of HC and CO emissions. Moreover, the overall emissions results are shown in Figure 2.10, where it is seen that the double pilot scheme provides the best emissions trade-off and lowest fuel consumption.

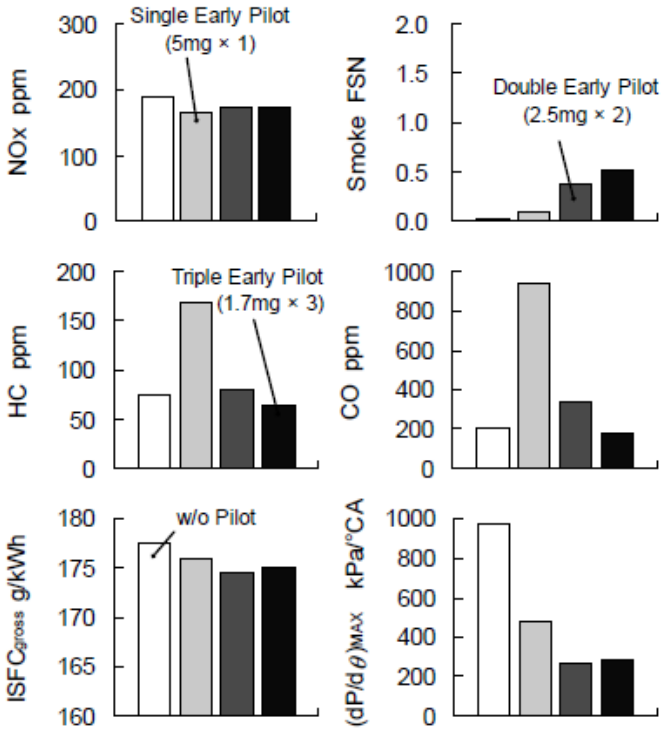

Figure 2.10: Emissions results of varying the number of pilot injections from zero to three [30].

In 2008, Ehleskog and Ochoterena [90] set out to further examine the effects of split main injections in hopes of understanding the relationship between main injection split dwell times and soot production. They employed the injection strategies previously investigated in Ehleskog 2007 [42] that involved a single pilot injection in conjunction with a main injection split. Rather than repeating the same engine tests, these injection strategies were tested in a high temperature, high pressure vessel with optical access to use a planar Laser Induced Incandescence (LII) analysis. They were able to repeat the results found previously, seeing that the addition of a pilot injection reduces soot, and splitting the main injection into two equal injection allows for further soot reduction; however, no clear relationship between dwell time and soot production was seen.

The same year, Vanegas et al. [91] experimented with pilot/main and pilot/main/post injection strategies on their 1.9 L four-cylinder CI engine with a compression ratio of 18.3:1. For

the pilot/main injection cases, the pilot injection mass was held at 12.5% of the total injected fuel mass and the main SOI was varied from 4° to -5° BTDC, while the pilot-main dwell time was set at 10°, 16°, and 22° for a total of 12 runs. The lowest NO_x emissions with dual injection was seen with a main SOI of -5° BTDC and a dwell of 22°, most likely because of the lengthened combustion duration. Moreover, HC and CO emission decreased with the dual injection strategy as compared to the single injection event when an advanced SOI and short dwell were used. Regarding smoke emissions, smoke increased compared to the single injection case for all dual injection schemes. For the pilot/main/post injection strategies, the pilot and post injections were again held at 12.5% of the total injected fuel mass and main SOI was varied from 4° to -5° BTDC, but this time with dwells of 13°, 19°, and 25° between pilot and main injections. The post injection timing was varied from 9° to 18° ATDC with a main/post dwell of 13° for the first set, 15° to 24° ATDC with a main/post dwell of 19° for the second set, and 21° to 30° ATDC with a main/post dwell of 25° for the last set. All 12 triple injection cases were able to achieve slightly lower NO_x levels than the dual injection cases, while CO and HC remained basically constant close to the nominal level seen for all the tests. The lowest soot emissions with triple injections were seen with a main SOI of 4° BTDC and a post SOI of 9° or 15° ATDC.

Concurrently, Mendez and Thirouard [44] implemented up to four fuel injections per cycle to explore HCCI/Highly Premixed Combustion (HPC) operation in the LTC regime. While LTC operation is not of interest here, they also produced results within the medium to high load range that were representative of conventional CI combustion. They used respectively low compression ratio engines along with the help of EGR for their tests, which is necessary to increase the ignition delay. This greater ignition delay provides more time for charge homogeneity, and coupled with lower temperatures, can reduce soot and NO_x. They tested five

small bore light-duty CI engines, three of which were single-cylinders, and two were four-cylinders. At mid load (IMEP of 7 bar) and 2000 RPM it was possible to lower fuel consumption by 8% using a duel injection strategy (SOIs of 7.4° and -5° BTDC) while achieving the same noise and soot levels as a single injection strategy. This was believed to be a result of better fuel distribution and, thus, optimized air usage, in addition to the cooling effect brought on by the second injection event that improved premixing. At high load (IMEP of 13 bar) and 2500 rpm, the NO_x versus soot trade-off was evident with two injections (SOIs of 32° and 19° BTDC). Here, the addition of a third injection (SOI of 4° BTDC) achieved a favorable effect on the trade-off by lowering soot without increasing NO_x emissions or fuel consumption.

In 2009, Lee et al. [31] carried out an investigation of single and double pilot injection strategies employing their 1.82 L single-cylinder CI engine with a compression ratio of 17:1. Experiments included testing at medium load and 1200 rpm with injection parameters as follows: the single pilot injection timing was varied from 10° to 80° before the start of the main injection event while the pilot quantity was adjusted from 10% to 50%. Furthermore, the timing of both pilot injections for the double pilot case were modified in the same range as the single pilot, though pilot quantities of either 15% or 25% were used. Main injection timing was varied from 28° to -4° BTDC for both single and double pilot injections, as well as using two different fuel pressures of 30 and 140 MPa. When the single pilot SOI was more than 40° before the main injection, a drastic decrease in NO_x was seen, suggesting partially premixed charge compression ignition (PPCI); however, this could also be due to cylinder fuel impingement causing less fuel to participate in combustion. Regarding smoke, a pilot/main dwell greater than 40° caused smoke emissions to increase due to the fuel impinged on the cylinder wall. The most advanced single pilot injection of 80° before the main SOI had a medium sized premixed burn phase according to

the heat release profile, but it also had the lowest NO_x emissions. This was said to be because the advanced pilot injection resulted in a low ambient cylinder temperature due to PPCI combustion causing relatively delayed combustion phasing. The double pilot injection resulted in a greater NO_x reduction because of a more homogenous mixture formed by the improved turbulent effects from the additional injection split. Smoke emissions were also further reduced with the double pilot injection due to the same principle of the rich fuel spray tip region not being replenished and shortened. For both single and double pilot injection cases, the indicated specific fuel consumption (ISFC) and HC emissions increased as pilot/main dwell and pilot fuel quantity grew. With a pilot double split of 15/15/70, an HC reduction of 50% was seen due to the decreased spray penetration and less fuel hitting the cylinder walls. Timing of the second pilot injection did not have a significant effect on the heat release rate, but the heat release of the main injection event was affected. Results showed that a double pilot injection strategy is more advantageous than a single pilot injection due to a greater simultaneous reduction of NO_x and smoke.

Concurrently, Mingfa et al. [32] published an effort exploring pilot/main, pilot/pilot/main, and main/post injection strategies in a heavy-duty CI engine. Their testing utilized a 6.5 L six-cylinder engine with a compression ratio of 17.5:1. Overall, 25%, 50%, and 100% load conditions were tested at 1849 rpm and 120, 140, and 160 MPa of rail pressure, respectively. Pilot and post injection quantities were varied for the single pilot and post injection cases, though the relative quantity was not reported. For all injection schedules, the main SOI was held as 0° BTDC, while the pilot dwell was varied from 8° to 40° for both the single and double pilot cases, and the main/post dwell was varied from 6° to 24°. It was seen that single pilot injections were not effective in reducing NO_x or PM at high load but saw reductions in

NO_x, CO, and BSFC at low load. The double pilot injections were able to reduce PM due to increased cylinder air utilization but came with a growth of NO_x emissions. Post injections offered benefits in both smoke and CO emissions. The addition of EGR was also studied, allowing for mitigated NO_x creation during the double pilot injection, and thus, having a favorable effect on the NO_x -PM trade-off. The addition of a post injection was stated to offset the added smoke emitted due to EGR use.

In 2013, Yang and Chung [92] experimented with up to four injections per cycle to explore the feasibility of simultaneous NO_x and PM reduction with their HSDI single cylinder CI engine. An AVL 5402 engine was used that had a displacement of 0.51 L and a 17:1 compression ratio and was operated at 2000 rpm and 5 bar IMEP. Initial tests were performed with two injection pilot/main strategies while varying the injection pressure from 30 to 180 MPa. The respectively high increase in injection pressure led to almost zero smoke emissions and attributed to the increased atomization leading to the rapid formation of a lean pre-mixture that reduces ignition delay. However, in this case, the reduction in ignition delay did not contribute to lower NO_x emissions. Instead, the rapid premixed burn of the pilot injection caused an increase in NO_x. The best case occurred with an injection pressure less than 100 MPa where a 50% smoke reduction was seen with slightly higher NO_x emissions. A four-injection pilot/pilot/main/post scheme was then tested at 58 MPa involving a 13% pilot with an SOI of 25° BTDC, followed by a second pilot with a 11% quantity and 16° BTDC SOI, the main injection had an SOI of 4° BTDC, and the 13% post injection was injected at 45° ATDC. The four-injection strategy produced a 55% reduction in particulates and no penalty in NO_x as compared to a single main injection event.

Concurrently, Barman et al. [93] used a design of experiment (DOE) approach to optimize the multiple injection strategy for their light-duty CI engine. The engine speed was varied from 700-2600 rpm over a range of loads and employed up to four injections. At low to medium loads, a high pilot quantity and large pilot/main dwell provided benefits in BSFC, as well as reductions in NO_x and soot. At full load, multiple injections were less effective in NO_x and soot reduction, though a reduction in BSFC was seen. Post injections were found to be an effective method for soot oxidation with a small penalty in BSFC. However, they discussed that a small improvement in BSFC could be achieved with high post injection separation and low injection quantities.

In 2014, the current Tier 3 emission standards (see Table 2.3) were proposed and scheduled to phase-in starting in 2017 [74]; hence, motivating the proceeding research. Moreover, the Euro 6 emissions standards (see Appendix) began to phase in during 2014. This new generation of U.S. emissions standards is significant because, for the first time, Federal emissions and the historically lower California emissions standards have been "harmonized". Here, the Tier 3 standards are now equal to the California LEV III standards.

Table 2.3: Tier 3 emissions standards for light duty vehicles, light duty trucks, and medium duty vehicles [94].

Tier 3 Certification Bin Standards [FTP, 150.000 mi]				
Bin	NMOG+NOx [mg/mi]	PM [1] [mg/mi]	CO [g/mi]	HCHO [mg/mi]
Bin 160	160	3	4,2	4
Bin 125	125	3	2,1	4
Bin 70	70	3	1,7	4
Bin 50	50	3	1,7	4
Bin 30	30	3	1,0	4
Bin 20	20	3	1,0	4
Bin 0	0	0	0	0

Suh [95] studied twin pilot injections on a low compression ratio engine the same year as the Tier 3 emissions standards proposal. They tested an HSDI single-cylinder engine modified

from a production four-cylinder that was further altered to reduce the compression ratio from 17.8:1 to 15.3:1. Twin pilot injections were compared to both pilot/main and single injection strategies, yielding a 2.1% increase in IMEP over the single injection case for both pilot strategies, as well as NO_x reductions of up to 45.7% without significant penalties in soot.

Also in 2014, O'Connor and Musculus [96] investigated the effects of load variation on the efficacy of soot reduction by close-coupled post injections in an effort to understand the soot oxidation mechanism further. Testing was carried out using an optical 2.34 L single-cylinder CI engine based on a Cummins N-14. The original compression ratio of 16:1 was reduced 11.2:1 to accommodate optical instrumentation; hence, the intake was artificially boosted to bring the effective compression ratio back to 16:1. Main injection timing was held at 13° BTDC while a 13.5-34% post injection quantity was set to an SOI of 6° ATDC under a range of EGR levels. Overall, they concluded that post injection usefulness decreases at higher loads, and the range of post injection durations that are effective also shrinks. This was attributed to the varying thermal conditions, dictated by load, that change the structure of the post fuel jet. Specifically, high temperatures and loads cause soot to form further upstream in the post jet, and in greater quantities, swaying the competition between soot oxidation and formation to yield more soot.

In 2015, Busch et al. [97] conducted a study that used a combination of physical engine testing, spectral analysis, and zero-dimensional thermodynamic modeling to provide insight into the possible physical mechanisms that contribute to combustion noise reduction with close-coupled pilot injections. The engine used was a 0.48 L single-cylinder CI version of a GM four-cylinder with a 16.7:1 compression ratio and was tested at 1500 rpm and 9 bar IMEP. Pilot quantities of ~6% with the SOI varied from 12° to 1° were used while the main injection SOI was adjusted from 0° to 2° to meet the load requirement. A 3 dB reduction in noise was achieved

without a change in exhaust emissions. This was said to be a result of two possible factors. The first involves the relative phase change between pilot and main combustion events that has two potential mechanisms at play. The initial mechanism has to do with the pressure rise and fall associated with heat release and expansion and how this affects pressure oscillations and combustion phasing. It was postulated that if there is not a significant pressure change after TDC or before the beginning of heat release, this impedes pressure oscillations in the critical frequency range (1.3 to 2.6 kHz). The subsequent potential mechanism is that combustion phasing can cause destructive interference in the critical frequency range and does not rely on interaction of compression or expansion of the cylinder; hence, only the pressure oscillations caused by heat release, though this thought was stated to be less likely. The second factor considered to be a cause of the close-couple pilot injection noise decrease is the suppression of pilot heat release due charge cooling brought on by the main injection. This could lead to broadband attenuation of sounds pressure levels over a wide frequency range; thus, decreasing combustion noise for a certain range of dwells. Here, simulations predicted this effect was only apparent for a small portion of the noise decrease seen.

In 2016, Biswas et al. [98] investigated multiple injections using a DOE strategy to improve BSFC and torque using a 5.7 L six-cylinder CI engine with a compression ratio of 17.5:1. The focus of the experiments were pilot/main/post and pilot/pilot/main/post strategies at a range of loads and speed of 10-100% and 1200-2400 rpm, respectively. Results showed benefits in BSFC with the pilot/main/post strategy at low loads, though at high loads the pilot/pilot/main/post scheme provided optimal BSFC. Regarding emissions, overall, the pilot/pilot/main/post strategy achieved lower PM, HCs, and CO, although with marginally higher NO_x levels.

In 2017, Diwakar and Domenech-Llopis [33] performed experiments in conjunction with a computational study to explore the fundamental physics behind combustion noise reduction with multiple injections in CI engines. They experimented with a light-duty 0.49 L single-cylinder engine with a compression ratio of 15.2:1 that operated at a constant speed of 2000 rpm and 5 bar BMEP. A five-pulse injection scheme was used that employed three pilot injections, a main, injection, and a post injection. The goal of testing was to analyze noise reduction when the dwell between the final pilot injection and main injection was varied while all other injection parameters remained constant. The results from varying the injection 3 to 4 delay from 0° to 4° shows a sweet spot at 2° that minimizes combustion noise, increases gross IMEP, and has little effect on NO_x. The optimal dwell time of 2° had the lowest corresponding rate of pressure rise, while still maintaining a relatively high average rise rate, as shown in Figure 2.11. This is said to be a result of the localized cooling effect from the 4th injection; thus, delaying premixed ignition to the point that the premixed spike is damped from interaction with the main injection.

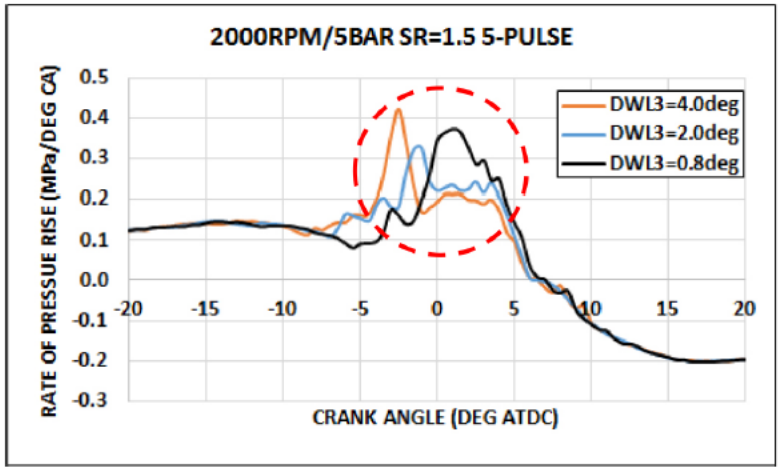

Figure 2.11: Illustration of how maximum pressure rise rate can be minimized while maintaining the average rate (blue line) to provide benefits in noise and IMEP [33].

Also in 2017, Jorques et al. [27] explored the effect that pilot injections have on main injection events and how they can be used to control the combustion process. The purpose of this was to increase the feasibility of closed-loop combustion control by decreasing cycle-to-cycle variation and the effects of external disturbances that are a detriment to combustion modes such as HCCI. Closed loop combustion involves the use of an in-cylinder pressure transducer that can be used to estimate heat release and facilitate precise combustion control. Testing was performed on a modified Scania D13 heavy-duty CI engine at an operating point of 1200 rpm with loads ranging from 2.5 to 15 bar IMEP, as well as a constant 10 bar IMEP with engine speed varied from 600 to 1800 rpm. After testing the effects of a small pilot injection on the main injection process with different combinations of pilot mass, dwell, fuel rail pressure, and combustion phasing, it was seen that combustion phasing and duration have a more significant effect on emissions and performance that the pilot injection alone. It was suggested that more pilot mass needs to be injected at higher loads to reduce the combustion duration, while at low load, the pilot/main dwell can be used to influence this process.

In 2019, Sadafale and Mittal [99] investigated dual injection strategies with a 0.55 L supercharged single-cylinder CI engine with a compression ratio of 16.3:1 as a means for validating their numerical simulations. Experiments at 1500 rpm and a range of low operating loads were carried out while varying the pilot SOI from 4° to 6° BTDC and main SOI from 5° to 7° ATDC. They concluded that simultaneous NO_x and soot reduction is possible with delayed dual injections in conjunction with EGR.

2.2.2. Summary of Diesel-Fueled Multiple Injection Strategies

The literature has brought forth a myriad of useful results pertaining to conventional diesel-fueled CI engines employing multiple injections. Many mechanisms have been proposed to explain the reduction of exhaust emissions, combustion noise, and fuel consumption possible with these strategies. This section will recount these efforts by summarizing the trends and physical mechanisms involved.

Starting with pilot injections, a wide range of injection timings and quantities for both the pilot and subsequent main injection events have been explored. This is in addition to a varying number of pilot injections per engine cycle. Pilot injection experimentation began with the goal of combustion noise and NO_x emissions reduction, which has been successful while also being effective in reducing the BSFC. Here, the general thought was that noise could be decreased through lowering peak cylinder pressure rise rates [33, 40, 73]. The study by Busch et al. in 2015 delved further into the noise reduction mechanism, showing that it only takes a pilot quantity of ~6% to attain significant reductions in combustion noise. This was mainly attributed to two possible mechanisms: first, the pressure rise and fall due to heat release and expansion can influence the relative pilot and main injection combustion phasing that may subsequently impede

pressure fluctuations in a critical frequency range, and second, combustion phasing that causes destructive interference may be present only due to pressure fluctuations as a result of heat release.

The original notion that NO_x reduction could be attributed to a decrease in peak heat release rate has been confirmed numerous times [28, 61, 65, 66, 68, 73]; however, a strong load dependency has also been reported [40, 61, 65, 66, 73, 85, 93]. Every pilot quantity has been explored that can still be considered a "pilot" injection (i.e., quantities less than 50%), and pilot injection timing has been tested as early as 90° (i.e., the intake stroke) [69]. Significant early injection events often come with piston/cylinder wall impingement issues, especially at low engine speeds and loads with associated low turbulence; hence, this causes oil dilution and spikes in HCs, CO, and PM emissions [29-31, 69]. In addition, pilot SOI has been investigated as late as 0° ATDC [75], with a main SOI as delayed as 10° ATDC. At low loads, optimal injection parameters for NO_x abatement appears include a small pilot quantity of 10-15% [60, 66, 91, 92, 100].

There are countless reports of pilot/main dwell times that are favorable, but they are relative to the phasing of the injections with respect to piston location, as well as the number of pilot injections. Nevertheless, pilot/main dwells ranging from 2°- 80° have been reported [31, 84]. At medium load, it has been reported that pilot influence starts to lessen and requires a larger pilot quantity (around 18%-30%) [27, 28, 31]. At high loads, pilot injections are often reported to have little to no influence on combustion [61, 66, 73, 93]; however, some researchers had success with NO_x and noise reduction at high loads [29, 67, 82]. This lessened pilot influence as load progresses has been thought to be a function of the decreasing premixed combustion phase (low load being predominately premixed), which necessitates other means of

combustion modulation such as main injection splitting. Furthermore, multiple pilot injections have been reported to be effective [28, 30, 31, 92, 95, 98], even at high loads [98], with even stronger effects at part load. It is generally agreed upon that double pilot injections are optimal [28, 30, 31, 92, 95]. An important takeaway from these results is that the use of a pilot injection allows for delayed main injection timing that benefits NO_x emissions, as well as potentially BSFC due to a lengthened combustion into the expansion stroke [61, 65, 91, 99]. While some researchers found a growth in PM emissions while using pilot injections [29, 30, 91], many have experienced reductions in PM with little to no penalty in NO_x production [92, 98]. Conversely, researchers have seen NO_x reductions with little to no penalty in PM levels [50, 65, 95] and even simultaneous NO_x and soot reduction [31, 57, 66, 75, 82, 88, 93, 99] as compared to a single injection event.

Main injection splits have been successful in reducing NO_x levels and combustion noise [8, 42, 44, 60, 67, 68, 72, 76] via the same mechanisms discussed via pilot injections. Moreover, main injection splits in conjunction with pilot injections have compounded benefits in NO_x and combustion noise [42, 60, 76]. Main injection splitting has been widely shown to increase fuel air mixing to reduce PM production [44, 60]. Here, the reports indicate PM reduction with little to no impact on NO_x [44, 60], or NO_x emission decreases with little to no impact on PM, as well as simultaneous PM and NO_x reductions [8, 60, 67, 76]. Furthermore, it has been reported than main injection splits can reduce BSFC by maintaining a respectively high heat release rate for a longer amount of time [42]. Main injection splits also brought forth the witness of an additional soot reducing mechanism. This was explained by the discontinuation of the fuel rich soot producing zone at the tip of the fuel jet that is not replenished because the proceeding injection is introduced into a high temperature and pressure environment caused by the preceding injection

event. This mechanism was first proposed by Han et al. in 1996 and has since been confirmed by multiple studies [71, 72]. Main injection splits have been investigated for up to four injections [42, 90] with optimal BSFC and PM reports resulting from two injections [42, 44, 80, 90]. A load dependency has also been observed, albeit with a lessened effect of favorable behavior as compared to pilot injections. Overall, it was been reported that main injection splits can be effective at all loads, with generally dampened effects at high load [60, 67, 93].

The literature has proven post injections to be effective for PM reduction without increasing NO_x emissions while only incurring a potentially small growth of BSFC [29, 34, 39, 76, 81-84, 91-93, 96]. Largely, the mechanisms that make post injections effective operate differently than main injection splits or pilot injections. While post injections do share the same quality of discontinuing the soot producing region at the tip an initial fuel jet, that benefit is lessened due to the lower temperatures and pressures occurring during the expansion stroke. Instead, post injection PM reduction is a function of an improved mixing and continued combustion that influences the soot production and oxidation battle. While temperatures are too low to have any BSFC improvements, temperatures are still high enough to contribute to the late stage soot oxidation phase seen only minimally during the traditional single injection event strategy. The post injection schemes proven to be the most effective deal with post injection quantities of approximately 10%-17% [29, 34, 39, 75, 81-83, 92, 96] and SOIs no later than 27° ATDC [75]. Furthermore, post injection effectiveness is highly dependent on load [83, 96]. This is similar to pilot injections since the soot producing diffusion phase becomes more predominate as load increases; hence, the soot production and oxidation battle naturally shifts.

While pilot, split, and post injections have been widely studied while employing only one of these respective injection schemes, it is unanimously agreed upon that pilot injection in

conjunction with post injection is the most beneficial [29, 75, 76, 81, 82, 91, 92, 98], with various methodologies of splitting the pilot, main, and post fuel quantities included [82, 92, 98]. Furthermore, different injection types benefit from dissimilar fuel pressures. With the reported tests employing fuel pressure ranging from 30-180 MPa [34, 92], it has been generally seen that pilot injections are most effective with respectively low fuel pressures [28, 34, 39, 92]. This is to minimize heat release rates from excessive fuel jet penetration, atomization, and mixing; however, this can be combated by splitting the pilot injection. Moreover, high fuel pressures with early pilot injection timing can cause lean misfires due to overmixing [34]. Post injections have been observed to benefit from higher pressures [34, 39, 92] because of the increased mixing that allows for late stage soot oxidation, although lower injection pressures still allowed for some post injection benefit. Overall, there has been a wide range of results from the literature with some studies focusing on BSFC improvements, while others concentrate on a single family of emission constituents. Interestingly, favorable literature results with one strategy might incur worse performance for a seemingly similar injection scheme in another paper. The overriding agreement is that multiple injection parameter calibration is delicate, and the optimal injection scheme will differ between any two setups. Nevertheless, the literature has illustrated the potential effects and sensitivities of multiple injections with diesel-fueled CI engines, along with generally agreed upon mechanisms to describe the resultant behaviors.

2.2.3. Multiple Injections with Biodiesel Fuels

There has been limited research on the effects of biodiesel fueled CI engines operating with multiple injections. To the author's knowledge, the earliest account of multiple injection strategies with biodiesel is from 1999 [101]. Most of the research has occurred between 2013 and 2019 and from these limited investigations only four biodiesel feedstocks (i.e., waste cooking oil

(WCO), coconut oil, soybean oil, and karanja oil) have been explored. Moreover, these efforts are divided into neat biodiesel research and those that incorporate biodiesel blends. Overall, biodiesel blends are popular because they are more feasible for large-scale implementation. This is due to the capability to realize emissions reductions without sacrificing fuel economy largely as a result of the lower energy content of biodiesel [102]. Thus, this review will begin by recounting the efforts of multiple injections with neat biodiesel, followed by the works pertaining to biodiesel and conventional diesel blends.

2.2.3.1. Neat Biodiesel

Neat biodiesel has been commonly shown to simultaneously reduce CO, PM, and HC emissions, but can increase NO_x emissions due to its greater oxygen content and higher adiabatic flame temperature if combustion phasing is not considered. Conversely, research such as the efforts by Magnus et al. [103], has shown neat biodiesel can actually achieve reductions in NO_x emissions by controlling heat release through appropriate injection timing helping to mitigate the advancement of combustion phasing primarily due to its cetane number. Thus, with the addition of multiple injections to further control the heat release of biodiesel, it is reasonable to believe there are additional gains possible with respect to emissions using neat biodiesel. Initially, studies in this area were conducted exclusively on small single cylinder CI research engines.

In 2008, Stringer et al. [102] began the research on multiple injection strategies with biodiesel using a 0.3 L single cylinder CI engine with a compression ratio of 19.5:1 operating at 4.0 bar IMEP and 1500 rpm. Tests were conducted using pilot injections (~16% total injection quantity for biodiesel and ~14% for conventional diesel) with neat soybean biodiesel at a fuel pressure of 80 MPa. Their results showed that simultaneous reductions in NO_x and PM can be

achieved with neat biodiesel using pilot injections when compared to conventional diesel. To note, the biggest reductions were a result of operating in a postulated LTC regime when employing a pilot SOI of 30° BTDC and main SOI of 10° ATDC.

Kim et al. [104] also investigated the use of neat soybean biodiesel with multiple injections in 2008. Using a 0.37 L single cylinder CI engine with a compression ratio of 17.8:1, their effort consisted of comparing a single injection case to a 50/50 split at an injection pressure of 100 MPa and 1500 rpm. The split injections significantly reduced NOx output compared to the single injection case. Moreover, unlike the single injection case, delaying injection for the split injection case resulted in slightly lower soot emissions. However, HC and CO emissions grew due to a longer combustion duration that also caused a reduced thermal efficiency.

The following year, Fang et al. [105] conducted a study with an optical 0.3 L single cylinder research engine with a compression ratio of 19.5:1. The use of the optical set-up allowed them to investigate simultaneous NO_x and soot reductions using a pilot injection strategy by measuring engine-out NO_x emissions and analyzing the natural flame luminosity during combustion. They concluded that the natural flame luminosity of the neat soybean biodiesel tested was always lower than conventional diesel at the same operating conditions, subsequently leading to lower soot emissions. Moreover, a NO_x reduction of up to 30% as compared to conventional diesel at the same operating point was seen using a pilot injection strategy with a respectively delayed main injection event.

In 2010, Yehliu et al. [106] was one of the first to investigate multiple injections with biodiesel utilizing a full-sized CI engine. They experimented with a 2.5 L four-cylinder engine with a compression ratio of 17.5:1. The single injection tests with soybean biodiesel resulted in

an increase in NOx emissions at high load over conventional diesel, along with increased particle concentrations at low load. With the addition of a pilot injection, the neat biodiesel fuel produced decreased NOx emissions, as well as a lower particle concentration compared to the conventional diesel fuel.

In 2011, Park et al. [100] experimented with neat biodiesel using a similar single cylinder research engine to that used by Stringer et al. in 2008; however, it had a slightly lower compression ratio of 17.8: l. This engine was operated at 1400 rpm and utilized a higher fuel pressure of 120 MPa. Experiments were carried out by comparing a single 10 mg injection to a pilot injection of 3 mg and main injection of 7 mg. The pilot SOI was varied from 30° to 10° BTDC with a fixed main SOI at 0° BTDC. They concluded there was an increase in IMEP to be had when using the pilot injection as compared to the single injection strategy due to a delayed main injection event extending combustion further into the expansion stroke.

Also in 2011, Qi et al. [107] set out to continue the research started by Stringer et al. in 2008 with neat soybean biodiesel; however, this time on a full-sized 2.4 L Ford Lion V6 with a compression ratio of 17.3:1 and with the addition of EGR. Their effort consisted of utilizing a pilot injection strategy at load points of 3 bar and 6 bar at 1500 rpm. The pilot injection timing was held constant at 14° BTDC for the lower load point and 16° BTDC for the higher load point, with both varying the main injection timing from 4° to -4° BTDC. They were able decrease NO_x emissions without any soot penalty, but with a small increase in BSFC by using a respectively delayed main injection timing and EGR.

In 2014, Chen et al. [43] studied the use of double post injections for DPF regeneration. It was seen that a mixed feedstock biodiesel (mainly soybean oil) produced lower HC and NO_x

emissions along with a small penalty in CO in comparison to diesel. Moreover, biodiesel exhaust temperatures were lower and produced a lower DOC conversion efficiency during the regeneration process.

Additional research was done by Jeon et al. in 2015 [108] using a 0.51 L single cylinder research engine with a compression ratio of 17.1:1. Their study consisted of comparing neat soybean biodiesel to conventional diesel using pilot injections at 4.4 bar and 1500 rpm. They investigated the effects of varying both pilot injection timing from 90° to 20° BTDC and pilot fuel mass from 2 – 6 mg (main injection quantity unknown). They found a reduction in brake specific energy consumption of up to 15.8% is possible for biodiesel when using multiple injections as compared to a single injection. They discussed that multiple injections could allow biodiesel to overcome the inherent disadvantages associated with its higher viscosity during spray development. Moreover, it was seen that the poor atomization of the biodiesel fuel caused an increased soot concentration in the middle of the combustion process compared to conventional diesel. However, its higher oxygen content and greater temperatures accelerated the soot oxidation process and resulted in lower overall soot emissions.

Concurrently, Mohan et al. [41] studied the effects of injection profile shaping using both injection pressure modulation and a pilot injection. A 2.5 L four-cylinder turbocharged CI engine with a compression ratio of 18.5:1 was operated with neat WCO biodiesel at various speeds and loads. Results of this study demonstrated that when a smaller pilot injection is used than the main injection, reductions in NO_x and PM as compared to the single injection case can be achieved under a medium engine speed and load scenario.

In 2017, Li et al. [109] explored the effects of post injections using neat soybean biodiesel. Tests were carried out on a 3.8 L four-cylinder turbocharged CI engine with a compression ratio of 17.5:1 at various engine speeds and an IMEP of approximately 10.6 bar. The main-post injection dwell was varied from 8° to 20°, and the post injection quantity was varied from 4% to 20%. They found that when increasing main post dwell and post injection rate, CO and HCs increase while NO_x decreased. Regarding particulates, PM increased with a greater dwell at low injection rates, then a sweet spot of lowered PM was achieved as injection rate was increased. Continuing to raise the injection rate subsequently resulted in the PM again increasing. Particle number grew with increasing dwell at low injection rates, while decreasing to a sweet spot before rising again at higher injection rates. The study concluded that the post injection dwell and rate greatly affect soot reactivity. Most notably, at higher injection rates a decreased activation energy was seen for the soot particles.

Lastly, in 2018 Babu et al. [110] experimented with a 0.55 L single cylinder CI engine with a compression ratio of 16.5:1. They investigated the effect of multiple injections using WCO biodiesel derived from sunflower oil. Timing of the first injection was varied from 19° to 25° BTDC, while the SOI of the second injection was varied from -5° to 0° BTDC. Additionally, the injected fuel quantity of the first injection was varied from 75% to 90% of the total injected fuel mass. Here, simultaneous reduction of HCs, smoke, and NO was achieved without compromising engine performance.

2.2.3.2 Biodiesel Blends with Conventional Diesel

Research involving conventional diesel blended with biodiesel began in 1999 when Choi et al. [101] set out to understand the effects of using high pressure injection in conjunction with

multiple injections and oxygenated fuel blends. Experiments were done on a 2.44 L single cylinder Caterpillar test engine with a compression ratio of 16.1:1. A blend of 20% soybean biodiesel was compared to conventional diesel while testing both single and split injection strategies, all at an injection pressure of 90 MPa. For the high load split injection case, a 50/50 fuel split was employed at 1600 rpm, while the low load case utilized a 61/39 split at 1700 rpm. It was found that the split injection strategy offered an additional reduction in soot emissions at high loads. This was on top of the inherent reduction achieved when using biodiesel. Moreover, at low loads, biodiesel only offered a small reduction in particulate emissions due to the premixed dominated combustion. However, the split injection case still provided an additional reductions in particulates. Overall, they were able to reduce particulates using biodiesel and multiple injections without any penalty to NO_x emissions.

To follow, there was an absence of blended biodiesel multiple injection research until 2013 when Dhar et al. [111] investigated the effects of karanja biodiesel blended with conventional diesel. They used a 0.51 L single cylinder CI engine with a compression ratio of 17.5 fueled with B0, B20, and B50 karanja biodiesel blends. Using a 10% pilot injection and respectively advanced injection timing, the B20 blend produced the lowest particle concentration of all the fuels, but at the expense of increased NO_x emissions. Dhar et al. [112] conducted another study in 2014, this time testing a B10 karanja biodiesel blend and saw similar results to the 2013 study.

It was not until 2018 that multiple injection research with multi-cylinder engines operating with biodiesel blended fuels began when How et al. [113] experimented with a 1.46 L turbocharged four-cylinder engine with a compression ratio of 18.25:1. They tested conventional diesel, as well as B20 and B50 coconut biodiesel blends using single, double, and triple injection

strategies at a constant 60 N-m load and 2000 rpm. The multiple injection schedules employed 50/50 and 33/33/33 fuel mass splits with constant dwell angles between injections. By using triple injections with delayed injection timing, they were able to reduce NO_x levels beyond that of conventional diesel with both biodiesel blended fuels. Moreover, they achieved simultaneous reductions in NO_x and PM with the B50 coconut biodiesel blend.

Later in 2018, Teoh et al. [114] continued the work of How et al. on the same test engine and used the same fuel blends, this time focusing on double split injections (50/50) and varying the dwell angle between the two injections. Again, they were able to reach simultaneous reductions in NO_x and PM as compared to conventional diesel. The best results were obtained with a respectively long dwell angel and delayed SOI, where there was a further reduction in NO_x as compared to the triple injection study, but at the cost of an increase in PM.

How et al. [115] conducted an additional study in 2019, using the same hardware and fuels as the previous two studies. Here, the effects of varying the double injection fuel masses was investigated; i.e., 25/75, 50/50, and 75/25 injection splits were applied at a constant dwell angle of 15° and varied SOIs from 12° to -2° BTDC. This time, the B50 blend with a delayed 25/75 split was found to be optimal, achieving reductions in NO_x and PM in comparison to diesel. This attained the lowest PM levels of the three studies along with NO_x emissions equivalent to the best case of the previous double injection study.

Most recently, Plamondon et al. [116] experimented with conventional diesel and a B20 WCO biodiesel blend using pilot injections. Their set up consisted of a Renault 1.5 L turbocharged four-cylinder engine operating at 2 bar BMEP and 2000 rpm. They tested a wide range of pilot SOIs from 64° to 11.5° BTDC at a fixed main SOI of 4° BTDC, in addition to

varying the dwell angle from 7.5° to 60°. Moreover, while they claimed to be using pilot injections, their "pilot" fuel masses ranged from approximately 58-64% (i.e., greater than 50%) of the total injected fuel mass. Their testing was concluded without attaining simultaneous reductions in NO_x and PM compared to diesel. In specific, they saw a reduction in NO_x while increasing PM. Overall, only the B20 fuel was able to achieve a reduction in both constituents with double injections as compared to the single injection event.

2.2.4. Summary of Biodiesel-Fueled Multiple Injection Strategies

Largely, the literature finds similarities with multiple injection operation between conventional diesel and biodiesel fuels with a few differences reported. To begin, the same NO_x reduction mechanism has been observed with the use of pilot injections and respectively delayed main injection timing [102, 105, 107]. Potential benefits in the IMEP (and effectively BSFC) as a result of pilot injection use was also reported [100] due to the same concept of the combustion process extending further into the expansion stroke. In addition, the same PM reducing tendency of post injections has been reported [109, 110]. Conversely, the qualities inherent to biodiesel fuels (i.e., greater cetane number, higher viscosity, and lower energy content compared to petroleum diesel) present deviations in favorable injection parameters compared to conventional diesel. For instance, slightly higher pilot injection quantities (around 15-25%) have been reported with single pilot injections [102, 115] when using neat biodiesel to counteract its larger cetane number.

A major difference in biodiesel multiple injection operation involves the variance in behavior of the soot production and oxidation battle. Due to the higher viscosity of biodiesel fuels, its correspondingly poorer atomization produces an increase in soot concentration in the

middle of combustion, but its higher oxygen content and greater adiabatic flame temperature accelerates the soot oxidation process [108]. Furthermore, respectively high post injection quantities (around 20%) have been reported to decrease the activation energy of soot particle oxidation [110]. The beneficial shift in soot production and oxidation inherent to biodiesel use is compounded by the addition of a post injection event, explaining why many researchers have seen lower PM levels with biodiesel compared to petroleum diesel when employing multiple injections.

Another difference involves the historical time period when the bulk of efforts have taken place with respect to CI fuel injection technology. While investigations involving conventional diesel-fueled CI engines employing multiple injections have presented a vast number of experiments with a wide range of injection parameters (e.g., timing and quantity to fuel rail pressure), most biodiesel multiple injection research has taken place when many of these injection parameters are generally understood. Hence, a smaller range for a given parameter has been explored with biodiesel; for example, fuel pressure tested involves a respectively reduced span of about 80-120 MPa [100, 102]. Another difference has been a stronger focus on PM emissions. Since Tier 3 PM emissions requirements approach zero, PM emissions must be understood in great depth; thus, the literature has offered more detailed insight into the PM production and abatement qualities when using multiple injections with biodiesel.

Overall, multiple injections with biodiesel fuels have been proven to be just as effective, if not more so than with conventional diesel. Most studies have reported the same NO_x and PM reduction potentials with biodiesel and that multiple injections are advantageous as compared to a single injection event. Moreover, a few have attained simultaneous reductions in NO_x and PM levels in comparison to conventional diesel with the same injection scheme; however, these

results have been limited to neat soybean biodiesel [102, 104, 105] and coconut biodiesel blends [113, 115]. Here, multiple injections with biodiesel allow for the inherent benefits of biodiesel (e.g., lower PM, HCs, and CO), while also overcoming disadvantages associated with its lower energy content and higher viscosity through flexible control of injection parameters. Now that a review of the literature has been brought forth that encompasses all conventional diesel and biodiesel-fueled CI engine operation within the multiple fuel injections regime, this information can be used motivate experimental efforts moving forward.

2.3. Conclusion

The summary sections presented prior highlight the schemes, parameters, and corresponding benefits involved with multiple fuel injection use for both diesel and biodiesel-fueled CI engines. While pilot injection strategies have proven to be useful for both fuels, there has been little to no exploration of injection timing associated with the maximum brake torque (MBT) condition. MBT for CI engines involves optimizing the injection timing so that the maximum amount of work can be extracted for a given amount of fuel. This condition is often quantified by achieving either an optimal peak pressure location from the pressure trace or by using a heat release analysis to correlate an ideal location for the 50% mass fraction burned point. For single fuel injections, achieving MBT has been linked to favorable performance in both power output and emissions [117]; thus, it would be of interest to expand this understanding to a CI engine operating with multiple injections. In specific, this includes discussing how this relationship differs between conventional diesel and biodiesel fuels. With an extensive consideration of how multiple injections affect pressure rise and heat release behavior, a strong foundation has been laid for delving further into the understanding of biodiesel fueled CI engines operating with multiple fuel injections.

Chapter 3 – Multiple Fuel Injection Experiments

3.1. Introduction

The experimentation conducted in this chapter is largely motivated by the opportunity to compare biodiesel combustion between single and multiple fuel injection operation when combustion is normalized by maintaining the same peak pressure for a given speed and load condition. This will help compare different fuel injection strategies on a fundamental level. In addition, this will provide the same analytical advantage for identical strategies compared between ULSD and biodiesel. Moreover, the single-cylinder engine used for experimentation in this effort operates with a respectively high compression ratio of 21.2:1. This compression ratio has only been approached by Carlucci et al., who tested multiple fuel injections with ULSD on an engine having a compression ratio of 19.8:1. Furthermore, the closest instances with respect to biodiesel operation occurred when Stringer and Fang each experimented with their respective 19.5:1 compression ratio engines fueled with soybean biodiesel. The higher compression ratio of the engine used in this work is expected to influence certain combustion parameters (e.g., ignition delay) that are critical players in performance and emissions when operating with multiple injections, regardless of the fuel being used. Lastly, results of multiple injection operation reported in the literature vary from setup to setup due to the different operating variables that may be introduced (e.g., boost, EGR level, etc.) when striving to attain optimum performance and emissions levels. Here, following the theme of fundamental analysis between normalized conditions, engine operation will be kept as simple as possible to allow for objective comparison between fuels and injection schemes.

The injection scheme of focus will be the single pilot and main injection strategy. While there are surely benefits to adding additional pilot or main injection events, not to mention a post

injection event, the fundamental effects of a single pilot injection must first be explored before additional injections can be added. The decision to analyze pilot injections rather than post injections comes from the fact that there is more insight to be gained from pilot injections. This is because they affect a wider range of engine performance and emissions parameters, while post injections generally only impact PM emissions. In addition, neat soybean-derived biodiesel will be the biodiesel fuel of choice. Neat biodiesel will be used to limit the variables considered (as opposed to biodiesel/ULSD blends) and provide a fundamental understanding of the influence of biodiesel. Most of the limited number of tests pertaining to neat biodiesel multiple injection experiments have been accomplished utilizing soybean biodiesel; thus, the selection of soybean as the feedstock will allow for comparison with these prior results and possibly facilitate a more comprehensive understanding of results obtained.

The remainder of this chapter will proceed by first describing the experimental setup and test procedures used, along with the methods of data collection and post-processing. Then, this will be followed by analyzing the multiple fuel injection test results with ULSD and biodiesel. Analysis will consist of the consideration of emissions, performance, heat release, and combustion noise to provide a holistic view of the trends and behaviors seen. To conclude, a summary of the results will be presented, highlighting the effects of pilot injection operation with an engine having a respectively high compression ratio that is fueled with biodiesel, as well as underline the differences seen between operation with the two fuels.

3.2. Experimental Setup, Procedure and Data Collection, and Post-Processing

3.2.1. Experimental Setup and Data Collection

Experiments were conducted within a single-cylinder CI test cell containing a Yanmar L100V engine fitted with a modern high-pressure electronic fuel injection system. The fuel injection system can operate with both petroleum diesel and biodiesel fuels. A detailed account of the implementation of this system can be found in Mangus 2014 [118]. Table 3.1 provides full specifications of the Yanmar L100V used in testing, as well as the Dyne Systems alternating current (AC) dynamometer (dyno) that regulates its speed while measuring the torque generated.

Table 3.1: Engine and dynamometer specifications [119, 120].

Engine	
Manufacturer and Model	Yanmar L100V
Type	Vertical Direct-
Aspiration	Naturally Aspirated
Cooling	Air-Cooled
Cycle	4-Stroke
Displacement	435 cc
Number of Cylinders	1
Number of Valves	1 Intake, 1 Exhaust
Bore	86 mm
Stroke	75 mm
Connecting Rod Length	118 mm
Crank Pin Radius	38 mm
Clearance Volume	2.1611 × 105 m3
Cylinder Head/Piston	5.8088×10^{-2} m^2
Compression Ratio	21.2:1
Intake Valve Close	122° BTDC
Exhaust Valve Open	144° ATDC
Continuous Rated Power	8.3 hp SAE; 6.2 kW
Maximum Speed	3600 rpm
Injection Pressure	47 MPa
Number of Injectors	1
Injector Holes	6
Injector Hole Diameter	0.17 mm
Aftertreatment	None
Engine Oil Used	Shell 15W-40

Dynamometer	
Manufacturer and Model	Dyne Systems, Inc.
Continuous Torque	21.1 ft-lbs
Continuous Power	12 hp
Speed	0-7500 rpm
Voltage	480 Volts AC
Phase	Three-Phase
Frequency	60 Hz
Controller	Dyne Systems, Inc.

As for instrumentation and experimental hardware within the test cell, all sensors listed are sampled at a rate of 10 Hz, excluding in-cylinder pressure measurements. Engine torque is measured by a FUTEK (model #TRS-605) torque transducer that provides readings from 0-200 ± 0.2 N-m. To note, the engine will be running in the dyno controller's "speed mode" that allows an exact engine speed to be chosen and maintained, while measured load (torque) is a function of fuel input and injection timing. The fuel injection system includes a high-pressure common fuel rail (Bosch model #261-B1-135-201) and a six-hole fuel injector from a Fiat Grande Punto MJTD 1.3. In addition, a Bosch high pressure fuel pump (model #CP3) is employed that is powered by an external direct current (DC) motor and can produce 40-200 MPa of fuel pressure. The last of the fuel system hardware is the Emerson ELITE Coriolis mass flow and density meter (model #CMF-010M having an uncertainty of ±0.03%) that is placed in-line between the fuel reservoir and pump. The fuel injection parameters are controlled by a Bosch Engine Control Unit (ECU: model #MS15.1) that communicates with Bosch ModaSport software that allows for calibration of injection parameters, permitting 0.02° of fuel injection timing resolution.

On the intake side, ambient air temperature and humidity are measured by an Omega (model #EWS-RH) sensor that has accuracies of ± 1.4 °C and ± 4% for temperature and relative humidity, respectively. Intake air flowrate is then measured by a Meriam (model #50MW20-2) volumetric airflow element with an uncertainty of ± 0.1%. The metered air then enters a 30-

gallon plenum to dampen pressure fluctuations presented by piston movement where intake relative humidity is measured by an Omega (model #HX92AC, accuracy of ± 3.1%) relative humidity sensor. From here, the air flows through a throttle valve used for the EGR system and then into a mixing box that can be used for the introduction of gaseous fuel through a dedicated port on the box. Within the mixing box, pressure and temperature are measured by an Omega (model #PX329, accuracy of ± 0.25%) pressure transducer and (model #KQXL) K-type thermocouple. In addition, a Bosch combined temperature and pressure sensor (model #A-261-260-253) is sampled within the box by the Bosch ECU. Furthermore, the same three sensors that the mixing box employs are incorporated downstream within the intake manifold to account for potential heat transfer.

During engine operation, a cylinder pressure measuring system is utilized. This includes a Kistler (model #6052C) piezoelectric in-cylinder pressure transducer that is mounted in the cylinder head (a detailed account of its implementation can be found in Mangus [118]). A Kistler (model #2614B4) pulse amplifier is employed to generate a usable signal from the raw pressure measurement. The resulting pressure signal is then phased by a Kistler (model #2614B1, uncertainty of ± 1.5%) analog crankshaft encoder employing 0.2° of resolution where the position signal is output to a Kistler (model #2614B2) digital signal converter. The final pressure trace that is reported after data logging is the average of 60 thermodynamic cycles with a subsequent uncertainty of ± 0.5%. Measurement of the in-cylinder pressure system is done by a rack mounted computer that utilizes a National Instruments (NI: model #PCIe-7841R) Peripheral Component Interconnect (PCI) card with a Field Programmable Gate Array (FPGA) chip. Lastly, exhaust temperature and pressure readings are measured by Omega K-type thermocouples and pressure transducers (models #KQXL and #PX329 with uncertainty of ± 0.25%, respectively) at

two separate upstream and downstream locations. All sensor measurements (besides in-cylinder measurements and ECU-dedicated sensors in the mixing box and intake manifold) are input and converted to savable data using an NI (model #cRIO-9014) compact-reconfigurable I/O (cRIO) real-time controller with an eight-slot chassis (model #cRIO-9114). All signals sent to the cRIO are processed by the Yanmar Performance Data Acquisition program (YDAQ-p). This is an in-house LabView code that incorporates front-end processing through a laptop running LabView, as well as back-end processing generated by the cRIO chassis that permits programming upwards of 100 MHz.

The exhaust is first sampled by an AVL smoke-meter (model #415SE) that reports filter smoke number (FSN) as well as soot concentration. Sample number and duration are used by the smoke-meter to produce an averaged output value that is dependent on engine load and is manually updated. The reason for varying the number of samples and sample duration has to do with the minimum and maximum measurement limits of the carbon deposits on the filter paper within the smoke-meter. At low load and respectively low PM emission, the lower measurement limit of the machine must be avoided by taking relatively long measurements to allow deposit build-up on the filter paper. Moreover, when a longer measurement is taken, less samples are needed to calculate an accurate average. As load increases, the higher measurement limit needs to be avoided, so sample time is reduced, and the number of samples is increased. Thus, at 0.5 and 4.5 N-m, two measurements are taken at a duration of 120 seconds each, while the 9.0 N-m load condition is sampled three times for 90 seconds each, four measurements are taken at 13.5 N-m for 45 second durations, and the 18.0 N-m condition is sampled four times at 9 seconds each. Exhaust species are then sampled by an AVL SESAM Fourier Transform Infrared Spectroscopy (FTIR) emissions analyzer (model #2030HY). After the system has been purged

with nitrogen, the FTIR is calibrated before testing using various span gasses such as oxygen, nitrogen, and specific hydrocarbon (HC) species. Here, constituents are measured continuously for five minutes at a sampling rate of 1 Hz. The sampled species include (but are not limited to) CO_2, CO, NO, NO_2, N_2O, CH_4, H_2O, NH_3, isocyanic acid (HNCO), hydrogen cyanide (HCN), formaldehyde (HCHO), acetaldehyde (CH_3CHO), and aromatic hydrocarbons. The emissions analyzer unit also houses a flame ionization detector (FID) used for measuring the total hydrocarbon (THC) content of the exhaust, which itself references a Magnos oxygen sensor to detect diatomic oxygen.

To note, before any data collection begins for a given operating point, engine oil and exhaust temperatures are monitored until steady-state conditions are achieved, meaning either temperature experiences fluctuations less of less than 1% over a 60 second period. Concluding a detailed account of the experimental setup, the data analysis techniques used to process experimental data will now be described.

3.2.2. Test Data Post-Processing

Various methods of post-processing these test data are used. The first method includes the in-house Test Cell Analysis (TCA) MATLAB code that consolidates data from all the test equipment employed to report brake specific emissions, efficiencies, as well as all averages and uncertainties within a single Excel document. The TCA code was developed by a previous student (see Langness [119]) to replace cumbersome and error-prone data processing that had to be done manually. The program consists of a graphical user interphase (GUI) that receives testing data files from the emissions analyzer, smoke-meter, YDAQ-p, and in-cylinder system. This code then filters all data using either a moving average filter or a curve-fit filter to the order

"*n*", which is user-selected in the GUI, and calculates brake-specific efficiencies. These efficiencies include the volumetric efficiency (η_v):

$$\eta_v = \frac{\dot{m}_{air}\bar{R}T_{intake}}{NM_{air}P_{intake}V_d} \tag{3.1}$$

where $\dot{m}_{air}$ is the mas flowrate of air entering the cylinder, $\bar{R}$ is the universal gas constant, N is the engine speed, M_{air} is the resulting mass of air in the cylinder, P_{intake} is the intake manifold pressure, and V_d is the displacement volume of the engine. Eqn. (3.2) is then used to compute combustion efficiency (η_c),

$$\eta_c = 1 - \frac{P_b}{\dot{m}_{fuel}}\left(bs_{CO}Q_{LHV_{CO}} + bs_{THC}Q_{LHV_{THC}} + bs_{H_2}Q_{LHV_{H2}}\right) \tag{3.2}$$

where P_b is the brake power produced by the engine, $\dot{m}_{fuel}$ is the mass flowrate of fuel, bs_{CO}, bs_{THC}, and bs_{H_2} are brake-specific CO, THC, and H_2 emissions, respectively, and $Q_{LHV_{CO}}$, $Q_{LHV_{THC}}$, and $Q_{LHV_{H_2}}$ are the lower heating values of CO, THC, and H_2, respectively. In addition, fuel conversion efficiency (η_f) is calculated as:

$$\eta_f = \frac{P_b}{\dot{m}_{fuel}Q_{LHV}} \tag{3.3}$$

Lastly, thermal efficiency is calculated with Eqn. (3.4), followed by the final calculation of importance, the net indicated mean effective pressure ($IMEP_n$), represented by Eqn. (3.5).

$$\eta_{th} = \frac{\eta_f}{\eta_c} \tag{3.4}$$

$$IMEP_n = \frac{W_{in}}{V_d} \tag{3.5}$$

where W_{in} signifies the net indicated work:

$$W_{in} = \int_{IVC}^{EVO} PdV + \int_{EVO}^{IVC} PdV = \left(\frac{P_1 + P_N}{2} \right)(V_1 - V_2) + \sum_{i=2}^{N} \left(\frac{P_i + P_{i-1}}{2} \right)(V_i - V_{i-1}) \quad (3.6)$$

and EVO and IVC represent exhaust valve opening and intake valve closing, respectively.

After TCA results have been obtained, post processing can then move on to a heat release analysis. Rate of heat release (RHR) is an invaluable parameter when studying the effects of multiple fuel injections, as it allows for the quantification of ignition delay and fuel injection charge-cooling, as well as a visual representation of the overall effect multiple injections have on combustion. Here, another in-house MATLAB code is used, of which, an all-encompassing account of the construction of the program can be found in Mattson and Depcik [121]. For the sake of brevity, only the main components of the code and subsequent equations will be highlighted.

The heat release model used can be described as a zero-dimension (0-D) apparent heat release model, as it only accounts for heat release as a function of time, as opposed to 1-D or multi-dimensional computational fluid dynamics (CFD) modeling. This 0-D model allows for efficient computation with added accuracy and stability brought on by the utilization of an Arrhenius-based expression for the rate of combustion and the input of an initial combustion efficiency that has already been found from the TCA code. While the model has zero spatial dimensions, it operates by considering three separate zones within the cylinder during combustion. Here, unburned, burned, and fuel zones are continually changing with respect to volume, temperature, species, etc. The program requires an experimental pressure trace, information from the performance results generated by the TCA tool, as well as (if biodiesel is being analyzed) additional information pertaining to the various fatty acid mass fractions present within the fuel. The fatty acid content of the soybean biodiesel fuel used here is tabulated in the

Appendix. The main governing equation employed in this model is the conservation of energy derived from the First Law of thermodynamics on a crank-angle basis:

$$\frac{dQ_{hr}}{d\theta} = \frac{dU_{CV}}{d\theta} + \frac{dW_{CV}}{d\theta} + \frac{dQ_{ht}}{d\theta} + \sum h \frac{dm_{CV}}{d\theta} \tag{3.7}$$

This equation states that the change in heat transfer due to heat release $\left(\frac{dQ_{hr}}{d\theta}\right)$ is balanced by the total change in internal energy of the cylinder $\left(\frac{dU_{cv}}{d\theta}\right)$, the change in work done $\left(\frac{dW_{cv}}{d\theta}\right)$, the change in heat transfer to the surroundings $\left(\frac{dQ_{ht}}{d\theta}\right)$, and the energy transferred in or out of the cylinder due to mass flow brought on by the fuel injection event $\left(\sum h \frac{dm_{cv}}{d\theta}\right)$ (which can represent a number of things such as the intake event, exhaust event, blow-by, etc.). From here, these four terms from the right-hand side of Eqn. (3.7) can be solved for individually. To simply visualize the process flow of the model, Figure 3.1 illustrates the solution method for a given time-step based off this governing equation.

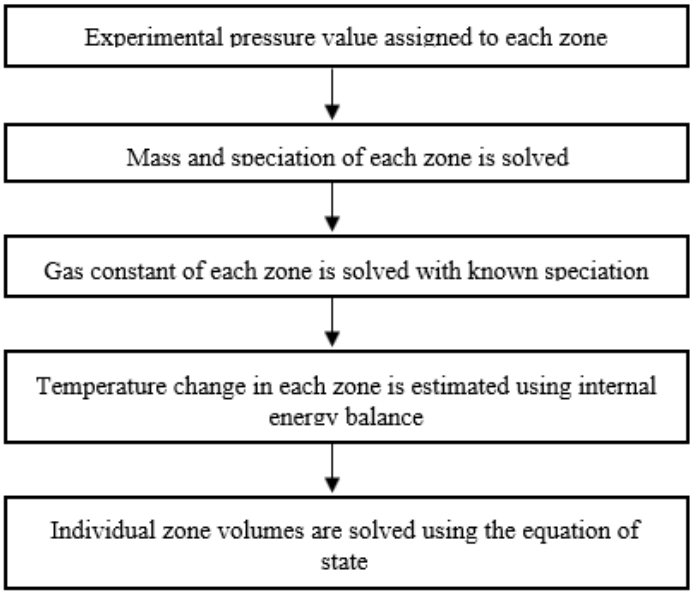

Figure 3.1: Process flow diagram executing the heat release model for a given timestep.

The total change of internal energy within the cylinder can be quantified by the summation of the change in internal energies of the different zones within the cylinder:

$$\frac{dU_{CV}}{d\theta} = \sum \frac{dU_i}{d\theta} = \frac{dU_u}{d\theta} + \frac{dU_f}{d\theta} + \frac{dU_b}{d\theta} \tag{3.8}$$

Here, $\sum \frac{dU_i}{d\theta}$ represents the summation of internal energy change of the different zones, and the subsequent subscripts *u*, *f*, and *b* of the individual terms indicate the unburned, fuel, and burned zones, respectively. These terms are each calculated from the same expansion of the change in internal energy for a given volume:

$$\frac{dU_i}{d\theta} = \left[\frac{\partial U_i}{\partial m_i}\frac{\partial m_i}{\partial \theta}\right] + \left[\frac{\partial U_i}{\partial T_i}\frac{\partial T_i}{\partial \theta}\right] + \left[\frac{\partial U_i}{\partial c_{v,i}}\frac{\partial c_{v,i}}{\partial \theta}\right] = T_i c_{v,i}\frac{dm_i}{d\theta} + m_i c_{v,i}\frac{dT_i}{d\theta} + T_i m_i \frac{dc_{v,i}}{d\theta} \tag{3.9}$$

where m_i, T_i, and $c_{v,i}$ represent the mass, temperature, and constant volume specific heat of an arbitrary zone. Next, the work term from Eqn. (3.7) can be computed as:

$$\frac{dW_{CV}}{d\theta} = p\frac{dV_{CV}}{d\theta} \tag{3.10}$$

where the volume of the cylinder with respect to crank angle (V_{cv}) is calculated by Eqn. (3.11) given by Heywood [122]:

$$V_{CV}(k) = V_{clear} + \frac{\pi b^2}{4}\left[c + r - r\cos(\theta(k)) - \sqrt{c^2 - (r\sin(\theta(k)))^2}\right] \tag{3.11}$$

Within this equation, $V_{cv}(k)$ is the cylinder volume at a given time step *k*, V_{clear} is the clearance volume, *b* is the cylinder bore, *c* is the connecting rod length, and *r* is the crank arm length. Next, the heat transfer term can be solved:

$$\frac{dQ_{ht}}{d\theta} = h_c\frac{dt}{d\theta}A_s(T_{CV} - T_w) + \sigma\frac{dt}{d\theta}A_s\left(\varepsilon_g T_{CV}^4 - \alpha_w T_w^{\ 4}\right) \tag{3.12}$$

where h_c is the convective heat transfer coefficient calculated using Woschni or Hohenburg correlations [123], T_{cv} and T_w are the average temperature of the three zones within the cylinder and cylinder wall temperature, respectively, ε_g is the emissivity of the bulk gas, α_w is the absorptivity of the cylinder wall, σ is the Stefan-Boltzmann constant, and the surface area of the cylinder (A_s) is derived from Eqn. (3.11):

$$A_s(k) = 2\frac{\pi b^2}{4} + \pi b\left[c + r - r\cos(\theta(k)) - \sqrt{c^2 - r\sin(\theta(k))^2}\right] + 4\frac{V_{clear}}{b} \tag{3.13}$$

Moreover, the bulk gas emissivity is variable and is calculated as:

$$\varepsilon_g = a_1 + a_2(p_g L_b) + a_3(p_g L_b)^2 + a_4(p_g L_b)^3 \tag{3.14}$$

where p_g is the combined partial pressures of carbon dioxide and water vapor within the cylinder, the a_i coefficients are given by Bahadori et al. [124-126], and L_b is the characteristic length for heat transfer to occur computed by the ratio of cylinder volume to surface area. There

are further steps within the algorithm to calibrate the amount of convective heat transfer in order to satisfy Eqn. (3.7); however, these algorithms will not be covered in this work. Lastly, the term dealing with the energy transfer due to fuel injection mass flow within the energy conservation equation can be solved by:

$$\sum h \frac{dm_{CV}}{d\theta} = \left[h_{fg} + c_f (T_{vap} - T_{inj}) + c_{p,f} (T_f - T_{vap}) \right] \frac{dm_{fa}}{d\theta} \tag{3.15}$$

Here, h_{fg} is the enthalpy of vaporization of the fuel, T_{vap} is the temperature of vaporization of the fuel, T_{inj} is the fuel temperature at injection, T_f is the temperature of the fuel zone, c_f is the specific heat of the liquid fuel, $c_{p,f}$ is the constant pressure specific heat of the fuel, and $\frac{dm_{fa}}{d\theta}$ is the fuel mass added and is modeled by a common expression for fuel flow rate during injection [127, 128]:

$$\frac{dm_{fa}}{d\theta} = C_d A_n n_h n_{inj} (2\rho_f \Delta p)^{1/2} \frac{dt}{d\theta} \tag{3.16}$$

In this equation, C_d is the discharge coefficient, A_n is the area of an individual nozzle hole through which fuel flows, n_h, is the number of injector holes per injector, n_{inj} is the number of fuel injectors, ρ_f is the density of injected fuel, and Δp is the difference in pressure between the injector nozzle and the cylinder. One last primary equation is needed for this model to execute, and that is the ideal gas law evaluated on the molar basis:

$$pV_i = n_i \bar{R}_i T_i \tag{3.17}$$

where n_i is the number of moles within a cylinder zone.

There are additional routines within the algorithm to account for speciation, fuel injection and ignition, rate of combustion, and temperature evaluation. Specifically, chemical processes

are modeled to account for the mass flow between zones before and during combustion. This is done using separate coupled global and local chemical reactions. Eqn. (3.18) shows the global reaction that is used speciate the bulk gas present in the cylinder at IVC from knowing air and fuel mass flowrates:

$$\xi(\mathrm{C_wH_xO_yN_z}) + \delta(\mathrm{g_2O_2 + g_3N_2}) + (\varepsilon_1 + \varepsilon_2)(\mathrm{g_4O_2 + g_5CO_2 + g_6H_2O + g_7N_2}) \rightarrow \lambda(\mathrm{g_4O_2 + g_5CO_2 + g_6H_2O + g_7N_2}) + \zeta(\mathrm{C_wH_xO_yN_z}) \tag{3.18}$$

Here, ξ and δ signify the number of moles of fuel and air, respectively, while ε_1 and ε_2 correspondingly represent moles of internal and external EGR. In addition, λ denotes the number of moles of exhaust species, and moles of unburned HCs is designated by ζ. Moreover, g_2 and g_3 represent the ratios of diatomic oxygen and nitrogen present in the air, respectively, while $g_4 - g_7$ quantify the fraction of each species per mole of emissions produced. Next, Eqn. (3.19) provides the formula for the local reaction equation used that is necessary to describe the flow of species between zones:

$$\mathrm{C_wH_xO_yN_z + l_2O_2 \rightarrow l_3CO_2 + l_4H_2O + l_5N_2} \tag{3.19}$$

where l_2 denotes the number of moles of oxygen needed to consume all moles of fuel (since this is an assumed stoichiometric reaction) and $l_3 - l_5$ represent the subsequent moles of exhaust species needed to balance the reaction. For the fuel injection event, Eqn. (3.16) is used to compute the mass flowrate of fuel into the cylinder and the ensuing ignition delay is modeled by an Arrhenius expression from Hiroyasu et al. [129]:

$$\tau = A\frac{dt}{d\theta}10^{-3}\left(\frac{p}{10^5}\right)^{-n_a} e^{\frac{E_a}{\bar{R}T_f}} \tag{3.20}$$

This equation includes the activation energy of the fuel (E_a), as well as the exponential and pre-exponential values n_a and *A* that can be found in the literature. From here, the start of combustion (SOC) can be calculated utilizing:

$$\int_0^{\theta} \frac{1}{\tau} d\theta \geq 1 \tag{3.21}$$

which states the condition for SOC is such that the current ignition delay value is smaller than the crank-angle distance between current and previous timesteps. Once SOC has been initiated, the rate of combustion of fuel can be used to control all ensuing entrainment processes as described in Eqn. (3.22), another Arrhenius-based expression:

$$\frac{dm_{fb}}{d\theta} \approx \frac{t_{step}}{\Delta\theta} \cdot K \cdot \rho_{CV}^2 \cdot y_f \cdot y_{O_2}^5 \cdot V_{CV} \cdot e^{\frac{-E_a}{\bar{R}T_{CV}}} \tag{3.22}$$

Here, the mass burn rate $\left(\frac{dm_{fb}}{d\theta}\right)$ is approximated using the bulk gas density (ρ_{cv}), the mass fractions of fuel and oxygen y_f and y_{O_2}, respectively, and a calibratable constant (K). Eqn. (3.22) is one of the contributing factors leading to the improved accuracy of this heat release model, as it allows for combustion to respond to changes in the pressure trace, as opposed to other 0-D models that use correlated combustion rates. From here, the rate of oxygen entrainment from the unburned zone can be calculated:

$$\frac{dm_{O_2}}{d\theta} = \frac{dm_{fb}}{d\theta} \cdot \frac{W_{O_2}}{W_{fuel}} \cdot l_2 \tag{3.23}$$

where W_{O_2} and W_{fuel} denote respective molecular weights of oxygen and fuel. The model is then able to compute the total change in mass (or entrainment) of CO_2, H_2O, and, N_2 in each zone by relating the entrainment of fuel and oxygen. Finally, there must be a means for evaluating the temperatures of the different zones after the occurrence of fuel injection. In short, this is done

using the form of the conservation of energy that balances the three different zones during combustion:

$$U_{CV} = U_u + U_f + U_b \tag{3.24}$$

This governing equation, in conjunction with numerous equations in between, eventually permits the arrival at two equations: Eqn. (3.25), used for determining the temperature of a given zone during combustion, and Eqn. (3.26), which calculates the temperature of the unburned zone during the time between fuel injection and combustion.

$$T_{b,n+1} = T_{b,n} - \frac{U_u(k) + U_f(k) + U_b(k) - U_{CV}(k)}{m_b(k) \cdot c_{v,b,n} - m_u(k) \cdot c_{v,u,n} \cdot \dfrac{m_b(k) R_b(k)}{m_u(k) \cdot R_u(k)}} \tag{3.25}$$

$$T_{u,n+1} = T_{u,n} - \frac{U_u(k) + U_f(k) - U_{CV}(k)}{m_u(k) \cdot c_{v,u,n} - m_f(k) \cdot c_{v,b,n} \cdot \dfrac{m_u(k) R_u(k)}{m_f(k) \cdot R_f(k)}} \tag{3.26}$$

These two equations are used to iterate for the temperature of a certain zone, then explicitly solve for the temperature in the remaining zones. They employ the masses of individual zones at given time-step $\left(m_i(k)\right)$, as well as the individual constant volume specific heats $\left(c_{v,i,n}\right)$ for the current iteration, and zone-respective gas constants $\left(R_i(k)\right)$ as a function of time. Following the end of a simulated cycle, the cumulative mass fraction burned (MFB, Y_{mb}) can be computed:

$$Y_{m,b} = 1 - \frac{m_{f,rem}}{m_{f,total}} \tag{3.27}$$

where $m_{f,rem}$ designates the remaining mass of fuel in the cylinder, and $m_{f,total}$ is the total amount of fuel that was injected. The algorithm then calculates the average of the Woschni and Hohenburg convective heat transfer coefficients to be used in Eqn. (3.12); thus, completing the

determination of all terms within the heat release equation. Following this, other useful metrics can be determined, such as gross indicated mean effective pressure ($IMEP_g$), gross brake-specific fuel consumption ($BSFC_g$), thermal efficiency, fuel conversion efficiency, and an updated combustion efficiency.

The final means of data processing used here is the numerical evaluation of combustion noise. Shahlari [130] provided a MATLAB code that has proven to correlate well to measured combustion noise when an in-cylinder pressure trace is given. It was reported that the program yielded a maximum difference of 0.4 dB when results were compared against those from an AVL noise meter. This code has since been used to compare the effects of different fuels, including waste cooking oil (WCO) biodiesel, on combustion noise and knock with the experimental setup used in this work [131].

Overall, the noise emanated from an internal combustion engine is more complex than the noise due to combustion alone. The energy associated with cylinder pressure by itself would produce a sound intensity on the order of 150-200 dB [132]. Fortunately, the presence of mechanical noise (or structure attenuation) acts to lower the effective sound intensity observed by at least 90 dB [133]. Shahlari's algorithm works like a traditional combustion noise meter and starts by filtering a Fourier transformed pressure trace to account for structure attenuation. The structure attenuation filter $\left(SA(dB)\right)$ is applied using Eqn. (3.28), which references an experimental curve fit shown in Figure 3.2.

$$SA(dB) = \begin{cases} \sum_{i=0}^{6} a_i f^i, 100 \leq f \leq 2300 \\ \sum_{i=0}^{6} b_i f^i, 2300 < f < 10000 \end{cases} \tag{3.28}$$

Here, the amount of intensity attenuation is based off the summation of products of six coefficients (a_i or b_i) derived from the curve fit shown in Figure 3.2, and the current frequency (f). A table of the coefficients used in the code can be found in the Appendix.

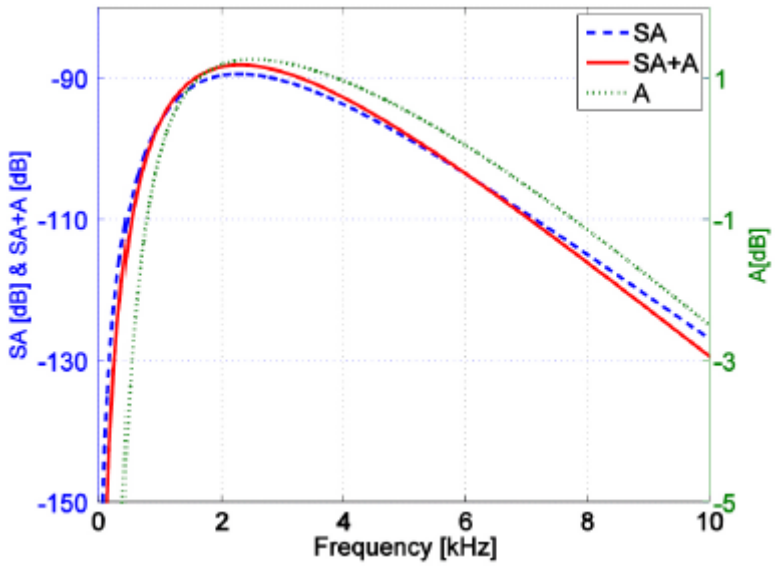

Figure 3.2: Experimental curve-fit to describe attenuation filters [130].

Figure 3.2 represents one of multiple attenuation curve-fits that can be found in the literature. Here, this one happens to originate from the AVL 450 Combustion Noise Meter instruction manual [134]. As with most combustion noise meters, there is an option within the program to add the additional A-weighting filter, which considers sound intensity as perceived by the human auditory system. Eqn. (3.29) is used to compute this A-weighting filer $\left(A(f)\right)$:

$$A(f) = 2 + 20 \cdot \log_{10}(R_A(f)) \tag{3.29}$$

where $R_A(f)$ is the frequency-based function:

$$R_A(f) = \frac{12200^2 \cdot f^4}{(f^2 + 20.6^2)\sqrt{(f^2 + 107.9^2 \cdot (f^2 + 737.9^2))} \cdot (f^2 + 12200^2)} \tag{3.30}$$

From here, the two filters can be combined with Eqn. (3.31) to represent the total transmission filer $(T(f))$:

$$T(f) = 10^{\frac{SA(f)+A(f)}{20}} \tag{3.31}$$

The final noise value given in dB is then computed using:

$$Noise(dB) = 20\log_{10}\left(\frac{P_{RMS}}{20\cdot[\mu Pa]}\right) \tag{3.32}$$

where P_{RMS} has been found by calculating the root mean square (RMS) value of the filtered pressure, and 20[μPa] is a reference pressure of 20 micro-Pascals corresponding the human hearing threshold. Upon the arrival at Eqn. (3.32), this analysis will useful for exploring how combustion noise is affected by the different fuels and pilot injection schemes employed in this effort. Now that the post processing procedures have been explained in detail, the experiments to obtain these data will be described next.

3.2.3. Experimental Procedure

Before multiple injection tests can be carried out, single injection experiments for both ULSD and soybean biodiesel are first conducted to allow for direct comparison between the respective fuels and ambient conditions. To note, 47 MPa of fuel pressure will be used for both the single injection and multiple injection experiments. While it is common for CI engines operating with multiple injections to utilize higher injection pressures (upwards of 100 MPa), this fuel injection pressure will allow consistency to be maintained with respect to previous experiments conducted within the lab. Moreover, it is known that pilot injections do not require the same level of injection pressure as compared to operation with both pilot and post injections. Five experiments for each fuel (properties listed in Table 3.2) will take place based on the load

condition of the engine. Of note, the fuel properties of soybean biodiesel were measured in 2013 when the fuel was produced at the University of Kansas; hence, the fuel was approximately seven years old when the following experiments were conducted. When biodiesel is stored for extended periods of time it becomes susceptible to degradation of many of its properties due to the oxidation of the fuel [135-137]. This oxidation occurs due to the formation of free radicals resulting from hydrogen abstraction from the methylene groups adjacent to the unsaturated methyl esters, which then react with atmospheric oxygen to reduce the caloric value of the fuel [137]. Moreover, because of the role of the unsaturated methyl esters in biodiesel oxidation, fuels with a higher unsaturation content are more susceptible to long-term storage degradation (i.e., soybean biodiesel). In addition to a reduction in energy content, long-term storage has been found to increase viscosity, density, and cetane number [135, 137].

Table 3.2: Fuel properties of the ULSD and soybean biodiesel tested [5].

Metric	ULSD	Soybean Biodiesel
Cetane Number [-]	~40	45 ± 3
Density [kg/m^3]	837.58 ± 0.01	881.25 ± 0.01
Energy [kJ/kg, MJ/m^3]	45636 ± 47, 38224 ± 0.10%	39798 ± 47, 35071 ± 0.12%
Kinematic Viscosity [cSt]	2.58 ± 0.008	4.17 ± 0.013
Flash Point [°C]	55.8 ± 5.3	164.9 ± 15.6
Oxygen Content [%wt]	~0	9.92 ± 0.06
Carbon content [%wt]	86.34 ± 0.20	77.22 ± 0.04
Hydrogen Content [%wt]	14.27 ± 0.10	12.87 ± 0.03

Different loads will be tested (i.e., 0.5, 4.5, 9.0, 13.5, and 18.0 N-m) that provide a good balance of pre-mixed and diffusion burn combustion, all at an engine speed of 1800 rpm. The injection timing for each fuel and load point will be based off previous efforts using this experimental setup where MBT has been achieved [5]. A compilation of these injection timings based on each fuel and load is given in Table 3.3. Here, the peak pressure location for each

single injection experiment will be important to quantify, as they will become a critical component for the subsequent pilot injection tests.

Table 3.3: Fuel injection timing used for single injection tests [5].

Load [N-m]	ULSD [°BTDC]	Soybean Biodiesel [°BTDC]
0.5	12.50	11.30
4.5	12.50	11.70
9.0	11.00	10.50
13.5	10.00	9.25
18.0	11.00	10.25

For each fuel, pilot/main schemes will be employed at each load point of 4.5, 9.0, and 13.5 N-m, signifying respectively low, medium, and high load operation. A range of pilot injection schemes have been selected based off practical and beneficial injection parameters found in the literature, while also being mindful of the number of experiments that can be feasibly conducted. Since a single pilot injection is the focus here, the greatest potential benefits pertain to reductions in BSFC and NO_x emissions. Thus, experimental bounds were chosen with these parameters in mind. The literature largely agrees that pilot injection quantities of 10-20% for low to medium loads are optimal while expecting respectively little response at high load. With regards to pilot injection timing, the main injection event is not intended to advance or delay from the original single injection location any more than necessary to maintain the original peak pressure location; hence, the lower bound for a pilot advance of 15° BTDC still provides a reasonable dwell between the most advanced single injection timing of 12.5° BTDC at 4.5 N-m with ULSD. Furthermore, pilot advance should not increase much past 25° BTDC in order to stay out of the PPCI/LTC regime [138] and maintain traditional CI combustion kinetics. The test matrix for each fuel is described by Table 3.4, which states that for each fuel type and load condition, timing of the pilot injection will be varied from 15°, 20°, and 25° BTDC. Then, the timing of the main injection event is calibrated such that the peak pressure location is equal to

the respective single injection load case mentioned previously. In addition, this sweep of pilot injection timing at each load point will be carried out for two different pilot injection quantities, 10% and 20%.

Table 3.4: Test matrix for load and pilot injection quantity.

Load/Pilot Quantity	10%	10%	10%	20%	20%	20%
4.5 N-m	15°	20°	25°	15°	20°	25°
9.0 N-m	15°	20°	25°	15°	20°	25°
13.5 N-m	15°	20°	25°	15°	20°	25°

Injection quantities are set in the Bosch MS15.1 ECU by specifying the amount of fuel mass for each injection event. Hence, a relative pilot injection fraction cannot be entered in the ECU. Furthermore, the pilot injection mass quantity cannot simply be calculated from the respective single injection fuel mass quantity. This is due to the influence of pilot injection quantity and timing on BSFC. Instead, an iterative approach is necessary to achieve both the desired relative pilot injection quantity and load condition. The procedure is as follows: first, an initial guess for the pilot injection quantity will be entered at the specified pilot injection (SOI_p) timing while utilizing the main injection (SOI_m) from the single injection case as a starting point. Then, the main injection will be varied to meet the desired peak pressure location that was determined during single injection testing (note: main injection fuel quantities are respectively high and will dominate the resultant peak pressure location). Subsequently, the main injection quantity will be varied to get close to the desired load point, and a new pilot injection quantity will then be calculated and entered. Next, this step will be repeated until the desired load is reached and the relative pilot injection quantity is achieved. Lastly, a final check of peak pressure location will be made to make sure it has been maintained. If unsuccessful, the procedure is repeated until all peak pressure, load, and pilot injection quantity conditions are

met. This completes the discussion of experimental methods and equipment used for these tests and the remainder of this chapter will discuss the results and trends observed.

3.3. Single Injection Results and Analysis

3.3.1. Results

Figure 3.3 provides the measured in-cylinder pressure and post-processed heat release results from the single injection ULSD experiments. Cylinder pressure follows the classic trend of a continually delayed peak pressure location resulting from an increase in diffusion-burn combustion as load increases. This is caused by the additional injected fuel mass necessary to meet the required load and a subsequent reduction in ignition delay (see Figure 3.4 and next paragraph), as well as the respectively delayed injection timing. Furthermore, similar peak pressure magnitudes are maintained between loads due to this delay in peak pressure location while the amount of combustion occurring during the expansion stroke grows.

The SOC values generated by the heat release code are used in conjunction with SOI to illustrate ignition delay in Figure 3.4. Of note, these values of ignition delay only account for the total duration between SOI and SOC, rather than the individual components of physical and chemical ignition delay. Here, ignition delay is seen to decrease slightly as load increases, which is caused by the greater amount of turbulence and increased cylinder temperatures that come with a higher load, thus, preparing the mixture for premixed SOC more quickly. Moreover, SOI moves closer to TDC as load increases due to the shortened ignition delay. This is to prevent a shift in the balance of pumping work to expansion work that maintains maximum thermal efficiency. In specific, a small amount of pressure rise before TDC is necessary to produce peak pressure post-TDC where volume is increasing most rapidly. It is also seen that SOI and SOC at

maximum load deviate from the previously described trend. This is attributed to the amount of injected fuel reaching a critical level at the chosen fuel pressure due to insufficient atomization and mixing; hence, injection must be advanced into the compression stroke. A greater fuel pressure could be employed that would allow SOI to continue to move closer to TDC, but modifying the atomization process would add an additional variable that would hinder comparison between operating points.

As for the rate of heat release, there is a general trend of decreasing peak RHR as load increases, caused by the greater fuel quantity that in-turn shifts combustion further into the expansion stroke; hence, leading to increased diffusion-burn combustion. In addition, the decreasing ignition delay acts to reduce the amount of fuel prepared initially that finds its way into the premixed combustion event. However, the 0.5 N-m case presents the lowest level of peak RHR, which could either be due to the small amount of fuel injected at that load and subsequent over-mixing, or the lack of turbulence that hinders preparation of the mixture for premixed combustion.

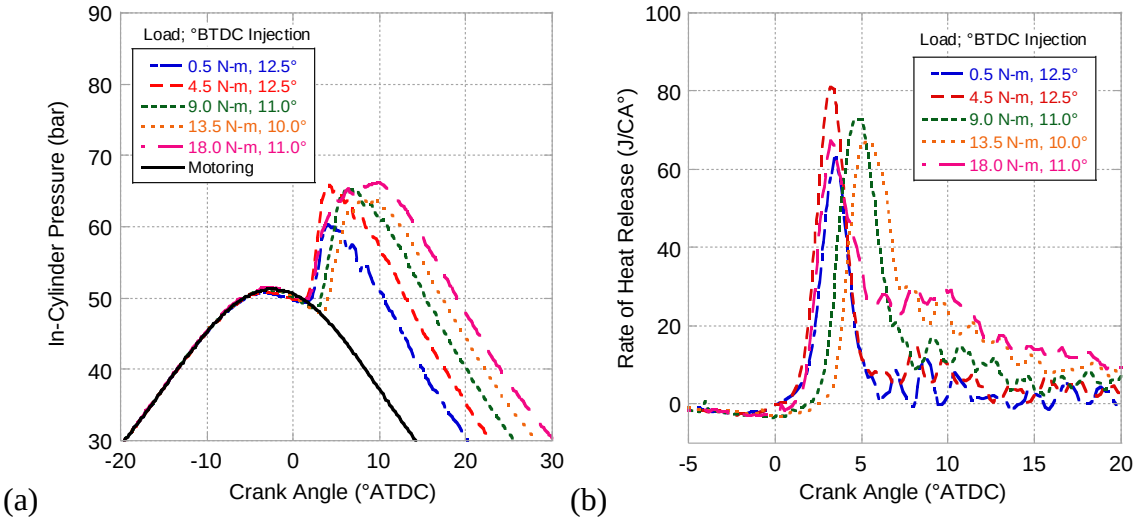

Figure 3.3: In-cylinder pressure (a) and RHR (b) results for ULSD single injection tests.

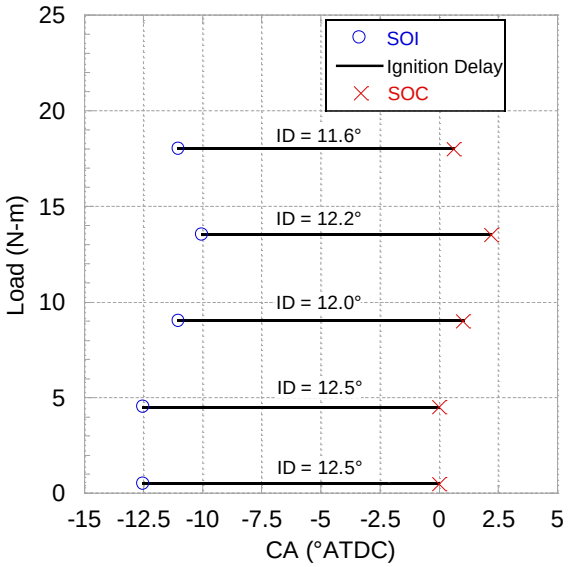

Figure 3.4: ULSD single injection ignition delay.

The previous work done by Mangus, et al. with respect to comparing ULSD to neat biodiesel fuels provides the groundwork for explaining the different behaviors seen here [5, 103]. Overall, they found that combustion advanced with biodiesel use and lower peak pressures were achieved, even when injection timing was adjusted for combustion normalization. These behaviors were attributed to several fuel properties, with the increased cetane number and viscosity of biodiesel being significant contributors. The greater cetane number in conjunction

with the oxygenated quality of biodiesel promotes earlier combustion. In addition, its higher viscosity limits the amount of fuel prepared for premixed combustion due to a hindered atomization process. The resulting reduction of premixed combustion then limits the peak pressure level that can be achieved. Furthermore, this reduction in peak pressure in conjunction with the lower energy content of biodiesel resulted in subsequent increases in BSFC as compared to ULSD. Another notable combustion difference they reported was the effect of biodiesel's greater adiabatic flame temperature. This results in more complete combustion (coupled with the added oxygen content) and subsequent decreases in partial products of combustion. Moreover, the same fuel properties presented by Mangus et al. that contribute to fundamental combustion differences between biodiesel and ULSD are the ones that further differ from ULSD when aging of the biodiesel fuel has occurred. Namely, the increased viscosity, cetane number, and oxygen content, coupled with a decreased energy content of aged fuel. Due to this, it is expected that these effects will be apparent in the heat release results for the proceeding experiments.

The in-cylinder pressure and RHR results for the soybean biodiesel tests are shown in Figure 3.5. Peak pressure phasing follows the same trend as the ULSD experiments, though with lower overall values. In addition, soybean biodiesel universally exhibits a lower amount of premixed combustion and a subsequent increase in diffusion-burn heat release. Ignition delay and SOC highlighted in Figure 3.6 and Figure 3.7, respectively, help to explain this behavior. Here, ignition delay is shortened for soybean biodiesel compared to ULSD and SOI (along with SOC, generally) occurs closer to TDC to maintain the balance of compression and expansion work. This is caused by biodiesel's higher cetane number and oxygenated quality (i.e., more fuel-air zones suitable for ignition) promoting earlier combustion; thus, decreasing the amount of fuel prepared for premixed combustion. Moreover, the increased viscosity of soybean biodiesel

hinders the atomization process which in-turn lowers the amount of fuel available for premixed combustion. This is countered somewhat by the lower volumetric energy of biodiesel that requires an increased amount of fuel injected to maintain load. This additional fuel produces a more pronounced latent heat effect as the fuel is vaporizing and lowers local mixture temperatures. This local mixture temperature reduction in conjunction with the higher flash point of soybean biodiesel can increase the ignition delay and the amount of premixed RHR. Overall, biodiesel's higher cetane number in conjunction with its lower energy content and worse atomization process are the dominant factors in reducing the energy available for premixed combustion while diffusion burn heat release grows to achieve the same load as ULSD. Finally, as expected, the heat release of the soybean biodiesel is respectively overall lower than Mangus, et al. due to the age of the fuel influencing its properties.

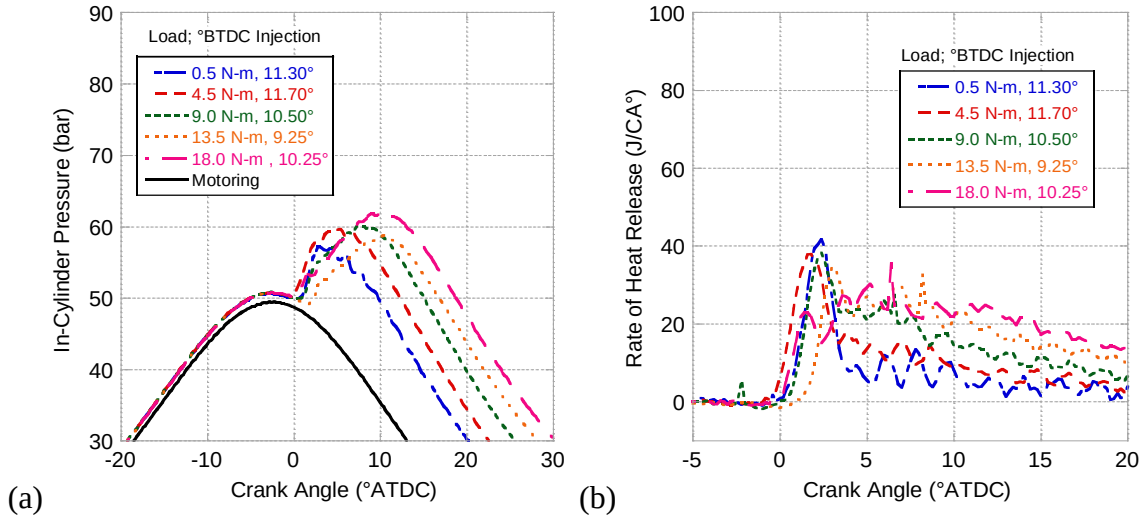

Figure 3.5: In-cylinder pressure (a) and RHR (b) results for soybean biodiesel single injection tests.

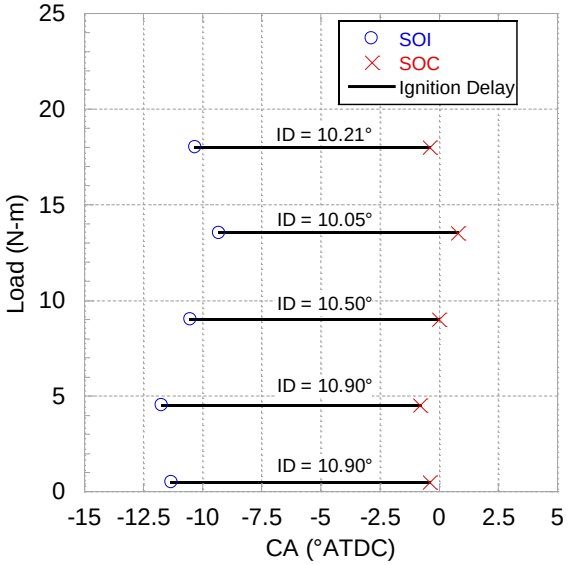

Figure 3.6: Soybean biodiesel single injection ignition delay.

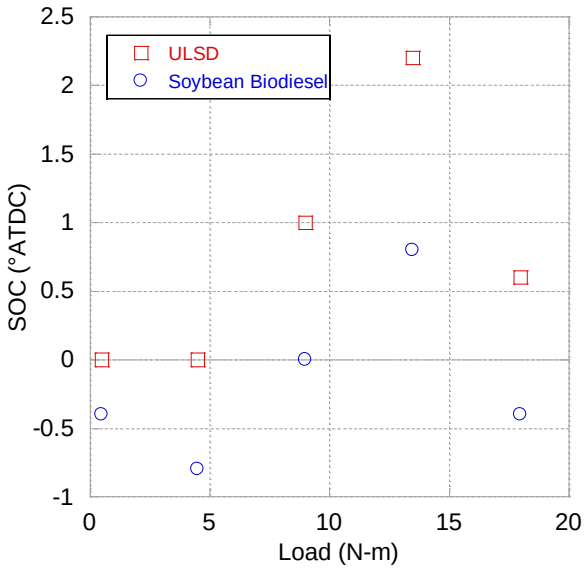

Figure 3.7: ULSD and soybean biodiesel single injection SOC event timing.

The peak pressure locations from the ULSD and soybean biodiesel single injection tests are presented in Table 3.5. The two fuels exhibit the same trend of continually delayed peak pressure location with increasing load; however, because of the greater pre-mixed heat release spike seen from the soybean biodiesel tests at 0.5 N-m, the resulting peak pressure location is closer to TDC. Conversely, the remaining load points for soybean biodiesel exhibit respectively delayed peak pressure timing. This is a function of a diminished constant volume-like combustion event and subsequent increase in diffusion-burn heat release shifting peak pressure further into the expansion stroke. These peak pressure locations will be used to calibrate timing of the main injection event for the subsequent pilot injection experiments. In addition, while these values represent the post processed averages over 60 thermodynamic cycles, the peak pressure locations achieved during testing will inevitably incur slight variances. During the experiments, the only means of verifying peak pressure location is to visually confirm its location, which is given by the real-time LabView pressure trace. Therefore, while the best attempts to maintain combustion normalization were accomplished there will inevitably be a

relatively small difference in peak pressure location between fuels (see Table 3.5). This effect will be more pronounced with the pilot injection experiments due to a greater impact on combustion phasing from two fuel injection events.

Table 3.5: Single injection peak pressure locations based on the average of 60 thermodynamic cycles.

	0.5 N-m	**4.5 N-m**	**9.0 N-m**	**13.5 N-m**	**18.0 N-m**
ULSD (°ATDC)	4.0	4.0	6.8	9.6	9.8
Soybean (°ATDC)	3.0	5.4	7.6	10.4	10.6

Results of the combustion noise analysis for both fuels are seen in Figure 3.8. These results correlate well with peak RHR trends seen, with the soybean biodiesel noise trending down with load as its pre-mixed RHR spike decreases. The ULSD tests follow the same trend except for the 0.5 N-m load point. Here, the noise level is relatively low, like the corresponding RHR peak. Overall, combustion noise produced by soybean biodiesel is lower than ULSD due to its decreased premixed combustion event.

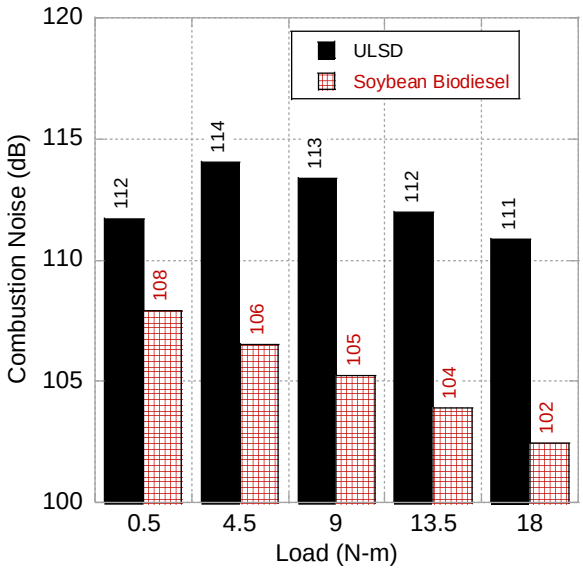

Figure 3.8: Comparison of combustion noise between ULSD and soybean biodiesel.

Recalling the production mechanism of NO_x constituents, NO_x forms at high temperatures in excess of 1,600° Celsius primarily during the premixed combustion process. Therefore, it is common to see high levels of NO_x emissions at low load where combustion is primarily premixed, with NO_x emissions decreasing as load grows and the amount premixed combustion subsequently diminishes as diffusion-burn combustion increases. Conversely, PM formation is largely a result of introducing un-atomized liquid fuel droplets during diffusion-burn combustion; thus, PM levels generally increase as load and the level of diffusion-burn combustion grows. The emissions results for ULSD are shown in Figure 3.9 where the traditional NO_x-PM tradeoff is illustrated. As load increases, fuel quantity grows and premixed-burn combustion decreases along with NO_x even as in-cylinder temperatures rise; whereas, PM subsequently increases as combustion becomes progressively more diffusion-burn dominant. Conversely, CO and THC trend in the same manner, as they are both inversely proportional to the combustion efficiencies reported in Table 3.6. Here, as temperatures rise with load, the level of incomplete combustion falls.

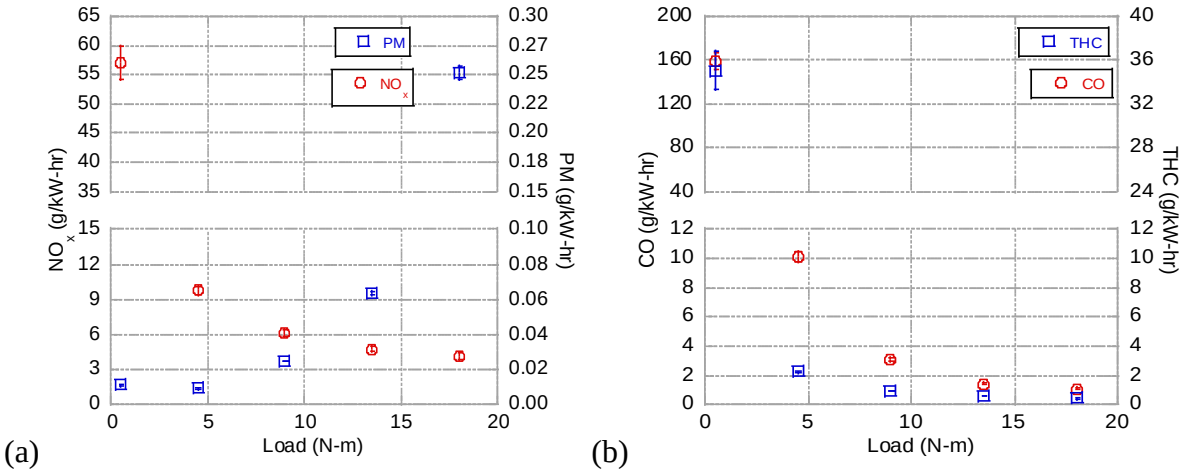

Figure 3.9: NO_x-PM (a)and CO-THC (b) emissions levels for ULSD single injection tests.

Table 3.6: Combustion efficiency vs. load between ULSD and soybean biodiesel.

	0.5 N-m	**4.5 N-m**	**9.0 N-m**	**13.5 N-m**	**18.0 N-m**
ULSD	95.8% ± 4.5	98.3% ± 2.4	99.2% ± 2.8	99.5% ± 3.2	99.5% ± 3.8
Soybean	98.6% ± 6.2	99.3% ± 4.2	99.6% ± 4.3	99.7% ± 4.7	99.6% ± 5.1

Mangus, et al.'s previous work also provides a foundation for comparing engine-out emissions between ULSD and neat biodiesel. They experimented with palm, jatropha, soybean, and beef tallow biodiesels, in addition to ULSD, with the goal of linking various fuel properties to the combustion event. Regarding NO_x emissions, when all fuels employed the MBT injection timing for ULSD, ULSD produced the greatest amount of NO_x at all loads other than 0.5 N-m. This was corroborated by heat release and in-cylinder temperature findings since ULSD exhibited the highest amount of premixed combustion (also seen in this effort) and often the greatest in-cylinder temperatures. When biodiesel injection timing was then delayed to re-phase combustion for MBT, further reductions in NO_x levels were seen for all biodiesel fuels. This was due to a lowering of in-cylinder temperatures and reduced gas residence times at the high temperatures necessary for NO_x production.

Of note, regarding the biodiesel fuels tested, soybean and jatropha exhibited the highest NO_x production. This is attributed to their larger premixed RHR spikes caused by higher unsaturation levels compared to the other biodiesels. Overall, the lower NO_x levels produced by neat biodiesel were attributed to the higher viscosity of biodiesel stemming from its longer molecular chain lengths and increased number of double carbon bonds. This increase in viscosity resulted in a reduction of the peak RHR, and subsequently less premixed combustion. The combustion behaviors seen here between biodiesel and ULSD in the current effort mirror that of Mangus, et al., as the soybean biodiesel exhibited reduced amounts of premixed combustion coupled with increased diffusion-burn combustion. This stemmed from its higher cetane number, higher viscosity, oxygenation, and lower energy content reducing the amount of fuel prepared for premixed combustion. Therefore, it is expected that the same reductions in NO_x emissions will be seen here due to the smaller premixed RHR spikes seen with the soybean biodiesel.

A previous effort by Churkunti, et al. [139] with the same experimental setup used here provides additional insight to NO_x production with biodiesel. They explored the effects of increasing fuel injection pressure for blends of WCO biodiesel ranging from neat ULSD to neat WCO. This was done to offset the viscosity impact on mixture formation as seen by Mangus, et al. While they found similar results pertaining to biodiesel NO_x emissions at the baseline fuel pressure of 50 MPa, raising the fuel injection pressure until similar peak cylinder pressures were seen between biodiesel blends and neat ULSD (at the lower injection pressure) resulted in NO_x emissions eventually rising beyond the baseline ULSD level. These increases were owed to a greater peak RHR that stems from the higher adiabatic flame temperature of biodiesel. Moreover, increasing the injection pressure of biodiesel led to a greater level of early combustion; thereby, allowing additional time for NO_x kinetics to take place. It was also noted

that the respectively high unsaturation level of WCO biodiesel contributed to more prompt NO formation, which also applies here to soybean biodiesel.

The NO_x emissions results for the soybean biodiesel here (Figure 3.10), correlate well with those reported by Mangus, et al., as NO_x levels are universally lower than ULSD and continue to decrease as load grows. This follows with respect to the lesser amount of premixed combustion presented in the heat release results due to the factors explained previously. In addition, these NO_x emissions levels are universally lower than the results obtained by Mangus, et al., with the largest differences at low loads. This makes sense regarding the 9.0 and 18.0 N-m because peak RHR values were also lower for these tests compared to Mangus, et al, which can be explained by the age of the fuel increasing its viscosity and cetane number, in addition to lowering its energy content. However, the 0.5 N-m results conflict between these two efforts because the peak RHR obtained here was larger than that of Mangus, et al., though the NO_x level was almost half. The higher RHR peak can be explained possibly by the increased viscosity of the aged biodiesel preventing over-mixing of the fuel at the respectively low fuel quantity used at 0.5 N-m; however, this does not explain the reduced NO_x level seen here compared to Mangus, et al. This is most likely due to the respectively small fuel quantity in combination with the variability experienced at 0.5 N-m.

With respect to PM emissions, Mangus, et al. showed that biodiesel largely produces more PM throughout the load range, except for the fully loaded condition at 18.0 N-m. Regarding soybean biodiesel PM emissions at the different loads:

- 0.5 N-m: soybean biodiesel (lowest of all biodiesels) < ULSD
- 4.5, 9.0, 13.5 N-m: soybean biodiesel > ULSD

- 18.0 N-m: soybean biodiesel (highest of all biodiesels) < ULSD

The unexpected increases in PM for biodiesel compared to ULSD below 18.0 N-m were explained by the higher energy content of ULSD introducing less carbon for potential PM, as well as the increased viscosity of biodiesel resulting in a greater amount of diffusion burn combustion. At full load, where both fuels exhibit diffusion-burn dominated combustion, the advantage of the oxygenated quality of biodiesel comes into play by leaning out rich fuel cores; hence, resulting in lower PM than ULSD. Furthermore, with increased fuel injection pressure, Churkunti, et al., found that neat WCO biodiesel produced slightly more PM than ULSD at 4.5 N, but significantly less at 9.0, 13.5, and 18.0 N-m; hence, helping to offset the impact of viscosity.

The PM results in Figure 3.10 correlate mostly with the results from Mangus, et al.:

- 0.5 N-m: soybean biodiesel << ULSD
- 4.5, 9.0 N-m: soybean biodiesel > ULSD
- 13.5, 18.0 N-m: soybean biodiesel < ULSD

The respectively large increase in PM for soybean biodiesel compared to ULSD at 0.5 N-m makes sense due to the corresponding decrease in NO_x described earlier. Furthermore, PM does not follow the same NO_x-PM tradeoff that ULSD does, nor that of the soybean biodiesel tested by Mangus, et al. at low to medium loads. However, the respectively large increases in PM at low to medium load compared to ULSD are accompanied by relatively similar decreases in NO_x. While soybean biodiesel presented increased PM emissions at low to medium load compared to Mangus, et al., reduced PM was seen at 13.5 and 18.0 N-m. Here, the increased

viscosity and cetane number of aged biodiesel can lead to a growth in diffusion burn and PM emissions; whereas, its increased oxygen level after ageing can result in lower PM emissions.

For emissions of partial products of combustion, namely CO and THC, Mangus, et al. showed that all fuels produce continually lower CO and HC levels with increasing load due to a hotter combustion event resulting in higher combustion efficiencies. However, because ULSD is a non-oxygenated fuel with a respectively lower combustion efficiency (e.g., Table 3.6), it produced more CO and THC under all loads. Soybean biodiesel specifically produced CO and THC levels less than or equal to ULSD at all loads. The lower levels of CO and THC emitted by the biodiesel fuels compared to ULSD was intriguing based on PM emission findings. In general, the increased viscosity of biodiesel fuels caused by more double carbon bonds should generate an increase in partial products of combustion during the diffusion-burn phase. Moreover, the higher density of the biodiesel fuels presents more opportunity for CO and HC production. However, biodiesel's longer combustion duration, higher adiabatic flame temperature, and oxygenated nature yielded more complete combustion overall.

The CO and THC results in Figure 3.10 present the same trends of being universally lower than ULSD and decreasing with load, as well as inversely correlating with combustion efficiency. However, the soybean biodiesel CO values obtained here are largely ~50% less than those given by Mangus, et al., and THC reductions are even greater. Given that the soybean biodiesel used here still attains combustion efficiencies in excess of 98% at every load point, the adiabatic flame temperature does not appear to be hindered, and the reductions in CO and THC can be linked to the increased oxygen content of the aged biodiesel.

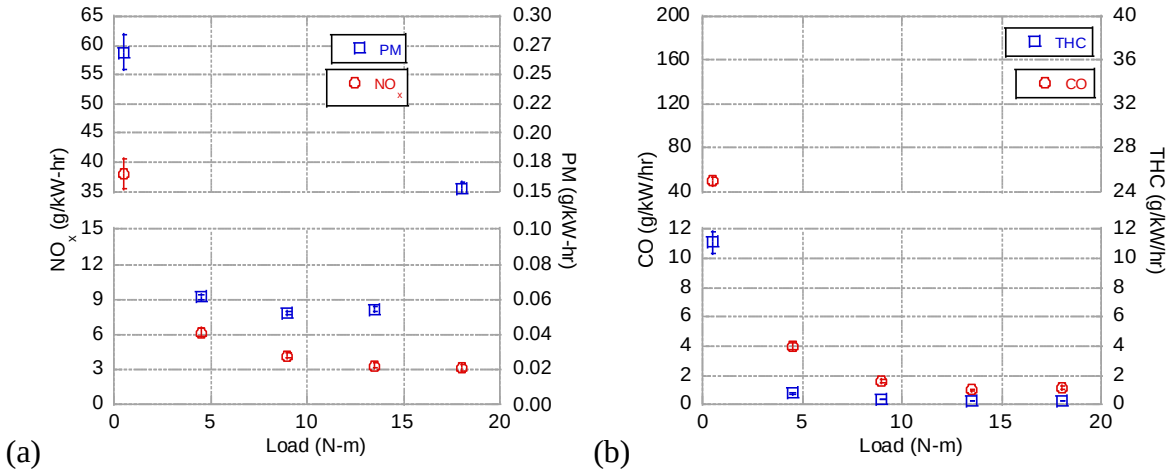

Figure 3.10: NO_x, PM (a), CO, and THC (b) emissions levels for soybean biodiesel single injection tests.

Lastly, BSFC (presented by Table 3.1) is an important baseline metric to analyze with respect to the pilot injection experiments to follow. The BSFC values of biodiesel are higher than ULSD due to its decreased energy content and lower amount of premixed combustion. Moreover, the soybean biodiesel BSFC values here are universally higher than those reported by Mangus, et al. This follows with respect to the reduced premixed RHR peaks seen and subsequently lower NO_x levels, as well with the fact that the age of the soybean biodiesel used here most likely incurred an increase in viscosity and decrease in energy content. Finally, these trends will be influenced by the introduction of a pilot injection event and the subsequent effect it will have on the atomization and vaporization process, similar to what was found by Churkunti et al. by increasing the injection pressure.

Table 3.7: BSFC results from ULSD and soybean biodiesel single injection tests.

	0.5 N-m	**4.5 N-m**	**9.0 N-m**	**13.5 N-m**	**18.0 N-m**
ULSD (g/kW-hr)	2555.3 ± 147.2	406.6 ± 3.0	283.0 ± 1.1	248.1 ± 0.7	235.1 ± 0.6
Soybean (g/kW-hr)	2981.6 ± 225.7	470.7 ± 6.1	339.7± 3.3	300.1 ± 2.9	288.7 ± 0.8

3.4. Pilot Injection Results and Analysis

Before delving into pilot injection results, a standard notation for referencing the different pilot injection schemes must be adopted to limit unnecessary description of each pilot injection test. Similar to what is seen in the literature, injection scheduling will be referenced using "*xx°/yy%*" notation, which denotes "*xx*" as the pilot injection timing in °BTDC, and "*yy*" as the relative pilot injection quantity compared to the entire amount of injected fuel for that cycle. In addition, if only pilot injection timing is being referenced, it will be indicated in the format of "-*xx* SOI_p", where "*xx*" represents pilot injection timing in °ATDC.

3.4.1. ULSD Results

While peak pressure was maintained (Table 3.8) within 1° of the desired location for the 4.5 N-m and 9.0 N-m load points, deviations of up to 2.4° exist for the 13.5 N-m tests. This occurred because of a discrepancy between the perceived peak pressure location and the post processed average peak pressure location. Subsequently, the target peak pressure location for the ensuing pilot injection tests was slightly more advanced (~8.2° ATDC) than the true post-processed single injection peak pressure location (9.6° ATDC). However, this change in desired peak pressure location for the 13.5 N-m pilot injection test does not appear to have hindered the realization of the trends relating to BSFC (discussed later). The cylinder pressure results from the ULSD pilot injection experiments are presented in Figure 3.11. The advancement of combustion is seen as the pilot injection timing is advanced and pilot fuel quantity is increased, thus, resulting in necessary main injection timing delay to maintain a consistent peak pressure location (values given by Table 3.9).

Table 3.8: Peak pressure location and magnitude of ULSD pilot injection tests (°ATDC/bar)

Load	Pilot Quantity: 10% Timing: 15° BTDC	20% 15°	10% 20°	20% 20°	10% 25°	20% 25°	Single
4.5 N-m	3.8°/65.90	4.6°/64.83	4.0°/62.82	4.8°/62.22	4.2°/62.35	4.6°/61.78	4.2°/65.83
9.0 N-m	6.8°/61.56	7.4°/62.03	6.2°/62.87	6.4°/62.28	6.6°/63.08	6.4°/63.98	6.8°/65.16
13.5 N-m	9.0°/65.50	7.2°/61.76	8.0°/65.24	8.8°/64.83	7.8°/65.14	8.8°/63.34	9.6°/64.04

Table 3.9: Main injection timing from ULSD pilot injection tests (°BTDC, relative change from single injection test).

Load	Pilot Quantity: 10% Timing: 15° BTDC	20% 15°	10% 20°	20% 20°	10% 25°	20% 25°
4.5 N-m	12.5° (-0.0)	12.0° (-0.5)	11.0° (-1.5)	10.0° (-2.5)	11.0° (-1.5)	10.0° (-2.5)
9.0 N-m	10.0° (-1.0)	9.0° (-2.0)	10.5° (-0.5)	9.0° (-2.0)	10.5° (-0.5)	9.5° (-1.5)
13.5 N-m	10.5° (+0.5)	7.5° (-2.5)	10.5° (+0.5)	8.5° (-1.5)	10.5° (+0.5)	8.0° (-2.0)

Pilot injection quantity had a larger effect than pilot timing on the required change in main injection timing. In addition, load played a part, as the 13.5 N-m load condition required a 0.5° advance in main injection timing at every 10% quantity pilot injection, as opposed to a main injection timing delay. Most notably, as load increases, the influence of the pilot injection on the pressure trace becomes more pronounced due to a larger amount of fuel being used. While all three loads experience a growth in cylinder pressure early in the expansion stroke (i.e., just after TDC), thus increasing the area under the work-producing portion of the pressure curve, all injection schemes other than the -15° pilot injections at 4.5 N-m see a growing cylinder pressure before TDC which inherently increases compression work.

While intuition would suspect that this greater compression work penalty would adversely affect BSFC, Figure 3.12 finds that BSFC was reduced for every single pilot injection experiment except for the 4.5 N-m 15°/20% experiment. Even the 25°/20% test at 13.5 N-m that

produced the greatest amount of pre-TDC pressure showed a slight decrease in BSFC as compared to the baseline 13.5 N-m value. Moreover, every experiment besides 20°/20% and 25°/10% at 13.5 N-m yielded reductions in peak pressure magnitude, which makes sense because less fuel is available for the main premixed combustion event. In addition, the cylinder is hotter when the main injection event occurs that minimizes its injection ignition delay. Therefore, less fuel is added in the main pulse that also has a smaller ignition delay; hence, one should expect a lower pre-mixed spike. However, the 20°/20% and 25°/10% experiments at 13.5 N-m that exhibited increases in peak pressure magnitude most likely did so because the amount of early combustion was significant enough to facilitate a greater starting pressure for the main combustion event. For the 25°/20% at 13.5 N-m test, it is possible that a significant amount of heat transfer occurred earlier that acted to lower the pressure. The fact that almost every pilot injection experiment yielded reductions in BSFC, even with lesser peak pressure magnitudes, illustrates how the benefit of an additional pressure rise immediately following TDC outweighs the drawbacks of increased pumping work and a reduced peak pressure magnitude.

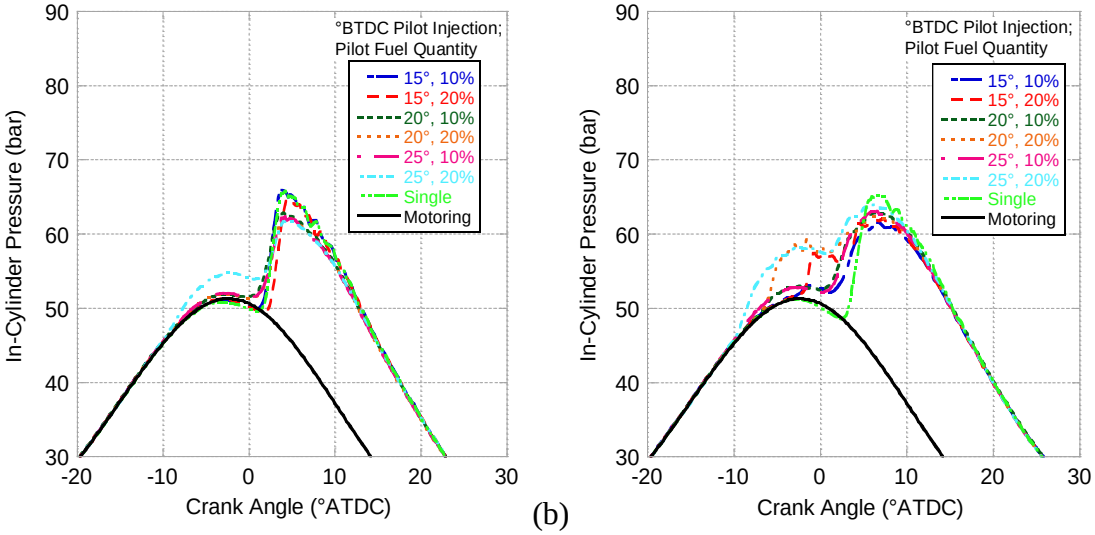

(a) (b)

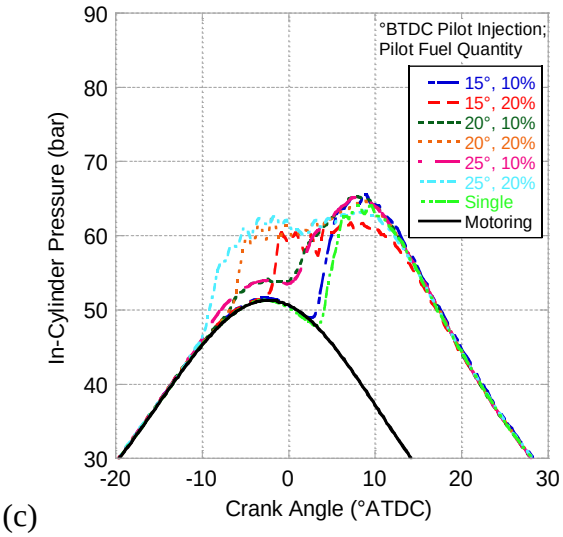

(c)

Figure 3.11: Cylinder pressure results for ULSD pilot injection tests at 4.5 N-m (a), 9.0 N-m (b), and 13.5 N-m (c).

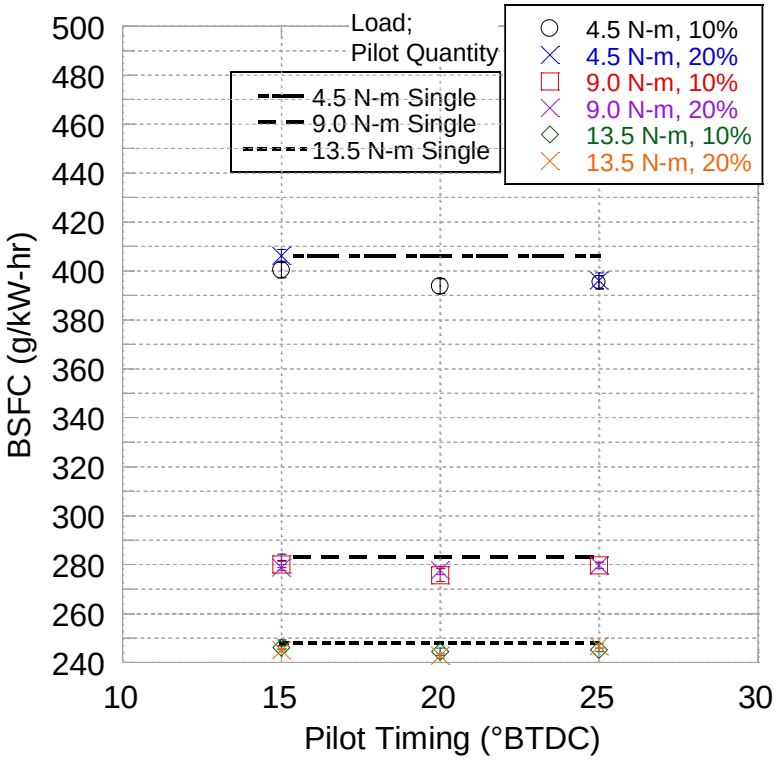

Figure 3.12: BSFC results from ULSD pilot injection tests.

Regarding BSFC, these tests indicate a 20° BTDC pilot injection timing "sweet spot" where the greatest improvements are seen unanimously throughout the load range. To note, a

mistake was made during the 4.5 N-m 20°/20% experiment that did not allow for complete post-processing; hence, this point is not plotted in Figure 3.12. However, during steady state data logging at this operating point, an "eye-balled" average BSFC value of ~400 g/kW-hr was written down from the real-time display on the data acquisition GUI, which follows in relation to the other tests. Furthermore, at a pilot injection timing of 20° BTDC, reductions in BSFC as large as 3.1%, 2.6%, and 2.2% were seen at loads of 4.5 N-m, 9.0 N-m, and 13.5 N-m, respectively. These reductions in BSFC are a result of relying less on peak pressure magnitude to create expansion work, and instead using the pilot injection to raise cylinder pressures at the beginning of expansion that creates more area under the work producing portion of the pressure trace. Conversely, there does not appear to be a clear trend in which pilot quantity is the most beneficial in reference to pilot timing or load.

Figure 3.13 provides the heat release results from the ULSD pilot injection tests, further demonstrating the effect that load has on pilot injection influence. The 4.5 N-m load point shows little response to the SOI_p of -15° in terms of peak RHR; whereas, the 15°/20% experiment shows a slightly delayed combustion and subsequently later peak RHR location. This might explain why this experimental point was the only one to not exhibit a decrease in BSFC. Conversely, the -20° and -25° SOI_p cases at 4.5 N-m all show reductions in peak RHR compared to the single injection baseline value. Here, the 25°/20% test is the only one to show noticeable heat release before the beginning of main combustion. The 9.0 N-m experiments all show a significantly reduced peak RHR compared to the single injection case. Moreover, while the pilot injection heat release spikes are similarly phased for both pilot quantities at a given SOI_p, it is apparent that the larger pilot quantity creates a greater pilot injection heat release spike and a further reduced peak RHR follows for the main combustion event.

Finally, the 13.5 N-m load points exhibit a similar trend to the 9.0 N-m test, where the 20% pilot quantities produce the largest pilot heat release spikes that continually lowers the peak RHR value for the main combustion phase. Here, the 15°/10% experiment is the only one to not yield a reduced peak RHR value. This test produced an identical, but slightly advanced, heat release profile in comparison to the single injection case. The same behavior was exhibited by the cylinder pressure results, indicating that the pilot injection was not sufficient to generate a significant level of early pilot combustion (possibly because of respectively high turbulence and over-mixing). As a result, there was no reduction in peak RHR; however, the increased mixing and residence time of the overall mixture brought on by the pilot injection resulted in a combustion advance of the main pulse. Here, all three 20% pilot quantity experiments produced pilot RHR spikes greater in magnitude than the subsequent main combustion peak RHR, although the pilot spikes are still lower than the baseline case. For 13.5 N-m, a 20% pilot fuel quantity provides enough fuel energy to sustain a combustion process. Hence, this results in an increase in cylinder temperature and associated turbulence prior to the main combustion pulse; thereby, making the main combustion process more akin to a diffusion burn phase. Overall, the reduction in the main combustion peak RHR with added pilot injection is a function of the pilot RHR magnitude that shifts the balance of heat release between pilot and main combustion events.

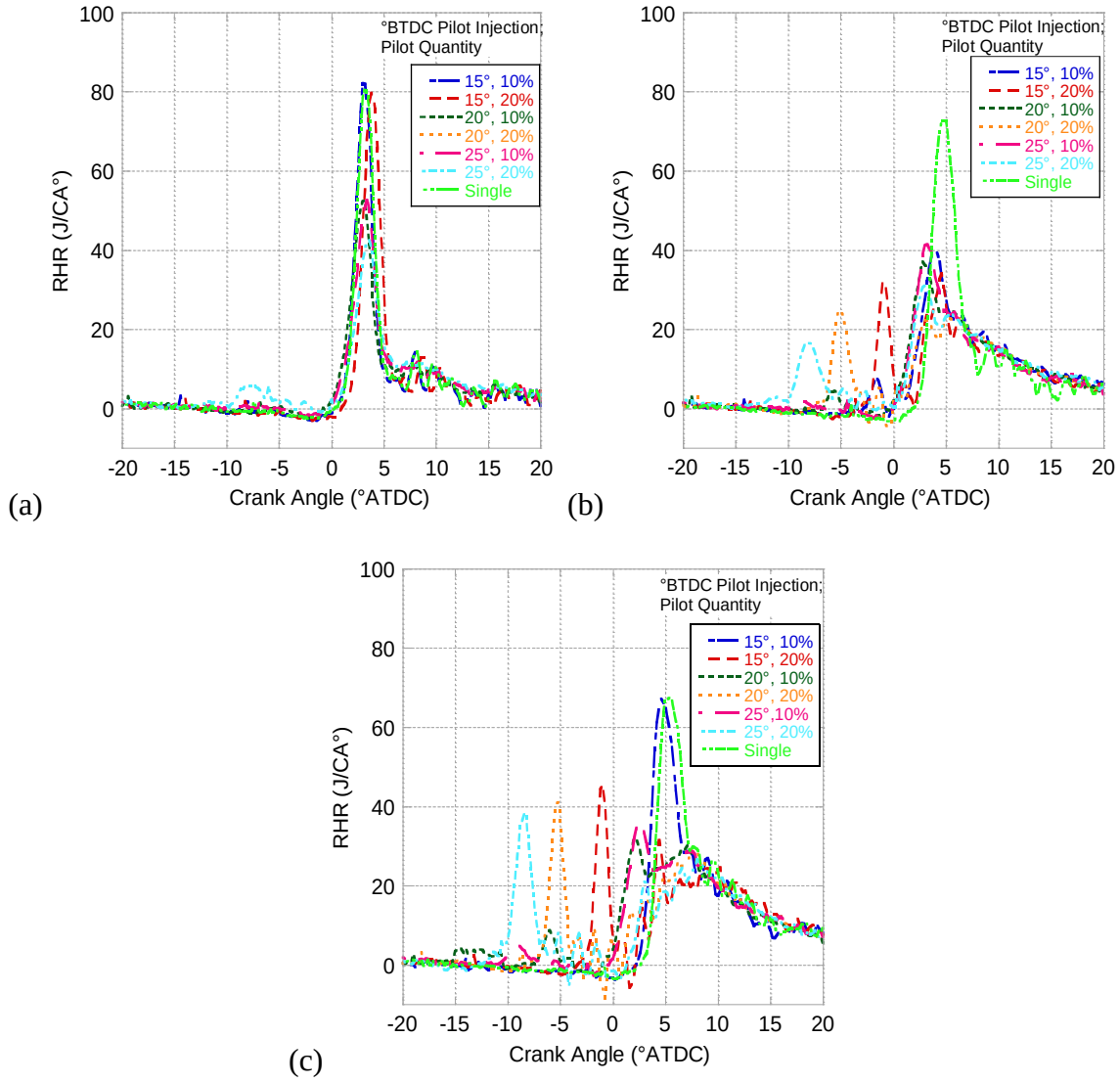

Figure 3.13: Heat release results for ULSD pilot injection tests at 4.5 N-m (a), 9.0 N-m (b), and 13.5 N-m (c).

Bulk gas in-cylinder temperature is also computed from the heat release code and is displayed in Figure 3.14 for the ULSD pilot injection experiments. These results largely mirror the cylinder pressure trace; however, the differences in temperature magnitude provide further insight into the formation of emissions. Moreover, the concept of pilot injection use is clearly illustrated here, as peak cylinder temperatures are generally lowered when there is a pilot combustion present, which can lead to reductions in NO_x emissions (shown later). Cylinder temperature will also help explain the trends in combustion efficiency and subsequent CO and

THC emissions levels. Furthermore, while peak temperature is largely reduced with the addition of a pilot injection, this is often coupled with a growth in cylinder temperature during the main injection ignition delay period. This promotes vaporization and chemical cooking of the main injection fuel pulse, which can subsequently reduce the main injection ignition delay. In addition, the average bulk gas temperatures from the ULSD experiments are included in Table 3.10 to provide further insight to the NO_x discussion to come.

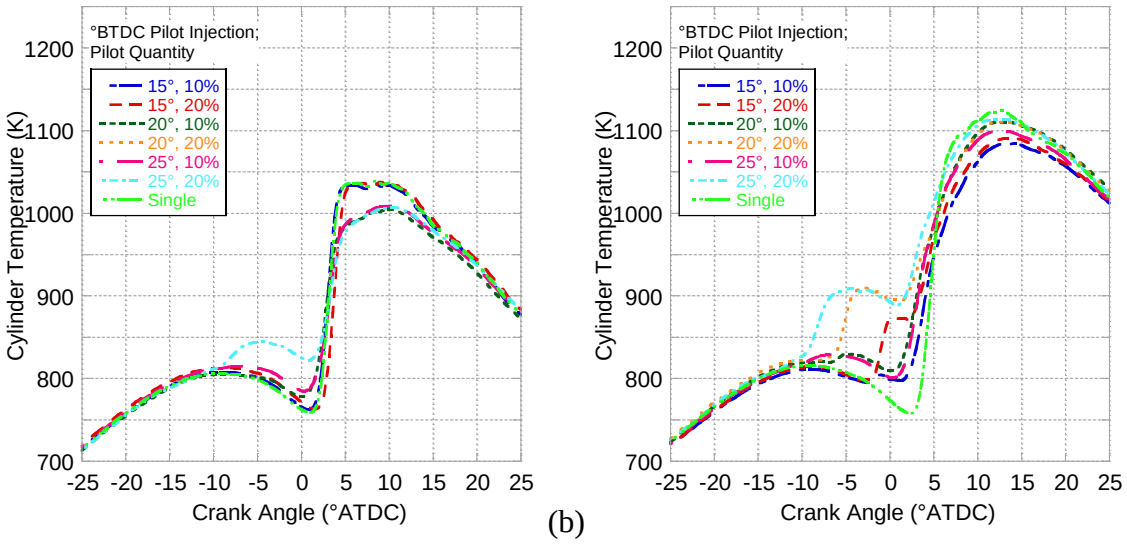

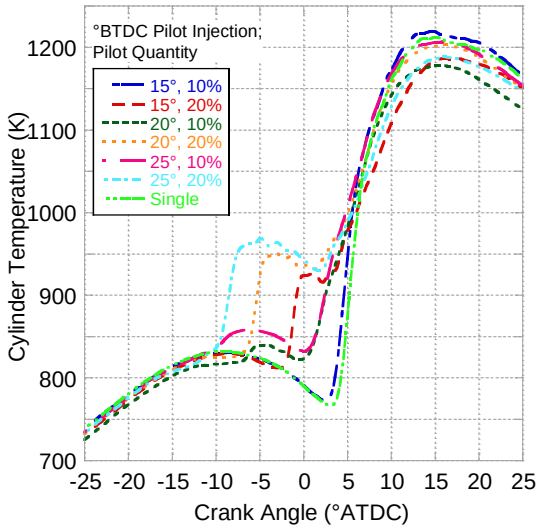

(c)

Figure 3.14: Bulk gas in-cylinder temperature for ULSD tests at 4.5 N-m (a), 9.0 N-m (b), and 13.5 N-m (c).

Table 3.10: Average bulk gas temperature (K) from -15° to 25° ATDC.

Load	Pilot Quantity: 10% Timing: 15° BTDC	20% 15°	10% 20°	20% 20°	10% 25°	20% 25°	Single
4.5 N-m	897	897	887	-	892	901	896
9.0 N-m	931	944	955	971	948	981	942
13.5 N-m	995	996	989	1024	1012	1027	986

The heat release model was also used to evaluate the SOC for both the pilot injection combustion (if present) and main injection combustion events. The method for deriving SOC and subsequent ignition delay differs for the pilot injection tests as compared to the single injection tests. While the heat release code can account for multiple injections, it is not set up to report more than one SOC event. In addition, pilot injection sometimes causes a small false RHR spike to be present shortly after the pilot injection event that can subsequently report a false SOC.

An example of this is shown in Figure 3.15 that has RHR and the second derivative of pressure plotted vs. CA for the 13.5 N-m 20°/20% test. The second derivative of pressure of the

motoring trace is also plotted for reference. An RHR spike is present at -15°, but with no associated spike in the second derivative of pressure. Analyzing the second derivative of pressure establishes SOC at -9.8°, which also makes sense due to the corresponding local minimum in RHR at the base of the RHR spike. When evaluating the second derivative of pressure, the criteria for the SOC is defined as when the value crosses from negative to positive along a spike signifying combustion [140]. While the second derivative of pressure technically hits zero multiple times at -15° and before, this is typical, as indicated by the motoring trace that exhibits similar behavior. Here, the true SOC will be preceded by a negative dip in the second derivative of pressure before crossing over to positive. Figure 3.16 presents the RHR vs. second derivative of pressure for the 4.5 N-m 15°/10% case. This case is noteworthy because it demonstrates how the second derivative of pressure will follow the same dip in the motoring curve until combustion starts with no pilot combustion present. Moreover, this illustrates how the SOC determined by the heat release code from RHR and SOC determined by the second derivative of pressure agree.

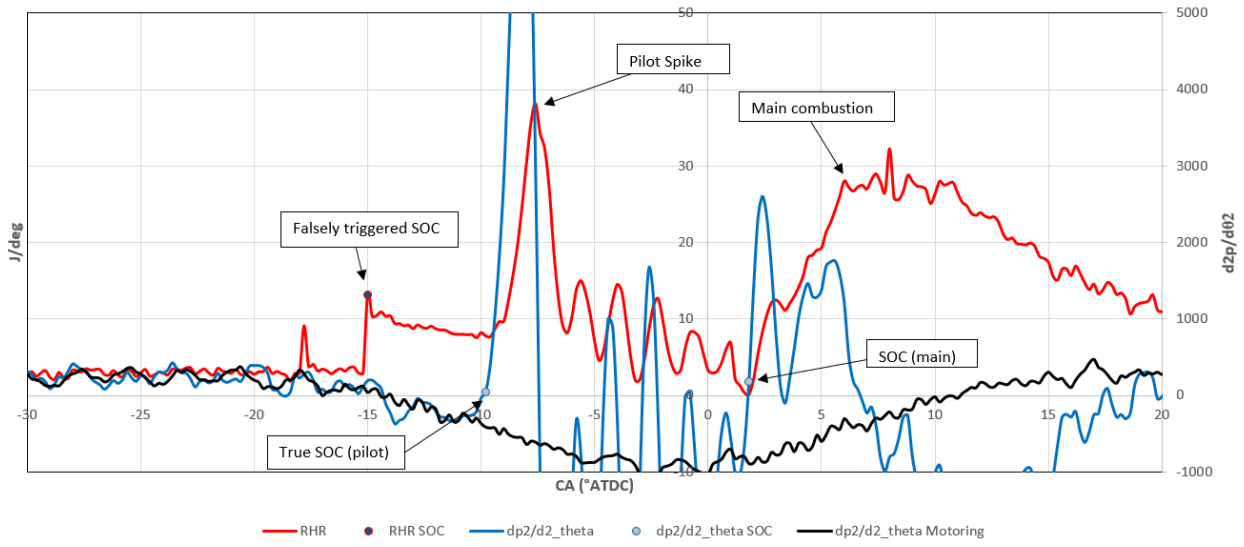

Figure 3.15: Demonstration of evaluating the second derivative of pressure to account for false SOC triggered by the RHR.

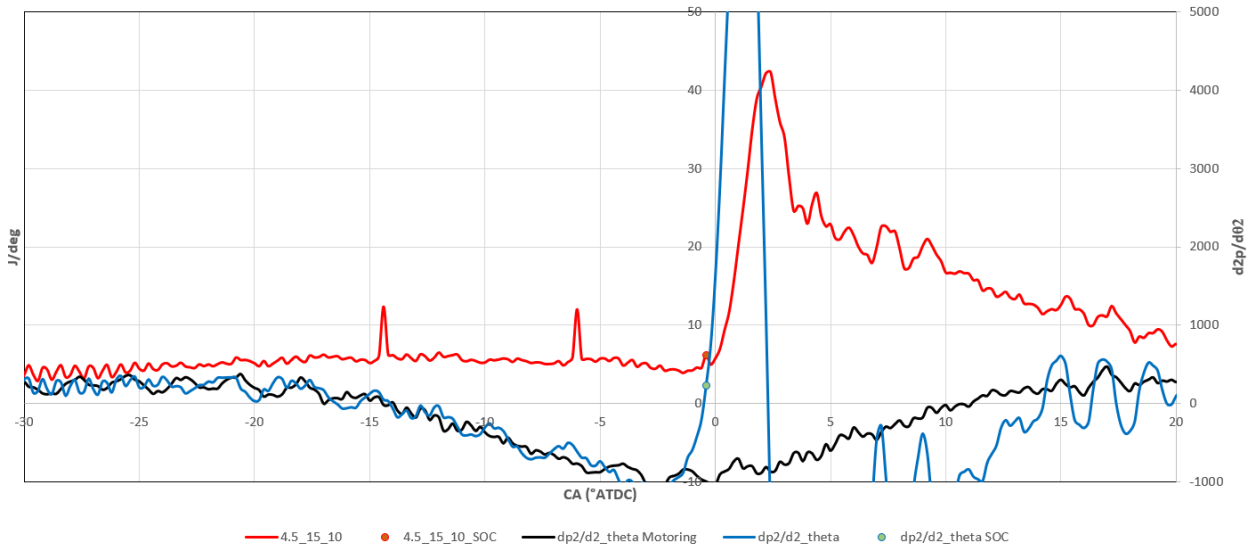

Figure 3.16: RHR vs. second derivative of pressure with no pilot combustion.

While Figure 3.15 illustrates the onset of the main combustion event following pilot combustion, this value of SOC is less straightforward to determine. Due to the oscillations in RHR and the second derivative of pressure, if the previous criteria was used to determine the main SOC, there would be multiple SOC events around -5° and -2.5°. Here, the main SOC was ascertained to occur at 1.8° using logic pertaining to both RHR and the second derivative of

pressure. Specifically, 1.8° is the point of negative to positive second derivative of pressure crossing, and more importantly, is associated with the largest second derivative of pressure spike following the pilot combustion spike. With respect to RHR, 1.8° also corresponds with the point closest to the local minimum RHR at the base of main combustion, further validating the main SOC placement determined here.

During the 20°/10% and 25°/10% tests at 4.5 N-m there is no appreciable heat release or second derivative pressure swing indicative of pilot combustion. However, there is a growth in cylinder temperature preceding the main injection SOC that deviates from the single injection case similar to the 20°/20% and 25°/20% experiments (seen in next paragraph) which experience noticeable pilot combustion. Since the bulk gas temperature is still significantly higher than the ignition temperature for ULSD (~530 K [141]), it is reasonable to assume there is some level of combustion occurring; albeit, respectively mild as a result of a globally lean and homogeneous mixture. Furthermore, the 20°/10% and 25°/10% tests exhibit reduced peak temperatures that are almost identical in magnitude to the 20°/20% and 25°/20% experiments. These temperature deviations indicate the cylinder was hotter preceding main combustion, which then resulted in lower peak temperatures stemming from reduced main injection ignition delay. This mild form of combustion appears to occur from either an inadequate amount of fuel injected necessary for a premixed pilot combustion event, or over-mixing of this respectively small pilot fuel quantity causing an assumed homogeneous mixture to weakly combust and raise the global temperature within the cylinder without a noticeable heat release (evident within a zero-dimensional heat release code).

The process of SOC determination was done for every pilot injection test to confidently obtain SOC timing for assessment of pilot and main injection ignition delays. The first of these

results are given in Figure 3.17 and Figure 3.18 for the ULSD pilot injection tests at 4.5 N-m. These results include the 20°/20% experiment at 4.5 N-m that is missing some post-processed data including heat release that is used for SOC determination. However, the routine within the heat release code that computes the second derivative of pressure was able to execute without the missing measurement data. The same method of SOC determination using the second derivative of pressure was used in conjunction with the raw pressure trace to determine SOC for this test. As seen in Figure 3.13 (a), there is only noticeable pilot combustion present during the 25°/20% test. Here, the 25°/20% and assumed 20°/20% experiments had the greatest amount of fuel and longest amount of time to vaporize, atomize, and mix to generate a pilot combustion event. Overall, the main injection ignition delay is seen to mostly decrease as both pilot quantity and timing increase. This is caused by the presence of pilot combustion further warming the cylinder before main combustion as seen in Figure 3.14 (a), necessitating a greater delay in main injection timing to maintain the desired peak pressure location. Here, the 15°/10% test was able to maintain the same main injection timing as the single injection case of 12.5° BTDC because the pilot injection had little influence on overall combustion, which is corroborated by almost identical peak RHR and BSFC values.

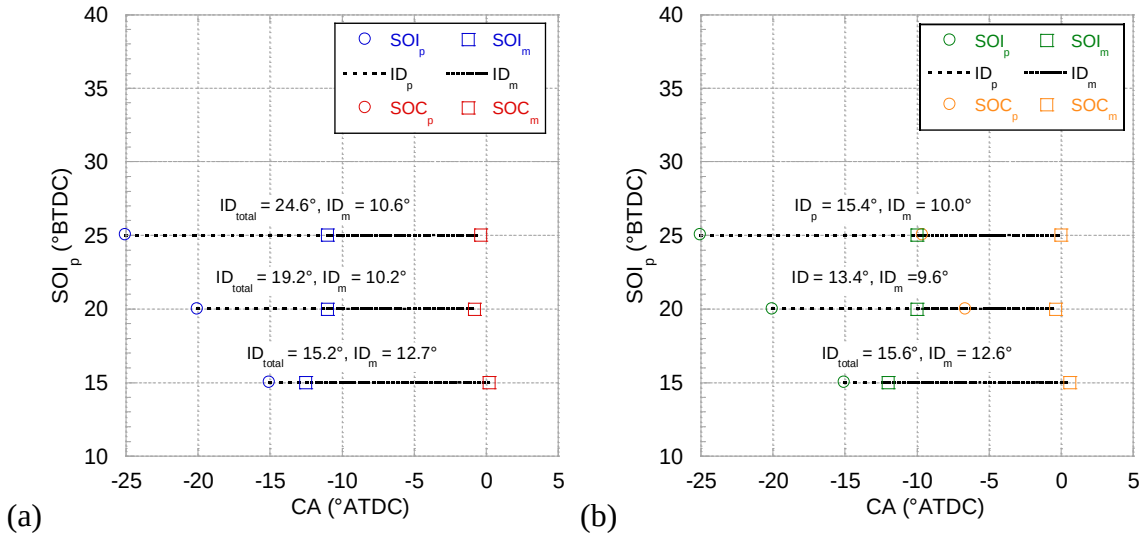

Figure 3.17: 4.5 N-m pilot injection ignition delay results for 10% (a) and 20% pilot quantities (b).

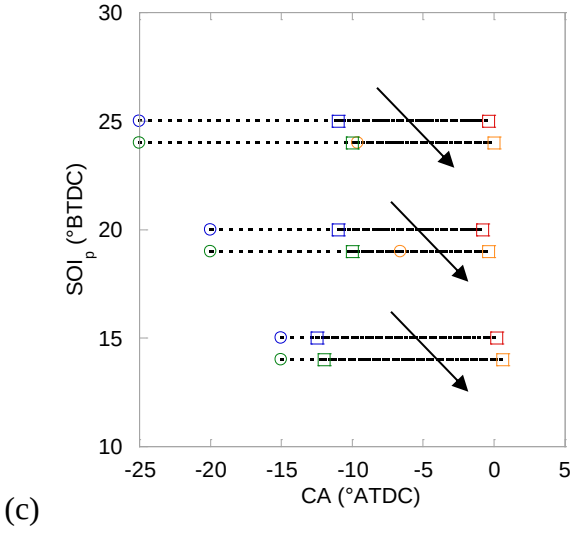

Figure 3.18: Comparison of 10% pilot and 20% pilot quantity ignition delay at 4.5 N-m.

The influence of pilot injection is greater for the 9.0 N-m experiments, as shown in Figure 3.19 and Figure 3.20. All tests experience noticeable pilot combustion, which advances into the compression stroke as both the pilot injection is advanced, and the pilot quantity grows. All tests exhibit a reduced main injection ignition delay compared to the 9.0 N-m single injection case. Here, the cylinder temperature rise during the main injection ignition delay period seen in Figure 3.14 (b) is more pronounced than the 4.5 N-m tests, as more fuel is being used for pilot

combustion in combination with the increased turbulence and mixing that comes with greater load. Furthermore, the pilot combustion ignition delay lengthens as a function of a greater pilot injection timing advance. Since the cylinder temperature preceding main combustion without the presence of pilot combustion reaches its peak at about 10° BTDC, fuel injected before this point starts its vaporization process at a lower temperature, thus, requiring more time for mixture preparation. The -25° SOI_p experiments had the greatest pilot injection ignition delay and smallest corresponding pilot RHR spikes of the 9.0 N-m tests. It is possible there is a pilot advancement limit based on a given speed, load, and quantity to avoid over-mixing of the air-fuel mixture (i.e., over-leaning). This also can explain the small gap between SOC_p and SOI_m for the 25°/20% test where the additional main injection fuel added to the mixture helps prevent the pilot injection from over-leaning. Given that pilot combustion for the 25°/10% experiment exhibited a milder combustion event, rather than premixed, this highlights that the 10% quantity case might be more susceptible to over-leaning, obviously because of the lesser amount of fuel available for pilot combustion.

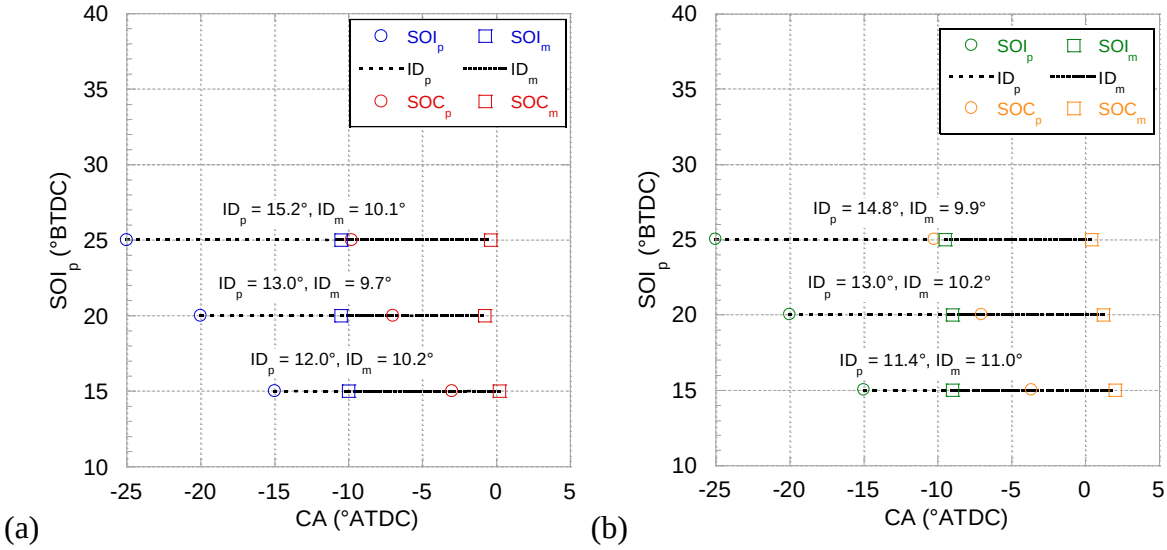

Figure 3.19: 9.0 N-m pilot injection ignition delay results for 10% (a) and 20% pilot quantities (b).

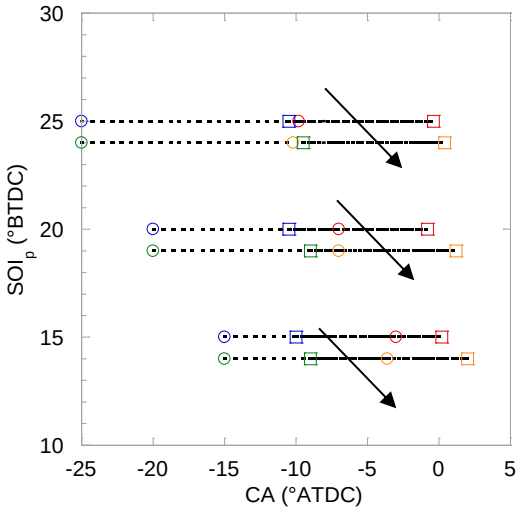

Figure 3.20: Comparison of 10% and 20% pilot quantity ignition delay at 9.0 N-m.

Overall pilot ignition delay continues to decrease for the 13.5 N-m experiments shown in Figure 3.21 and Figure 3.22, with the same trend of increasing delay as a function of pilot advance. Here, there is a noticeable temperature increase preceding main combustion for all 13.5 N-m tests (including the single injection case) compared the 9.0 N-m tests. This is due to an increase in fuel quantity injected that additionally explains a reduction in pilot ignition delay. However, the 15°/10% test does not experience pilot combustion, seemingly due to the opposite

reason the 25°/10% test at 9.0 N-m only had a weak pilot combustion event. Instead of over-leaning, due to the proximity of the main injection event, the pilot mixture was not able to mix quick enough to initiate a separate and noticeable combustion event. At this load, SOI_m is advanced for the 15°/10% experiment compared to the single injection test (-10.5° as opposed to -9.0°). With the respectively large amount of fuel used at 13.5 N-m, the main injection event caused this insufficiently mixed, globally rich mixture inadequate for a separate pilot combustion. Furthermore, due to the delayed main injection event, the pilot mixture can achieve autoignition for the 13.5 N-m 15°/20% experiment. It is also notable that the gap between SOC_p and SOI_m has continually grown with load for the 25°/20% case as a result of a decrease in pilot injection ignition delay and an additional delay in main injection timing that comes with a load increase.

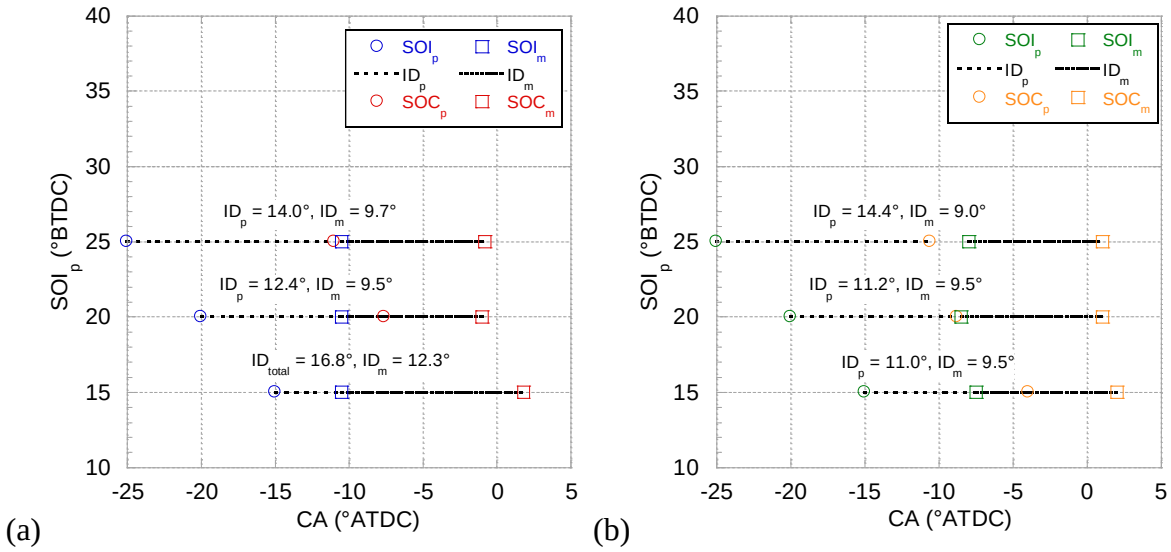

Figure 3.21: 13.5 N-m pilot injection ignition delay results for 10% (a) and 20% pilot quantities (b).

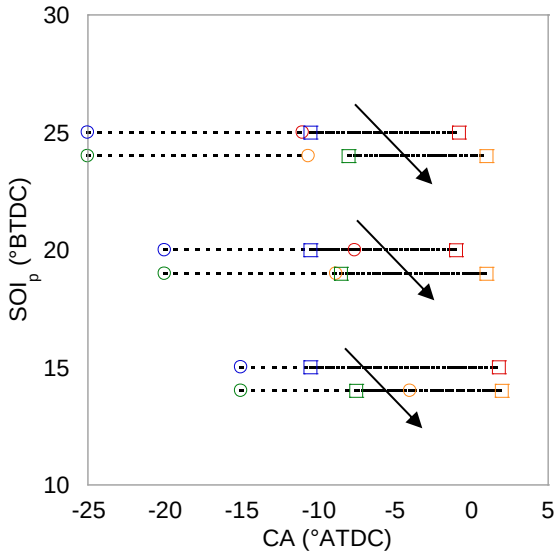

Figure 3.22: Comparison of 10% and 20% pilot quantity ignition delay at 13.5 N-m.

Similar to the single injection cases, combustion noise resulting from the pilot injection tests (Figure 3.23) correlates respectively well with peak RHR values. Due to the significant amount of premixed combustion present at 4.5 and 9.0 N-m, all significant reductions of the main combustion premixed RHR pike result in substantial combustion noise reduction. Furthermore, while the combustion noise from each pilot injection test at 9.0 N-m is largely the

same, it is evident that the small variations in combustion noise correlate with the respective peak pressure magnitude ranking. At 13.5 N-m, it appears there is a trend present between the 20% pilot quantity tests at 13.5 N-m. As pilot injection timing advances, the pilot combustion heat release spike both advances and slightly reduces in magnitude along with a small decrease in combustion noise. This points to the possibility that both pilot peak RHR and relative phasing to the main combustion event plays a role with the latter more likely the primary influencer. This makes sense when looking at the overall results at 13.5 N-m, as the 20°/10% and 25°/10% experiments attain combustion noise reductions as great as the 4.5 and 9.0 N-m tests because they still produce reduced main combustion RHR levels without significant pilot RHR spikes, unlike the 20% experiments at 13.5 N-m that did not achieve the same reductions in combustion noise due significant pilot combustion events. Overall, whether peak RHR occurs during the pilot heat release spike or in the main combustion heat release, the peak RHR value largely dictates the level of combustion noise, and reductions of up to 6, 7, and 7 dB are seen at 4.5 N-m, 9.0 N-m, and 13.5 N-m, respectively.

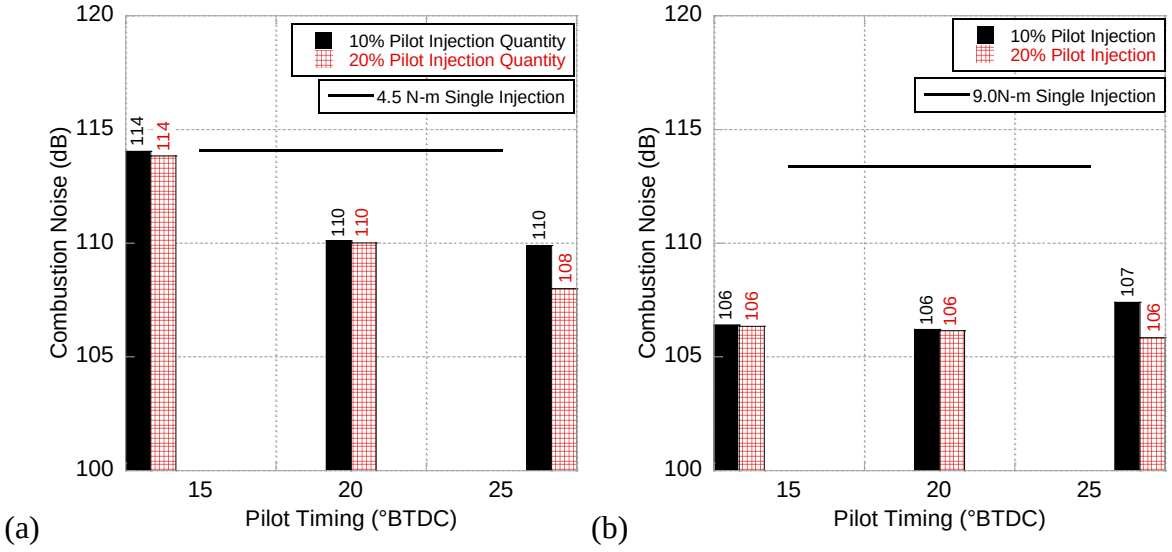

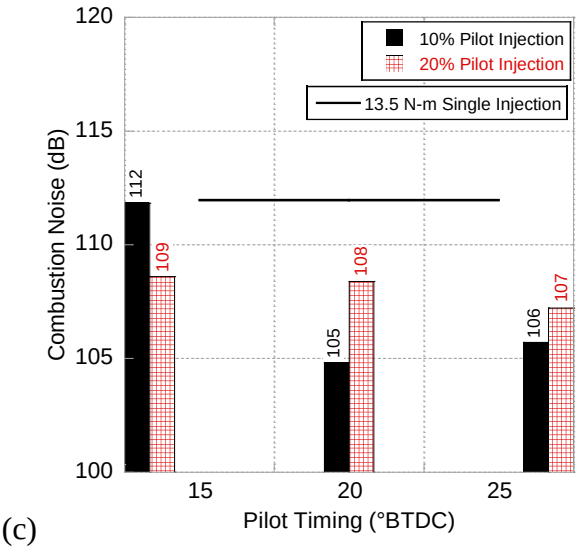

(c)

Figure 3.23: Combustion noise results for ULSD pilot injection tests at 4.5 N-m (a), 9.0 N-m (b), and 13.5 N-m (c).

Emissions results from the ULSD pilot injection tests are given by Figure 3.24 and Figure 3.25. At 4.5 N-m, the reduction in peak RHR for each test correlates well with the corresponding decrease in peak cylinder temperature and NO_x. Furthermore, while the 25°/20% experiment exhibited the lowest peak heat release and NO_x emission level, its peak bulk gas temperature and overall temperature profile during main combustion are largely the same as the 20°/10% and 25°/10% experiments. In addition, there is a significant temperature rise during pilot combustion of the 25°/20% experiment. This points to a possible NO_x emissions reduction potential due to a lessened heterogeneity since this test had the greatest amount of time to mix a significant pilot fuel amount. This decrease in heterogeneity can lead to less NO_x producing hot spots (which are not apparent in the bulk gas temperature results). Referring back to the average bulk gas temperatures in Table 3.10, the results are largely the same for each experiment at 4.5 N-m. However, in the presence of a pilot injection, there is a general trend of a greater temperature rise preceding main combustion that results in lower overall temperatures during expansion while keeping the average bulk gas temperature fairly constant. In addition, the 25°/20% exhibited the

highest average bulk gas temperature, furthering the point that the decrease in heterogeneity is a significant contributor to the NO_x emissions reduction seen here.

At 9.0 N-m, while all pilot tests exhibit reductions in both peak RHR, peak cylinder temperature, and NO_x, the benefits in NO_x reduction are respectively uniform between the different pilot injection events. This is the case even though their heat release and temperature results vary significantly. In general, NOx production is dependent on the level of combustion heterogeneity (i.e., hot spots lead to NOx emissions), the timing of the combustion event (i.e., the earlier the combustion process, the greater amount of time for thermal NOx kinetics, but more heat transfer losses to lower the temperature), and in-cylinder temperatures. The earlier the pilot injection event, the greater the homogeneity, but the more time for NOx kinetics and the potential of an overall larger average cylinder temperature. Furthermore, a greater amount of pilot fuel augments these outcomes (homogeneity↑ time ↔ average cylinder temperature ↑). Therefore, in deference to the 4.5 N-m experiment, while NOx emissions still did decrease overall, the competing effects of increased homogeneity, more kinetics time, and higher average cylinder temperatures appeared to balance out each other between the different pilot experiments. The average bulk gas temperature results at 9.0 N-m largely reflect this, as all but one pilot injection test produced a higher average temperature than the single injection experiment, but due to the increase in homogeneity there is a universal reduction in NO_x emissions.

Interestingly, the pilot injection experiments at 13.5 N-m did not significantly affect NO_x emissions. Like the 9.0 N-m discussion, there was a balance between heterogeneity, kinetics time, and bulk gas temperatures that precluded the pilot injection experiments from differing

significantly. Moreover, the overall greater fuel quantity brings about higher cylinder temperatures for a longer duration; hence, NO_x emissions remained respectively uniform.

In addition to the NO_x reductions seen at 4.5 and 9.0 N-m, the NO_x-PM tradeoff was demonstrated, as any decrease in NO_x emissions from the baseline value brought an increase in PM levels of similar relative magnitude. This is caused by the decrease in temperature associated with NO_x reduction that in-turn increases PM levels by reducing combustion efficiencies. Moreover, the RHR results indicate that when the respective pre-mixed spike decreases and the level of diffusion burn grows, so does PM as to be expected. This is readily apparent for the 4.5 N-m experiments, as both 15° pilot injection tests had RHR profiles nearly equivalent to the single injection test while finding identical PM levels. Whereas, the remaining 4.5 N-m experiments exhibited significant reductions in premixed combustion and a subsequent growth in PM. Furthermore, all 9.0 N-m tests exhibited noticeable reductions in premixed combustion with a corresponding growth in PM. Therefore, even if the level of heterogeneity decreases, this is a respectively small effect on the production of PM as it primarily forms during the diffusion burn phase. In other words, while the extents of the fuel/air mixture might be more homogeneous and have a reduced number of hot spots, the inner fuel injection core remains relatively intact (the principal source of PM [24]) and now there is a greater amount of diffusion burn for the main injection pulse. Finally, for 13.5 N-m, PM grows as there is a significant increase in the level of diffusion burn and no trade-off between NO_x and PM is seen.

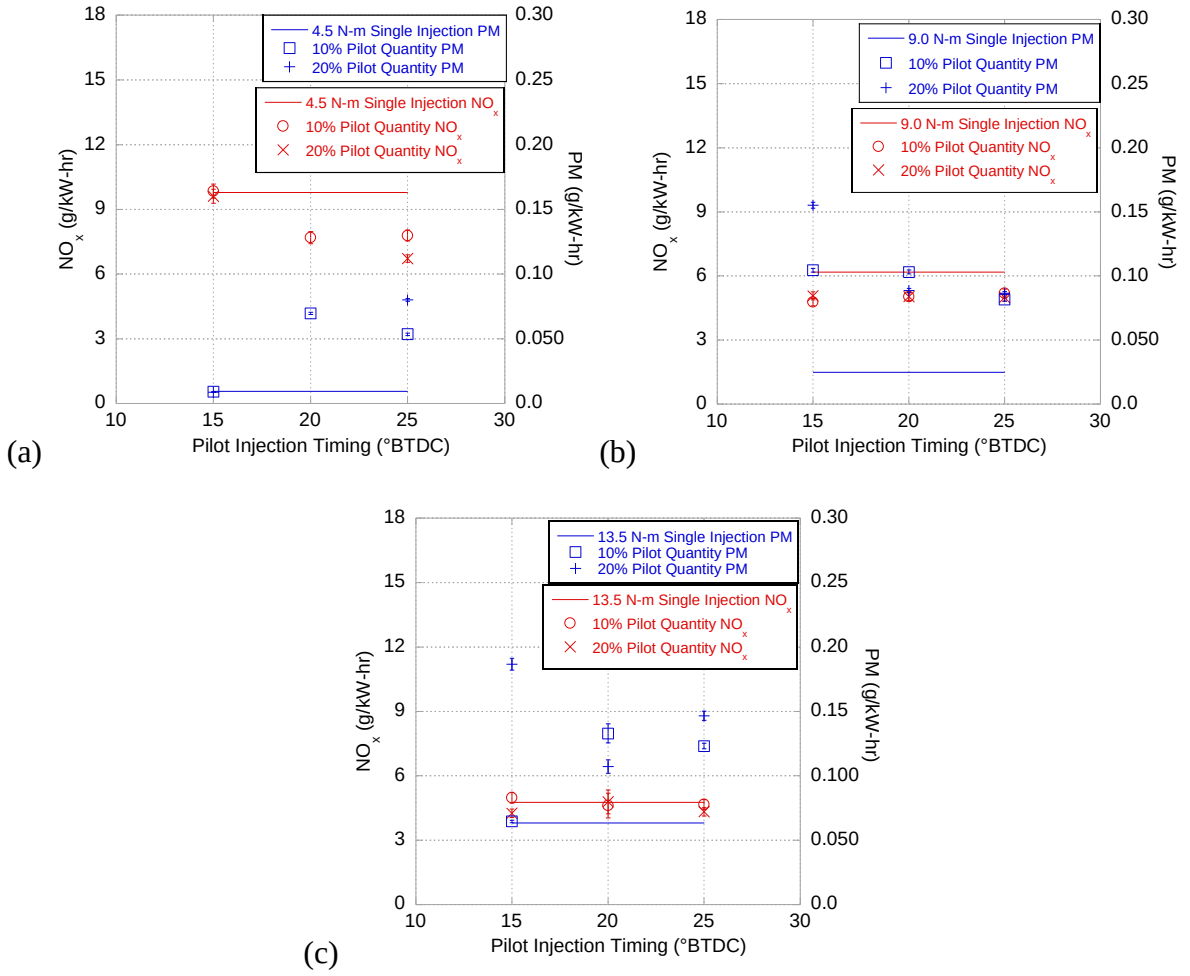

Figure 3.24: NO_x and PM emissions for ULSD pilot injection tests at 4.5 N-m (a), 9.0 N-m (b), and 13.5 N-m (c).

CO and THC emissions correlate relatively well with the previously discussed BSFC results, as the 20° SOI_p sweet spot is seen again, which makes sense because BSFC, CO, and THC are all linked to combustion efficiency (Table 3.10). The 20° SOI_p ideal timing provides the best compromise between lowering the cylinder temperature (adversely impacting combustion efficiency) and enhancing the time for mixture preparation before ignition (i.e., more homogeneity and not a significant amount of over-leaning). Moreover, for a given pilot injection timing and load, the 10% quantity pilot injection largely produces less CO and THC emissions than the corresponding 20% pilot injection experiment. This agrees well with the findings of

Okude et al. who concluded that smaller pilot injections are effective in reducing partial products of combustion since they have a decreased injection penetration that is less susceptible to piston and cylinder wall impingement [30]. Furthermore, the effect of load is apparent regarding CO and THC, as the largest reductions were attained at 4.5 N-m where the least amount of turbulence is present, and the greatest potential gains can occur from better spray characteristics. Also of note, the 25°/20% experiment at each load was the only point to yield significant increases in THC, presumably due to the respectively low cylinder temperatures at the time of the -25° SOI_p and subsequent cylinder wall or piston impingement potential. Finally, the results at 4.5 N-m are of interest as the simultaneous reductions in CO and THC are coupled with a respectively low peak cylinder temperature but with a slightly increased combustion efficiency. Here, a mild pilot combustion event coupled with a more homogeneous mixture yielded fewer hot spots and lower temperatures while resulting in an overall greater level of oxidation.

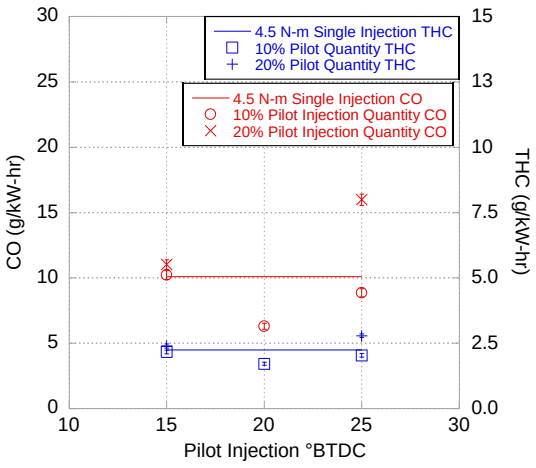

(a)

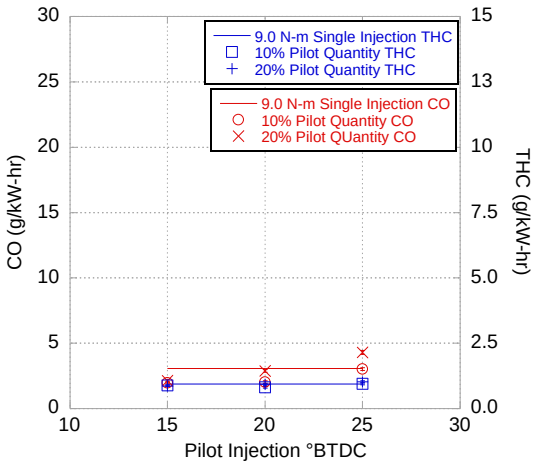

(b)

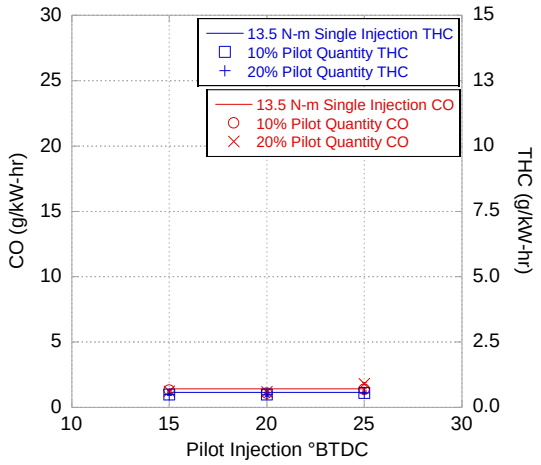

(c)

Figure 3.25: CO and THC emissions results for ULSD pilot injection tests at 4.5 N-m (a), 9.0 N-m (b), and 13.5 N-m (c).

Table 3.11: Combustion efficiency results from ULSD pilot injection tests.

Load	Pilot Quantity: 10% Timing: 15° BTDC	20% 15°	10% 20°	20% 20°	10% 25°	20% 25°	Single
4.5 N-m	98.3% ± 2.2	98.2% ± 2.2	98.8% ± 2.4	-	98.5% ± 2.3	97.5% ± 1.8	98.3% ± 2.4
9.0 N-m	99.3% ± 2.4	99.3% ± 2.5	99.3% ± 2.9	99.2% ± 2.5	99.2% ± 2.4	98.9% ± 2.4	99.2% ± 2.8
13.5 N-m	99.5% ± 3.4	99.5% ± 3.2	99.6% ± 8.5	99.5% ± 7.9	99.5% ± 3.3	99.4% ± 3.2	99.5% ± 3.2

3.4.2. Soybean Biodiesel Results

The peak pressure locations of all the soybean biodiesel pilot injection results are tabulated in Table 3.12, showing that peak pressure location was well maintained for all tests and the biggest deviation was 0.4° from the single injection location. However, the 25°/20% test at 13.5 N-m is 0.8° off due to the pilot knock causing instabilities at this point. Also, 9.6° ATDC is the peak pressure location of main combustion during this test, though the pilot event produced a combustion peak located at 3° BTDC that was greater in magnitude than the main combustion peak. Table 3.12 provides the main injection timing that was needed for each pilot injection test

to maintain the same single injection peak pressure location at each load. All tests required a main injection timing delay from the baseline, and in general, the 20% quantity tests required the same or greater main injection timing delay than the 10% quantity test at the same pilot injection timing.

Table 3.12: Peak pressure location and magnitude of soybean biodiesel pilot injection tests (°ATDC/bar).

Load	Pilot Quantity: 10% Timing: 15° BTDC	20% 15°	10% 20°	20% 20°	10% 25°	20% 25°	Single
4.5 N-m	5.6°/57.31	5.4°/58.42	5.2°/58.12	5.2°/58.39	5.6°/57.78	5.6°/56.80	5.4°/59.67
9.0 N-m	7.6°/58.76	7.8°/58.97	7.6°/58.80	7.2°/60.13	7.4°/59.26	7.4°/59.61	7.6°/60.28
13.5 N-m	10.2°/58.68	10.6°/57.71	10.8°/56.98	10.4°/58.23	10.4°/56.64	9.6°/58.19	10.4°/58.79

Table 3.13: Main injection timing from soybean biodiesel tests (°BTDC, relative change from single injection test).

Load/Pilot Quantity/Pilot Timing (°BTDC)	10% 15°	20% 15°	10% 20°	20% 20°	10% 25°	20% 25°
4.5 N-m	11.00°(-0.70)	11.50°(-0.20)	11.00°(-0.70)	10.50°(-1.20)	11.0°(-0.70)	10.0°(-1.70)
9.0 N-m	10.25°(-0.25)	10.25°(-0.25)	10.00°(-0.50)	9.50°(-1.00)	10.25°(-0.25)	9.50°(-1.00)
13.5 N-m	8.25°(-1.00)	7.00°(-2.25)	8.25°(-1.00)	7.40°(-1.85)	8.50°(-0.75)	7.60°(-1.65)

There are several fuel property differences between soybean biodiesel and ULSD that will influence the pilot combustion event. The greater viscosity and density of soybean biodiesel will decrease the amount of fuel that is adequately prepared for pilot combustion since biodiesel will generate a more compact fuel spray and greater heterogenous mixture. Conversely, these factors could also limit overmixing and over-leaning of the fuel spray. Moreover, the greater

cetane number of soybean biodiesel will promote pilot combustion and reduce the ignition delay; again, growing the level of heterogeneity. Overall, the expected greater amount of heterogeneity (even with more fuel oxygen available) and reduced fraction of fuel prepared for pilot combustion will yield a less significant pilot combustion event. This coupled with a less energetic fuel will show a significantly reduced premixed heat release with a greater extent of diffusion burn combustion. However, the larger cetane number of the soybean biodiesel in combination with a lessened overmixing potential could produce pilot combustion at the extents of the fuel spray not previously present during the ULSD experiments.

The in-cylinder pressure traces from the soybean biodiesel pilot injection tests are given in Figure 3.26. Although the pilot injection influence on combustion advance and pre-TDC peak pressure grows with load, the pilot combustion pressure rise is largely dampened compared to the ULSD tests. Fewer pilot schemes for the soybean biodiesel exhibited a significant pilot combustion pressure rise greater than the motoring curve near TDC with only the 13.5 N-m experiments showing more pilot combustion events than ULSD (albeit at a lower level). The greater CN of soybean biodiesel had a significant effect on the timing, as it caused pilot combustion to advance while requiring a main injection timing delay to maintain peak pressure location. While it was originally thought that soybean biodiesel might prevent overmixing in certain cases, this was not generally the case except for the 20°/20% experiment at 4.5 N-m. Here, it does appear that the greater heterogeneity of the biodiesel fuel spray is preventing a significant pre-mixed heat release that would grow the pressure more dramatically.

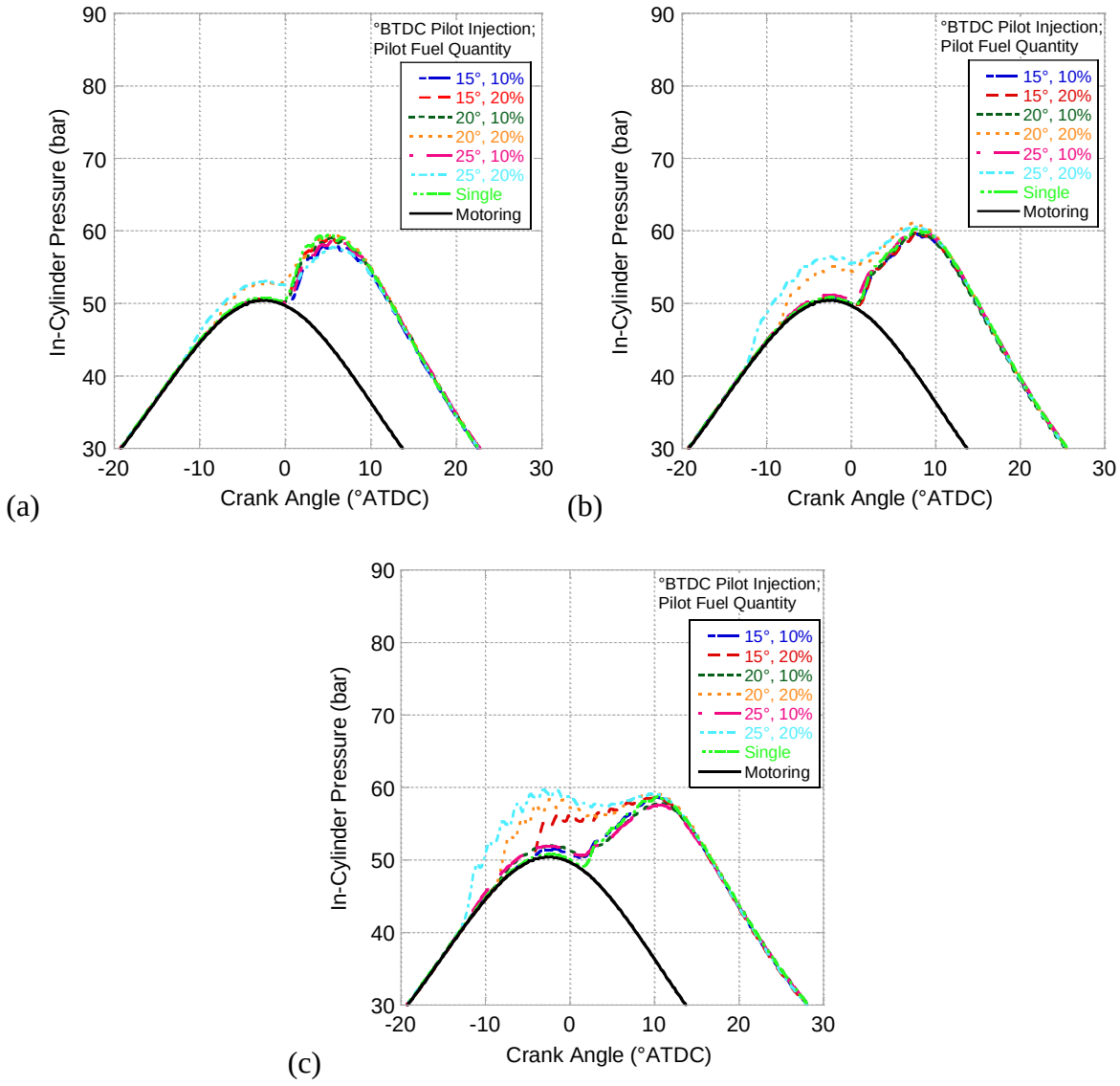

Figure 3.26: Cylinder pressure results for soybean biodiesel pilot injection tests at 4.5 N-m (a), 9.0 N-m (b), and 13.5 N-m (c).

BSFC results for the soybean biodiesel pilot injection tests are given in Figure 3.27. While the ULSD tests all produced improvements or no change in BSFC, with reductions generally being damped with an increase in load, the soybean biodiesel tests only show significant improvements at 9.0 N-m. This is due to an increased level of diffusion burn combustion (shown next) that is present with soybean biodiesel; hence, biodiesel burns more like a constant pressure event as evident when comparing in-cylinder pressure traces. As a result,

adding a biodiesel pilot grows the pressure before TDC without significantly adding to the expansion work. By investigating the area underneath the curves between ULSD and soybean biodiesel pilot experiments between TDC and peak pressure, the relative gain in expansion work for ULSD is seen and reflected in the BSFC. In other words, soybean biodiesel does not benefit significantly from the same tradeoff of increased expansion work at the expense of more compression work. Moreover, the BSFC results for the 13.5 N-m tests are the only experiments to demonstrate a (somewhat) global trend. While no significant improvements were seen, it appears that a close-coupled pilot injection (closer to the main injection) might produce more desirable results. Overall, BSFC reductions for soybean biodiesel compared to baseline single injection were limited to 0.6%, 1.5%, and 0.2% for 4.5, 9.0, and 13.5 N-m, respectively.

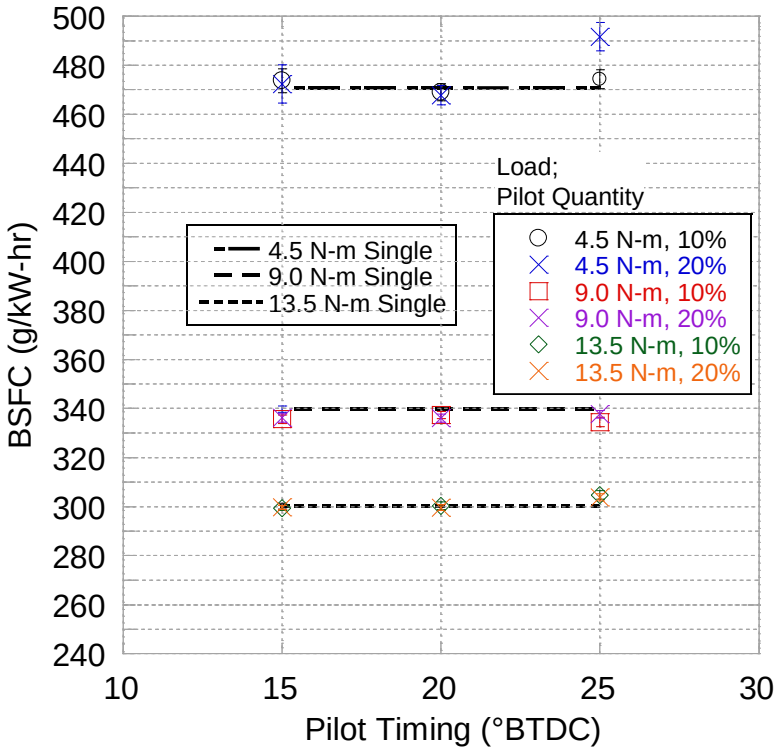

Figure 3.27: BSFC results from soybean biodiesel tests.

Figure 3.28 provides further insight via the heat release results. Soybean biodiesel pilot injections yielded significantly less reduction of the main injection premixed spike compared to ULSD. Furthermore, Figure 3.29 compares the 20°/20% experiments between soybean biodiesel and ULSD at 9.0 and 13.5 N-m. This illustrates how soybean biodiesel produces a lesser premixed pilot combustion event and a greater amount of diffusion burn during main combustion; thus, demonstrating a more constant pressure style of combustion. Referring back to Figure 3.28, at 9.0 and 13.5 N-m, many experiments produced pilot combustion spikes larger than the subsequent premixed spike of the main injection combustion event. Here, the earlier pilot combustion event results in a respectively hot cylinder prior to the main injection pulse. This, in combination with a greater CN of soybean biodiesel, reduces the ignition delay of the main injection event; hence, this nearly eliminates the premixed phase of main combustion.

Furthermore, while the level of diffusion burn heat release following the premixed spike of main combustion remained relatively constant for the ULSD experiments, it largely increased for many of the soybean biodiesel pilot injection experiments.

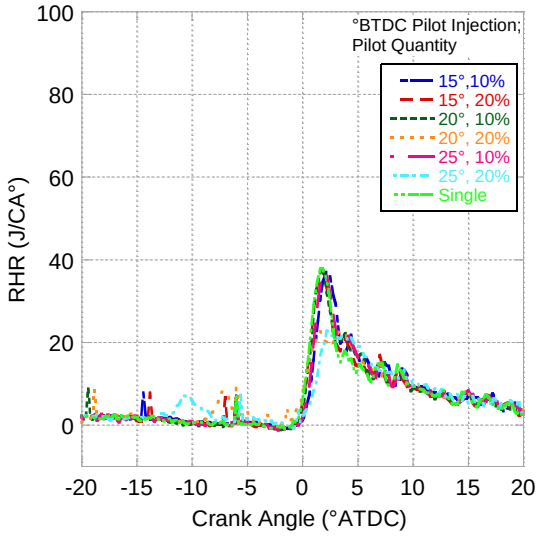

(a)

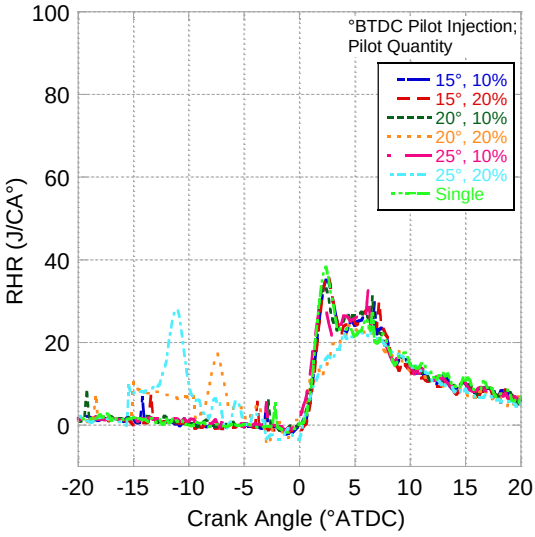

(b)

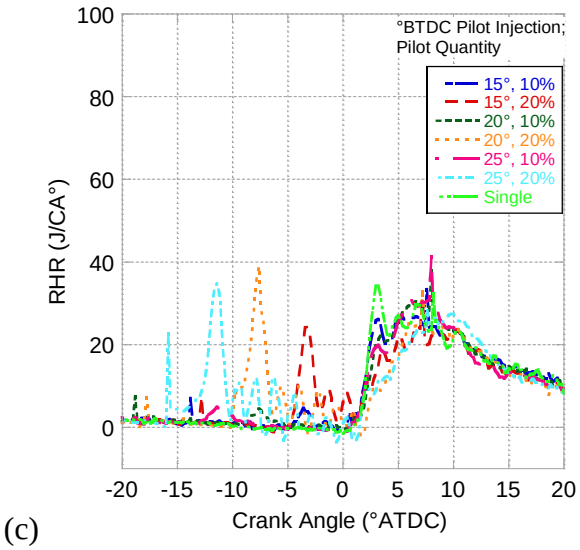

(c)

Figure 3.28: Heat release results for soybean biodiesel pilot injection tests at 4.5 N-m (a), 9.0 N-m (b), and 13.5 N-m (c).

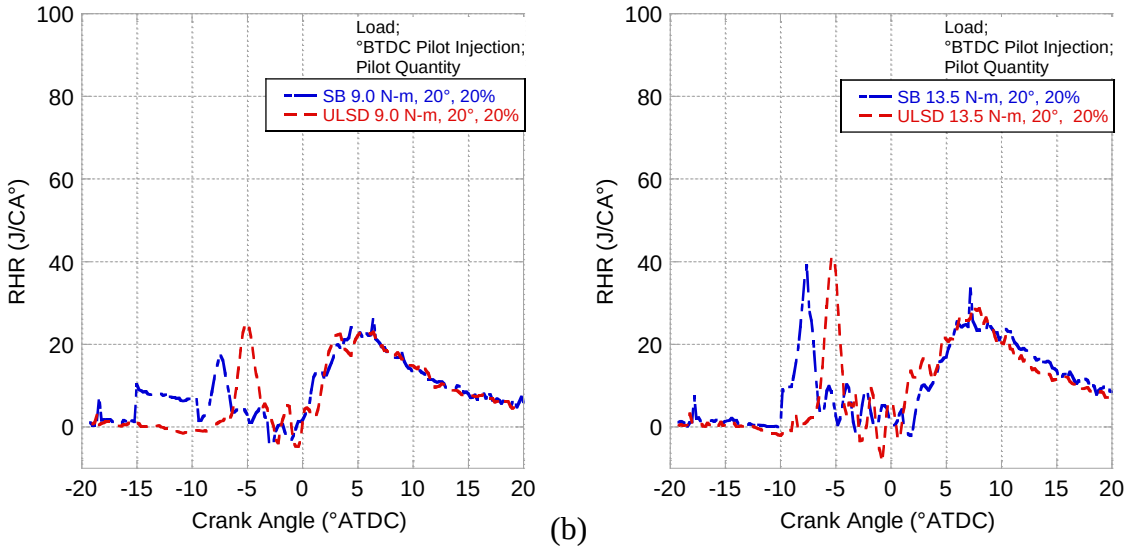

(a) (b)

Figure 3.29: Comparison of soybean biodiesel and ULSD 20°/20% pilot injection experiments at 9.0 N-m (a) and 13.5 N-m (b).

While the soybean biodiesel pilot experiments do not dramatically increase the peak in-cylinder temperature (given in Figure 3.30 and Table 3.14) as much as the ULSD experiments, they generally exhibit higher temperatures during main combustion. This is due to the greater level of diffusion burn for biodiesel resulting in a more muted temperature rise. This increase in diffusion burn also results in main combustion temperatures occurring slightly later in the

expansion stroke in comparison to ULSD. This earlier timing of the pilot combustion temperature rise with the soybean biodiesel experiments, in conjunction with the delayed peak temperature, helps to illustrate why there were minimal BSFC improvements for the pilot injection experiments.

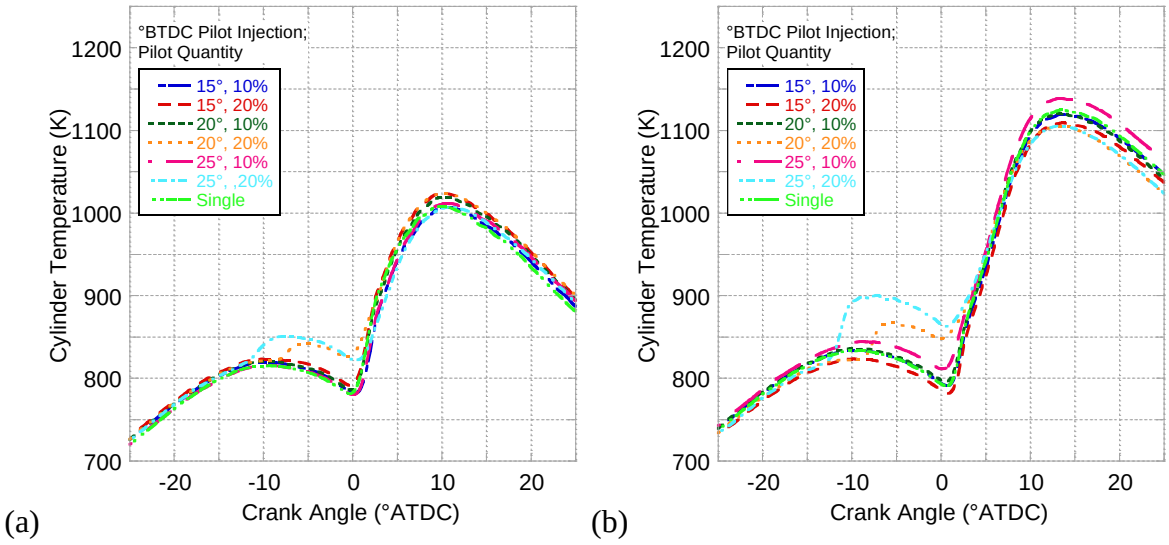

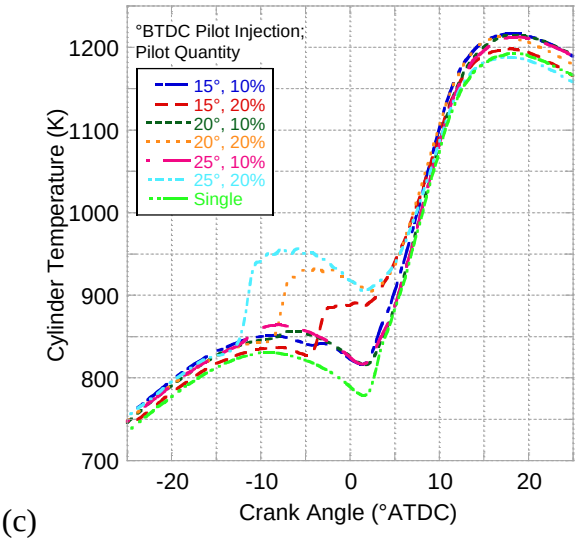

(c)

Figure 3.30: Bulk gas temperature from soybean biodiesel experiments.

Table 3.14: Average bulk gas temperature (K) from -15° to 25° ATDC.

Load	**Pilot Quantity: 10% Timing: 15° BTDC**	**20% 15°**	**10% 20°**	**20% 20°**	**10% 25°**	**20% 25°**	**Single**
4.5 N-m	893	905	901	912	894	904	893
9.0 N-m	953	943	956	959	970	971	956
13.5 N-m	995	997	990	1019	991	1023	969

Figure 3.31 through Figure 3.35 give the ignition delay results for the soybean biodiesel pilot injection tests. While, at each load, soybean biodiesel has largely the same or slightly reduced main injection ignition delay compared to ULSD, the greatest differences lie in the pilot injection ignition delay. For all soybean biodiesel experiments that produced pilot combustion, the pilot injection ignition delay was reduced by as much as 4° relative to ULSD due to its greater CN. However, at 9.0 N-m, soybean biodiesel exhibited pilot combustion for only two 20% pilot quantity tests, while ULSD achieved pilot combustion for all 10% and 20% tests. This is likely due to differences in mixture preparation between the two fuels resulting from the

greater viscosity and density of soybean biodiesel. Revisiting the idea that less than 15° of pilot timing advance could potentially be beneficial for BSFC at 13.5 N-m, it is clear from the ignition delay results at -15° SOI_p that the main combustion injection event would have to be further delayed and likely shift peak pressure away from the single injection location. Though because of the large peak pressure levels seen at this load, it may not be necessary to maintain the same single injection peak pressure location for optimal BSFC.

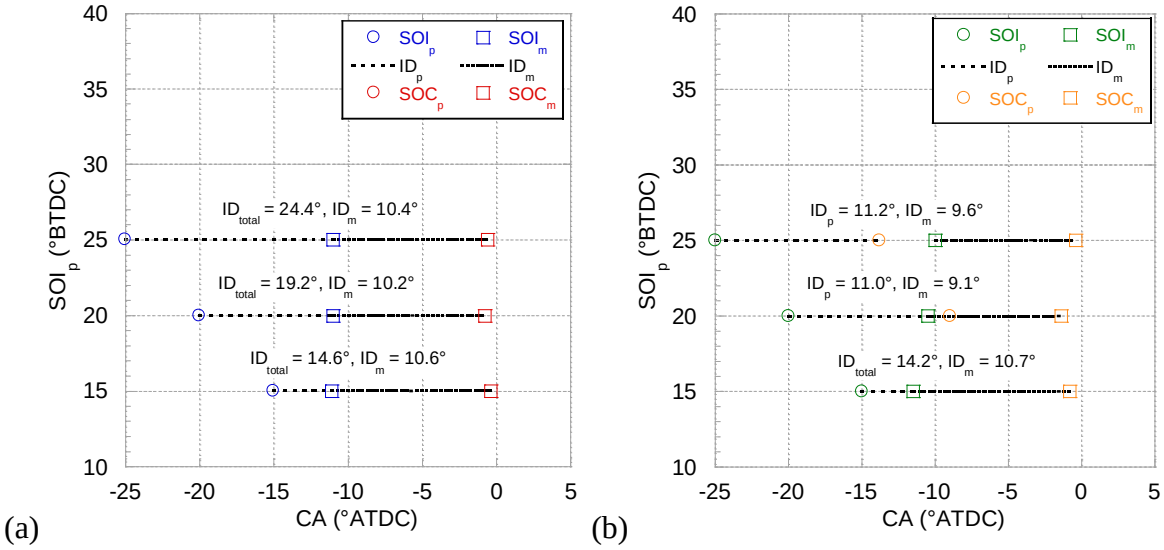

Figure 3.31: 4.5 N-m pilot injection ignition delay results for 10% (a) and 20% (b) pilot quantities.

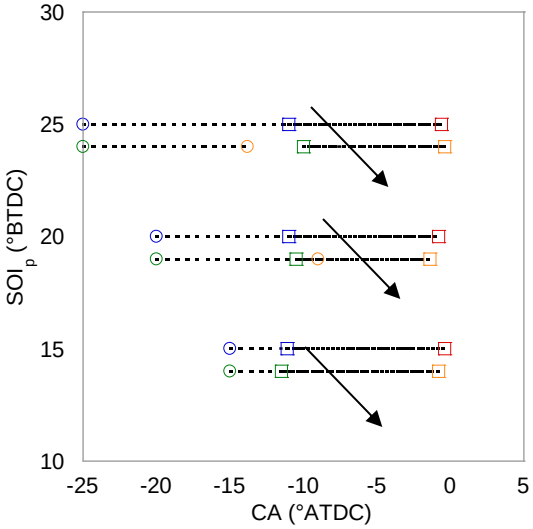

Figure 3.32: Comparison of 10% and 20% pilot quantity ignition delay at 4.5 N-m.

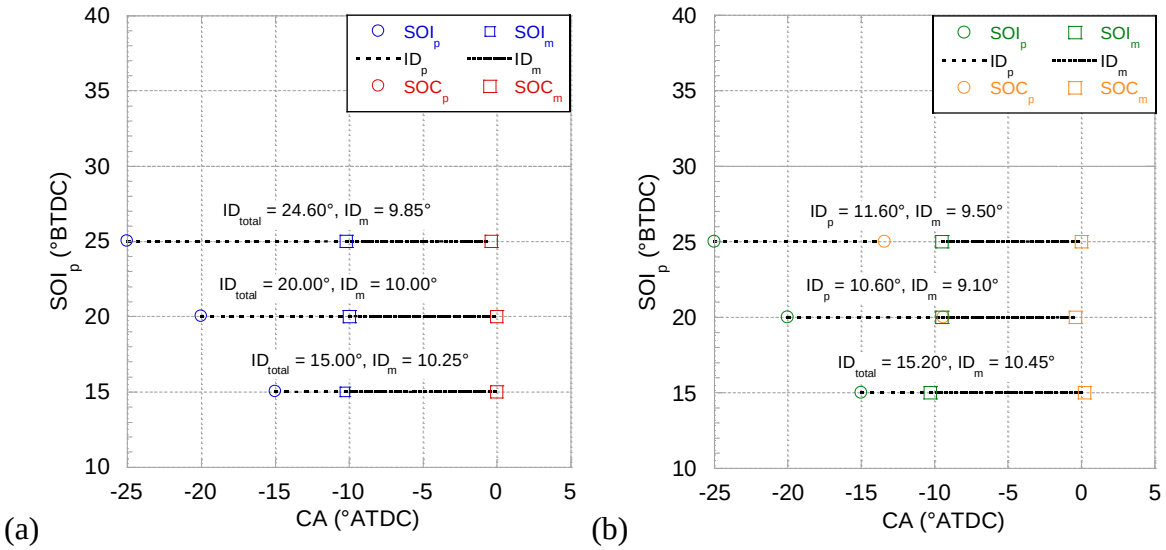

Figure 3.33: 9.0 N-m pilot injection ignition delay results for 10% (a) and 20% (b) pilot quantities.

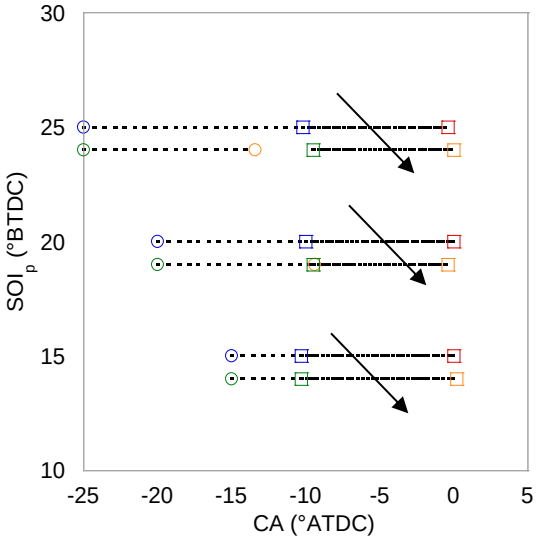

Figure 3.34: Comparison of 10% and 20% pilot quantity ignition delay at 9.0 N-m.

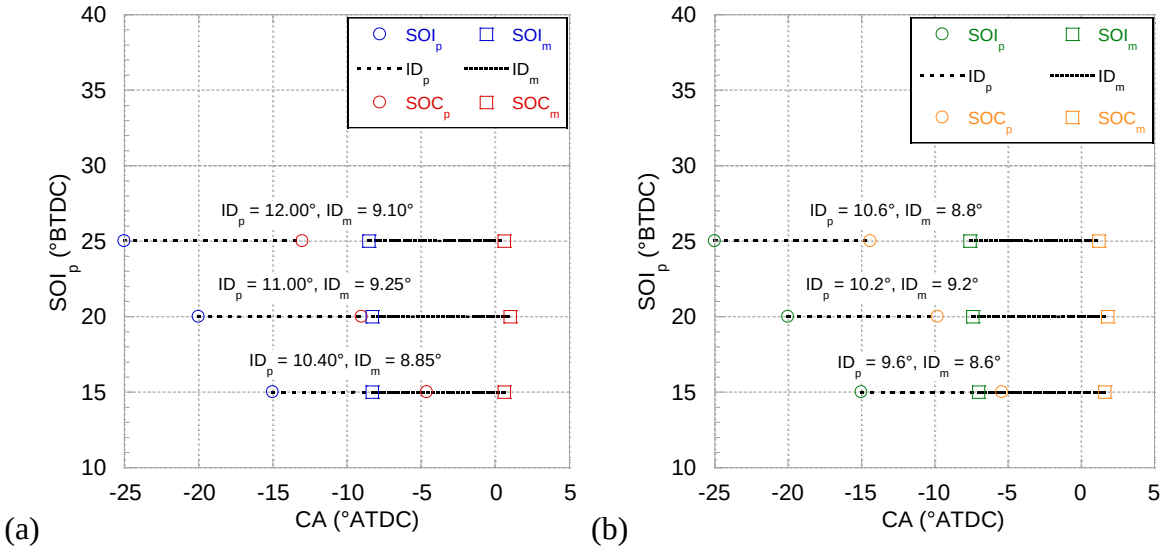

Figure 3.35: 13.5 N-m pilot injection ignition delay results for 10% (a) and 20% (b) pilot quantities.

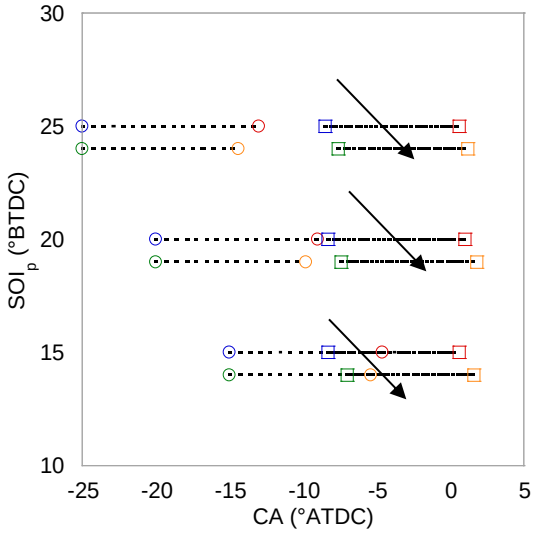

Figure 3.36: Comparison of 10% and 20% pilot quantity ignition delay at 13.5 N-m.

Figure 3.37 illustrates a dampened pilot injection influence on combustion noise with soybean biodiesel similar to the heat release and cylinder pressure results. The 4.5 and 9.0 N-m results tell a similar story as ULSD, as large reductions in the premixed RHR spike of main combustion result in a noticeable combustion noise reduction. However, the reductions in peak RHR were limited compared to ULSD due to the overall greater amount of diffusion burn present. The 13.5 N-m combustion noise results still largely illustrate how peak RHR correlates

with noise levels, although there is the additional influence of pilot knock that raises noise beyond the single injection level. In Figure 3.38, looking closely at the pressure during pilot combustion experiments sees the pressure waves characteristic of ringing combustion. When the pilot fuel injection is advanced along with the larger quantity of fuel, a greater pilot pre-mixed spike occurs, and greater pressure waves are seen. Hence, this results in an augmentation of combustion noise.

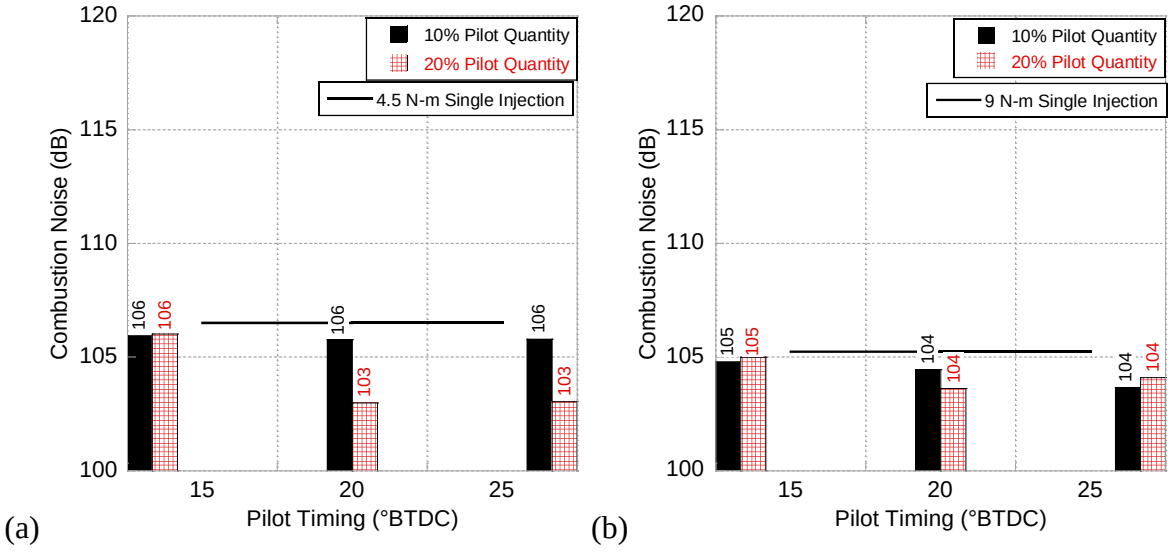

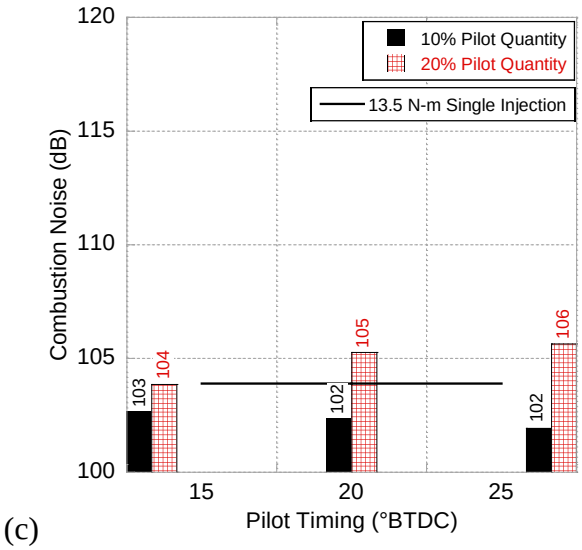

(c)

Figure 3.37: Combustion noise results from soybean biodiesel pilot injection tests at 4.5 N-m (a), 9.0 N-m (b), and 13.5 N-m (c).

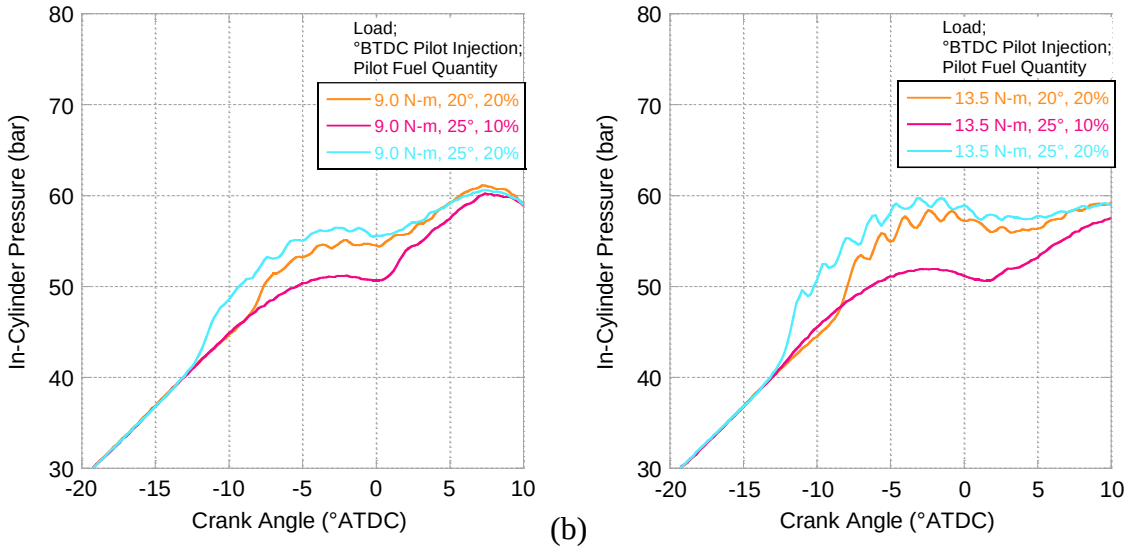

(a) (b)

Figure 3.38: Ringing pilot combustion during 9.0 N-m (a) and 13.5 N-m (b) experiments.

NO_x emission levels were largely unaffected by the addition of a pilot injection for soybean biodiesel, as shown in Figure 3.39. As stated before, NO_x production is dependent on the level of heterogeneity, the timing of the combustion event, and in-cylinder temperatures. Overall, the level of heterogeneity should decrease somewhat via a pilot injection as there is more time to mix the fuel and air. However, for biodiesel, combustion starts sooner and generally

sees an overall hotter cylinder. In addition, NOx emissions are largely tied to the level of premixed burn and soybean biodiesel has a reduced amount of premixed combustion during both pilot and single injection experiments. The combination of all these factors results in NOx emissions being almost constant with pilot injection timing and amount. Pilot injection influence on PM levels was also significantly less for soybean biodiesel compared to ULSD. Although cylinder temperature was higher for many of the experiments, the only significant change in PM was an increase when there was a noticeable growth in the diffusion burn phase brought on by the pilot injection experiments.

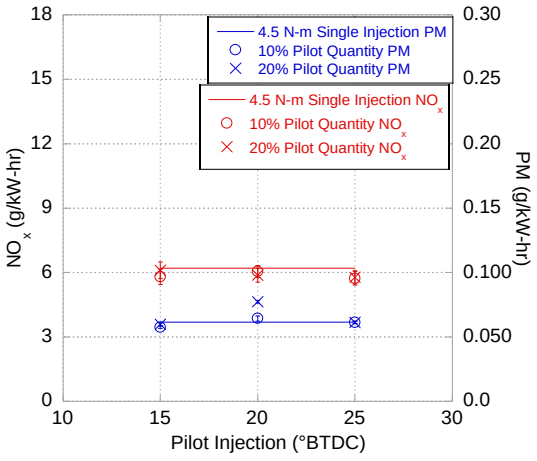

(a)

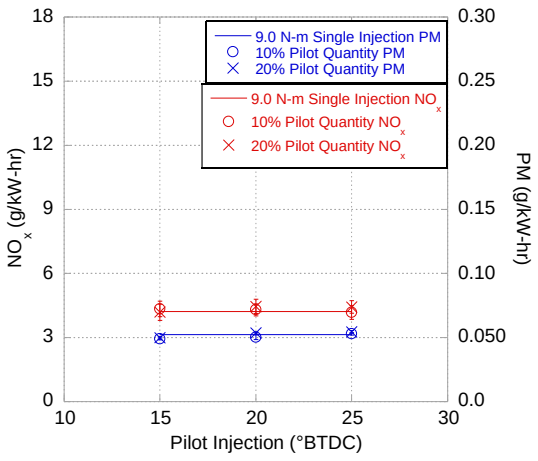

(b)

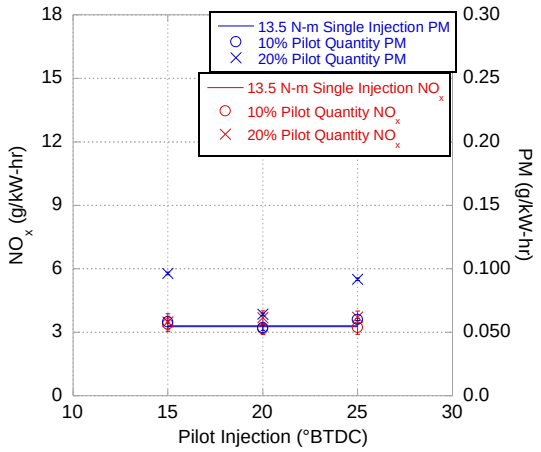

(c)

Figure 3.39: NO_x and PM emissions results for soybean biodiesel pilot injection testing at 4.5 N-m (a), 9.0 N-m (b), and 13.5 N-m (c).

Largely, the soybean biodiesel experiments exhibited a reduced response to pilot injection regarding CO and THC emissions as compared to ULSD, as illustrated by Figure 3.40. The combustion efficiency results in Table 3.15 tell the same story, as there is little deviation from the baseline single injection combustion efficiency at each load. Overall, the greater level of diffusion burn seen with the pilot injection experiments is balanced by generally hotter temperatures and along with the oxygenated quality of the fuel; hence, CO and THC emissions remain mostly constant.

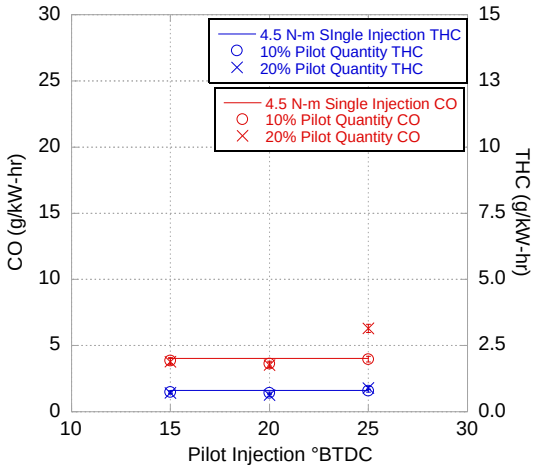

(a)

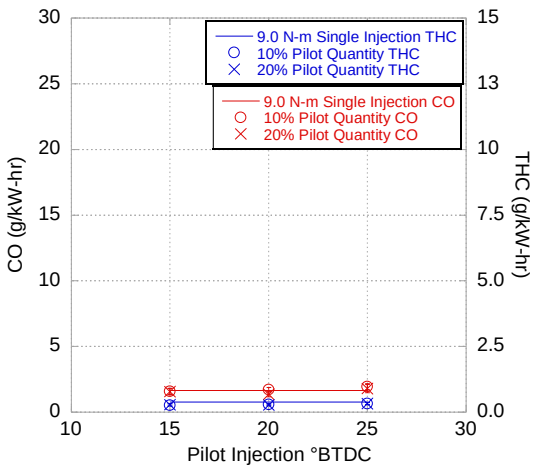

(b)

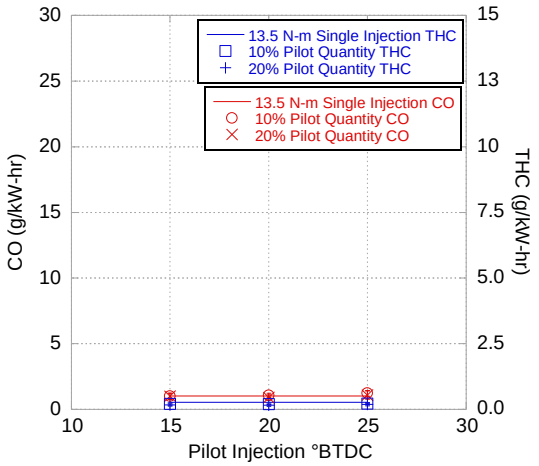

(c)

Figure 3.40: CO and THC emissions results for soybean biodiesel pilot injection tests at 4.5 N-m (a), 9.0 N-m (b), and 13.5 N-m (c).

Table 3.15: Combustion efficiency results from soybean biodiesel pilot injection tests.

Load	**Pilot Quantity: 10% Timing: 15° BTDC**	**20% 15°**	**10% 20°**	**20% 20°**	**10% 25°**	**20% 25°**	**Single**
4.5 N-m	99.4% ±4.0	99.4% ± 4.2	99.4% ± 3.2%	99.4% ± 3.7%	99.3% ± 3.7%	99.1% ± 3.4	99.3% ± 4.2
9.0 N-m	99.6% ± 5.1	99.6% ± 4.5	99.6% ± 4.2	99.7% ± 4.7	99.6% ± 4.3	99.6% ± 3.5	99.6% ± 4.3
13.5 N-m	99.7% ± 4.4	99.7% ± 5.4	99.7% ± 6.1	99.8% ± 6.3	99.7% ± 4.5	99.7% ± 5.6	99.7% ± 4.7

3.5. Conclusions

Experimentation was carried out to compare the fundamental differences in combustion between ULSD and soybean biodiesel fuels. Baseline single injection tests were conducted initially for both fuels over the entire load range of the Yanmar L100V single cylinder engine at 0.5, 4.5, 9.0, 13.5, and 18.0 N-m. Following the single injection tests, multiple injection experiments were conducted at 4.5, 9.0, and 13.5 N-m while varying the timing of a single pilot injection from 15° to 25° BTDC and employing pilot injection quantities of 10% and 20%. In order to normalize combustion between all tests, the single injection peak cylinder pressure crank

angle location at each load for both fuels was maintained during the corresponding pilot injection test by calibrating timing of the main fuel injection event. Following the experiments, the data were post-processed and analyzed via performance, heat release, combustion noise, and emissions findings.

A single pilot injection aided in reducing fuel consumption across the entire tested load range for ULSD, though reductions of any significance were restricted to 9.0 N-m for soybean biodiesel. The combustion of the pilot injection event leads to an increase in expansion work that is greater than the growth of compression work; hence, more crank angles are utilized for useful power. Comparing these results to the literature, ULSD attained reductions in BSFC of up to 12.14, 7.22, and 5.29 g/kW-hr at 4.5, 9.0, and 13.5 N-m, respectively, which matches the single pilot injection results of Ishida et al. almost exactly. However, the soybean biodiesel experiments were only able to achieve BSFC reductions of 2.91, 5.21, and 0.73 g/kW-hr at 4.5, 9.0, and 13.5 N-m, respectively. Overall, it was determined that soybean biodiesel would benefit from additional mixture preparation to increase its premixed combustion potential and lessen diffusion-burn combustion. This is due to the increased viscosity and density of soybean biodiesel, which is exacerbated by the age of the fuel used here, and leads to a more constant-pressure like combustion event. This points to an increase in fuel pressure being necessary for soybean biodiesel to reap similar benefits from a single pilot injection as compared to ULSD. Moreover, while maintaining the single injection main combustion peak pressure location at each load was effective in normalizing combustion, there appeared to be potential fuel consumption gains at medium to high loads if the overall combustion event was delayed. This observation has implications pertaining to emissions as well, as it is common in the literature for the lowest NO_x emissions results to be realized when the main injection event is significantly delayed; hence, the

potential benefit in BSFC from re-phasing combustion would likely be coupled with reduced NO_x levels as well.

Regarding emissions, the ULSD experiments behaved as expected for a single pilot injection following the NO_x-PM tradeoff at low to medium loads. At 4.5 and 9.0 N-m, all reductions in peak RHR resulted in reductions in NO_x and a subsequent increase in PM as combustion shifts towards an increased ratio of diffusion-burn to premixed. However, at 13.5 N-m, little change in NO_x emissions were seen, along with almost universal increases in PM. While NO_x levels remained largely unchanged between all soybean biodiesel experiments, they were also universally lower than NO_x levels produced by the ULSD tests, which is largely due to the amount of diffusion-burn combustion present for the soybean biodiesel tests. While ULSD's baseline PM levels were the lowest at 4.5 N-m and 9.0 N-m, most of the 4.5 N-m experiments between the two fuels produced similar PM levels, and at 9.0 N-m soybean biodiesel produced universally lower PM emissions than the ULSD pilot injection tests. At 13.5 N-m, both fuels produced similar baseline PM levels, but soybean biodiesel largely maintained the baseline PM level, while ULSD saw significant increases during most tests.

Combustion noise was found to be predominantly affected by peak RHR, as reductions in both were attained using a single pilot injection for each fuel. In addition, peak pressure magnitude and phasing between the pilot and main combustion events were seen to have a small influence. At 4.5 N-m, soybean biodiesel universally produced significantly lower combustion noise levels than ULSD, due to ULSD combustion being almost entirely premixed at this load; whereas, soybean biodiesel still exhibited a significant amount of diffusion-burn combustion. Soybean biodiesel continued to produce lower levels of combustion noise throughout the load range as a result of having less premixed combustion present. As a result, the pilot injection

strategy had little potential to reduce combustion noise from soybean biodiesel due to its largely diffusion burn combustion profile. Moreover, at high loads and pilot quantities, the greater CN of soybean biodiesel caused pilot combustion advance that resulted in ringing combustion indicative of knock, which brought combustion noise beyond the single injection level.

The results of the ULSD experiments have shown that there are benefits pertaining to fuel consumption, emissions, and combustion noise when operating with a single pilot injection. Conversely, the soybean biodiesel experiments exhibited little advantage besides respectively small reductions in combustion noise and emissions. Overall, the vast subject of multiple fuel injections with compression ignition engines, specifically ones operating with biodiesel fuels, can be further explored with a greater understanding of the fundamental behavior that multiple fuel injection events bring about.

Chapter 4 – Conclusions

The first chapter of this thesis explained the motivation behind biodiesel fueled CI engine research, which is mainly driven by the potential for biodiesel to produce less life cycle CO_2 emissions than ULSD. The advantages and disadvantages of biodiesel were detailed based on its fuel properties, specifically highlighting the drawbacks keeping it from the same level of proliferation as ULSD, such as its increased fuel consumption and perceived high NO_x emissions. A brief overview of modern fuel injection technology then introduced how electronic fuel injections systems contribute to added combustion flexibility in CI engines. In specific, multiple fuel injection strategies can be used to reduce fuel consumption and engine-out emissions.

A literature review of multiple injection use with CI engines was then conducted in the second chapter which encompassed efforts involving CI engines fueled with both conventional diesel and biodiesel. Moreover, this chapter first provides the basis for understanding this research by detailing the fundamentals of conventional CI combustion, along with the formation of pertinent emissions constituents. The literature involving multiple injection efforts with conventional diesel was then summarized. This section illustrated the mechanisms at-play with multiple injections and how they influence performance and emissions. It was shown how pilot injections can be used to limit peak RHR and cylinder pressure rise rate, which subsequently reduce NO_x and combustion noise, although these effects are often reduced at high load. Accounts of pilot injection influence on BSFC varied, although there were many researchers that showed how BSFC can be reduced when combustion is lengthened into the expansion stroke. Furthermore, there were numerous accounts of how post injections can be employed for PM oxidation with little to no effect on other emissions or fuel consumption. In addition, the

literature agrees that the presence of both pilot and post injections are the most beneficial, and how splitting the individual pilot, main, and post injection events into multiple sub-injection events also increases effectiveness.

Overall, the literature pertaining to biodiesel use illustrates how multiple injections are just as beneficial, if not more, than multiple injections with conventional diesel. Biodiesel fueled CI engines already benefit over conventional diesel with respect to partial products of combustion due to biodiesel's greater adiabatic flame temperature and combustion efficiency. The added flexibility of multiple injections helps to overcome the disadvantages of biodiesel, such as its greater viscosity and lower energy content. This is apparent through the scenarios where biodiesel was able to attain simultaneous reductions in NO_x and PM relative to conventional diesel; however, this only occurred with neat soybean and coconut biodiesel. Furthermore, differences due to the fuel properties of biodiesel are still apparent. With pilot injections, it is common for a greater pilot quantity to be used to counter the larger CN of biodiesel that would otherwise advance pilot combustion. Moreover, it was shown how the presence of a post injection augments the beneficial nature of biodiesel to produce less PM. The advantageous shift in the soot production-oxidation battle inherent to biodiesel is caused by increased soot production during the middle of combustion due to an increase in viscosity, but this is then overcome by the higher adiabatic flame temperature of biodiesel, which accelerates soot oxidation. The addition of a post injection then furthers this soot oxidation to allow for overall lower soot levels than conventional diesel.

In chapter three, experimentation was conducted using the CI single-cylinder test cell at KU that compared pilot injection use between aged soybean biodiesel and ULSD. These experiments were largely driven by the opportunity to contribute to the sparse amount of

literature available pertaining to multiple injection use with CI engines fueled with neat biodiesel. However, more novel aspects of this work include how the Yanmar L100V used for testing has a higher compression ratio than any engine used in efforts pertaining multiple injection use found in the literature. Moreover, the goal of this work was to compare how the fuel property differences between biodiesel and ULSD and the introduction of a pilot injection affect combustion on a fundamental level, rather than the popular literature method of modulating injection parameters until the most desirable results have been obtained. This was achieved by conducting single injection experiments for both fuels to which the pilot injection tests could then be compared, while also maintaining the same single injection peak pressure location during subsequent pilot injection experiments by modulating main injection timing to normalize combustion. Soybean biodiesel was chosen for these experiments due to its larger prevalence in the literature to compare to the results obtained here. As for the injection parameters, a single pilot injection was chosen to provide an initial understanding of multiple injections. The pilot injection strategy has the widest range of influence on combustion. Furthermore, the sweeps of pilot injection timing and quantity were limited to 15°-25° BTDC and 10-20%, respectively, in order to stay out of the possible regime of LTC kinetics and limit the number of experiments by starting with what has been proven to be effective in the literature.

Combustion results of the ULSD pilot injection experiments showed how the pilot combustion event becomes more pronounced as both pilot injection advance and quantity are increased, with quantity as the primary influence, and this caused the need for main injection delay in most experiments to maintain peak pressure timing. More pilot combustion was present at medium and high loads due to a greater amount of fuel injected; however, the effects of pilot combustion on heat release were the greatest at small and medium loads where premixed

combustion can be significantly reduced. These results agree with the literature findings that the primary effect of a pilot injection, a reduction in main combustion peak RHR, is achieved through shortening of the main injection ignition delay by injecting the main fuel quantity during hotter cylinder temperatures. These reductions in peak RHR caused an increase in diffusion burn combustion and affected emission and combustion noise, which will be reviewed later in this chapter.

As expected, the fuel property differences between soybean biodiesel and ULSD, such as soybean biodiesel's greater viscosity, density, and cetane number, yielded a lesser pilot combustion event due to higher stratification, shorter ignition delay, and overall less fuel prepared for pilot combustion. While it was anticipated that soybean biodiesel might achieve pilot combustion in extents where ULSD did not combust, due to soybean biodiesel's greater CN and oxygen content, this was largely not the case. In addition, it appears the age of the fuel caused viscosity increases that inhibited pilot combustion during a few tests where ULSD did experience pilot combustion. This greater viscosity of the aged soybean biodiesel also limited its premixed combustion potential and peak pressures were greatly reduced compared to ULSD. However, pilot combustion is inherently premixed, and this allowed soybean biodiesel pressure rise during pilot combustion to approach that of ULSD. The general findings from the soybean biodiesel experiments were that the introduction of a pilot injection, while significantly influencing combustion, did little to influence emissions, performance, or combustion noise. This was largely due to the already dominant level of diffusion-burn combustion for soybean biodiesel as a function of its increased viscosity. Heat release results showed how the respectively low amount of premixed main combustion during single injection experiments was all but eliminated when pilot combustion was present.

Overall, soybean biodiesel presented a higher BSFC than ULSD due to its lower energy content, and fuel consumption for the single injection soybean biodiesel experiments was also higher than what was previously found in the lab by Mangus et al. This is attributed to the age of the soybean biodiesel used in this testing, as aging of biodiesel causes an increase in viscosity and decreases energy content. However, the trends seen in these experiments still offer valuable insight into the fundamental effects of multiple injection use with biodiesel. The ULSD experiments proved that a single pilot injection can be effective in reducing BSFC over the entire load range. Reductions of up to 12.14, 7.22, and 5.29 g/kW-hr were observed at 4.5, 9.0, and 13.5 N-m, respectively, which also reflect the decrease in pilot injection effectiveness as load increases (as seen in the literature). However, a different mechanism for this fuel consumption reduction was seen compared to what is generally accepted in the literature. Many authors in the literature reference the fact that a pilot injection improves BSFC by allowing for delayed main injection timing that lengthens combustion further into the expansion stroke, thus, extracting more work. Whereas, the results obtained in this effort elucidate that it is possible to increase cylinder pressure at the beginning of expansion that aids in additional work extraction. The main injection event often required a slight delay, but it did not significantly cause combustion to occur any further in the expansion stroke than the single injection. Pilot combustion was seen to raise cylinder pressures at the onset of the expansion stroke, effectively bolstering the main combustion event so that it can take advantage of higher pressures spanning more crank angles while still maintaining the same peak pressure location and similar peak pressure magnitude. However, the pre-TDC cylinder pressure rise due to pilot combustion presents a tradeoff between compression work and expansion work which will mitigate BSFC benefits if the pilot combustion event is too great or to advanced.

Unlike the ULSD experiments, soybean biodiesel was only able to attain reductions in BSFC of 2.91, 5.21, and 0.73 g/kW-hr, respectively, although the mechanism was the same. This was mainly due to the increased viscosity and density of the fuel hindering mixture preparation of the main injection event, in-turn limiting peak pressure and its constant volume like combustion potential. As a result, the early expansion pressure rise caused by pilot combustion is slightly less in magnitude, but it also does not bolster main combustion pressure rise in the same way as ULSD because peak pressure is lower. Furthermore, the greater CN of soybean biodiesel causes pilot combustion to occur earlier which takes away from any BSFC benefit by increasing compression work. A higher fuel pressure could be used to counter the increased viscosity as facilitate mixture preparation; thus, benefitting BSFC. Moreover, additional pilot injections or main injections could be employed to potentially overcome this higher viscosity incurred by the aged biodiesel.

Combustion noise correlated strongly with peak RHR for all experiments, with noise reductions during the pilot injection experiments being proportional to the corresponding reduction in peak RHR. Furthermore, combustion noise was dictated by overall peak RHR, whether it occurred during pilot or main combustion, although the relative phase between combustion events was seen to play a small role as well. ULSD specifically, was able to attain combustion noise reductions of 6, 7, and 7 dB and 4.5, 9.0, and 13.5 N-m, respectively. Whereas, soybean biodiesel was limited to reductions of 3, 1, and 2 dB and 4.5, 9.0, and 13.5 N-m, respectively. However, soybean biodiesel exhibited universally lower combustion noise than ULSD due to its higher viscosity and lower level of premixed combustion. Hence, the 4.5 N-m experiments still have a relatively high amount of premixed combustion that could be damped by a pilot combustion event. Furthermore, the ringing combustion present during the 20°/20% and

25°/20% experiments brought combustion noise 1 and 2 dB beyond the single injection level, respectively.

Like the combustion noise results, ULSD exhibited significant reductions in NO_x emissions when peak RHR was decreased due to the presence of pilot combustion. Reductions of 3.06, 1.41, 0.51 g/kW-hr at 4.5, 9.0, and 13.5 N-m, respectively, were attained while employing a pilot injection event. These results further mirror the relationship found in the literature between load and pilot injection effectiveness, as there is less potential to minimize large RHR spikes as premixed combustion decreases with load. However, the NO_x benefits seen here only approach what is shown to be possible in the literature, most likely because the main injection event was not significantly delayed, which was done to maintain the single injection peak pressure location. Moreover, significant increases in PM were associated with any decrease in NO_x due to a growth in diffusion burn combustion, illustrating the NO_x-PM tradeoff that is common in the literature when employing a single pilot injection. There were no reductions in PM seen for any ULSD pilot injection experiment, as PM emissions often doubled from the baseline single injection quantity.

Conversely, soybean biodiesel exhibited only small decreases in NO_x emissions in the presence of pilot injections, as the greatest reduction was 0.46 g/kW-hr at 4.5 N-m. This was due to how little premixed combustion was present as a result of the increased viscosity and density of biodiesel, which was exacerbated by the age of the fuel. The soybean biodiesel single injection NO_x quantities were already significantly lower than ULSD, and as a result, there was little potential for a pilot injection to provide any benefit. While many experiments even showed slight increases in NO_x, soybean biodiesel still yielded universally lower NO_x levels than ULSD. Furthermore, while baseline soybean biodiesel PM levels were higher than ULSD at 4.5 and 9.0

N-m due to its hindered atomization process, PM was largely unaffected by the presence of a pilot injection. As a result, PM emissions were no worse at 4.5 N-m for soybean biodiesel compared to ULSD, and at 9.0 and 13.5 N-m, PM levels for soybean biodiesel were largely lower.

The ULSD pilot injection testing exhibited decreases in CO and THC emissions that correlate well with BSFC reductions and increases in combustion efficiency. However, significant changes in emissions of these partial products of combustion were limited to low load. Soybean biodiesel on the other hand, produced little change in CO and THC emissions when a pilot injection was introduced. The oxygenated fuel's already high combustion efficiency was largely unaffected by the additional mixing provided by the pilot injections, although the increase in average cylinder temperature would lead one to believe otherwise. However, emissions of these species were universally lower for soybean biodiesel compared to ULSD, and additional mixture preparation that could be had with higher fuel pressures or additional fuel injections could potentially increase this advantage, especially at low to medium loads.

Overall, the results of ULSD testing have illustrated the benefits, drawbacks, and limitations of pilot a single pilot injection. The results here corroborate literature findings that indicate the need for additional injection events; whether that be though additional pilot, main, or post injections, to reach the full potential of multiple injection use and achieve simultaneous reductions of NO_x and PM. The soybean biodiesel experiments yield a similar conclusion, in addition to the need for higher fuel pressures when operating with biodiesel (especially aged biodiesel) for BSFC benefits. However, the soybean biodiesel pilot injection tests showed universally lower NO_x, CO, and THC emissions, as well as largely lower PM emissions compared to ULSD, pointing to the potential for biodiesel to outperform ULSD with respect to

emissions if injection parameters were optimized and more advanced multiple injection strategies were employed. While biodiesel has a lower energy content than ULSD and will always incur an increased fuel consumption, the small decreases in BSFC with soybean biodiesel due to pilot injections seen here can be further improved with additional mixture preparation.

4.1. Future Work

The aim of this thesis was to provide a holistic view of multiple fuel injection use in CI engines so that these strategies could then begin to be paired with biodiesel use. The literature review provided knowledge of the various multiple injection strategies and their effects on combustion, followed by experimental efforts that provided initial testing with a biodiesel-fueled CI engine operating with multiple injections. By investigating the most basic multiple fuel injection strategy, the pilot injection, this work was able to accomplish the first step in attaining a fundamental understanding of multiple fuel injection operation with biodiesel. The completion of this work now allows for additional and more complex multiple injection strategies to explored.

The next basic strategy to be investigated will be the post injection for PM control. Especially for ULSD, where the pilot injections illustrated the traditional NO_x-PM tradeoff and subsequent increases in PM, this will be beneficial. While soybean biodiesel largely showed decreased PM compared to ULSD when a pilot injection was present, the addition of a post injection could be used to further this advantage. After exploring the post injection, efforts involving more complex injection strategies can be implemented that involve splitting of the pilot, main, and post injection events to realize the full potential of multiple injections with biodiesel.

There is also more work that can be done pertaining to the aged biodiesel used in this work. It was shown how the age of the fuel was most apparent in the resulting increased viscosity that greatly reduced the amount of premixed combustion present. In-turn, this limited pilot injection influence since the effects of a pilot injection event are the most apparent during premixed combustion. Additional experiments can be conducted in the future that test aged biodiesel at higher fuel pressures in order to combat the higher viscosity incurred by its age. Moreover, the potential effects of water absorption with aged biodiesel should be investigated, as biodiesel is known to have a significantly greater moisture absorption potential (approximately 15 – 20 times more [142]) than conventional diesel. This is particularly important because plant-based ethanol fuels are known to potentially form an aqueous bottom layer in the presence of significant moisture absorption, which can inhibit engine starting [143], not to mention the potential engine damage or unfavorable effects on combustion.

References

1. Gerpen, J.V., *Biodiesel processing and production.* Fuel Processing Technology, 2005. **86**(10): p. 1097-1107.

2. Sheehan, J., et al., *Life cycle inventory of biodiesel and petroleum diesel for use in an urban bus. Final report*. 1998, Office of Scientific and Technical Information (OSTI).

3. Demirbas, A., *Importance of biodiesel as transportation fuel.* Energy Policy, 2007. **35**(9): p. 4661-4670.

4. Ban-Weiss, G.A., et al., *A numerical investigation into the anomalous slight NOx increase when burning biodiesel; A new (old) theory.* Fuel Processing Technology, 2007. **88**(7): p. 659-667.

5. Mangus, M., et al., *Comparison of neat biodiesels and ULSD in an optimized single-cylinder diesel engine with electronically-controlled fuel injection.* Energy & fuels, 2014. **28**(6): p. 3849-3862.

6. Canakci, M. and H. Sanli, *Biodiesel production from various feedstocks and their effects on the fuel properties.* Journal of industrial microbiology & biotechnology, 2008. **35**(5): p. 431-441.

7. *Alternative Fuel Price Report, April 2020*. 2020: U.S. Department of Energy.

8. Montgomery, D.T. and R.D. Reitz, *Effects of Multiple Injections and Flexible Control of Boost and EGR on Emissions and Fuel Consumption of a Heavy-Duty Diesel Engine*. 2001, SAE International.

9. Mohan, B., W. Yang, and S.K. Chou, *Fuel injection strategies for performance improvement and emissions reduction in compression ignition engines—A review.* Renewable and Sustainable Energy Reviews, 2013. **28**: p. 664-676.

10. Pundir, B., *Engine emissions: pollutant formation and advances in control technology*. 2007: Alpha Science International, Limited.

11. Winter, L. *2020 Chevrolet Silverado's New, Advanced 3.0L Duramax Turbo-Diesel Redefines Expectations: No-compromize engine delivers refinemnet, performance and efficiency* 2019; Available from: https://media.chevrolet.com/media/us/en/chevrolet/vehicles/CorvetteGS/2020.html.

12. Khair, M.K. and W.A. Majewski, *Diesel Emissions and Their Control*. 2006: SAE International.

13. Environmental Protection Agency. *Diesel Fuel Standards and Rulemarkings*. 2020 [cited 2020 1/21]; Available from: https://www.epa.gov/diesel-fuel-standards/diesel-fuel-standards-and-rulemakings.

14. Reşitoğlu, İ.A., K. Altinişik, and A. Keskin, *The pollutant emissions from diesel-engine vehicles and exhaust aftertreatment systems.* Clean Technologies and Environmental Policy, 2015. **17**(1): p. 15-27.

15. Zheng, M., et al., *Biodiesel engine performance and emissions in low temperature combustion.* Fuel, 2008. **87**(6): p. 714-722.

16. Demers, D. and G. Walters, *Guide to exhaust emission control options.* BAeSAME, Bristol, 1999.

17. Faiz, A.W., Christopher S. Walsh, Michael P., *Air pollution from motor vehicles*. Air pollution from motor vehicles.

18. AA/MKA5, R.B.G.A.A.S.M.A.D.D. and T. Raatz, *Emissions-control technology for diesel engines*. 2005: Robert Bosch GmbH, Automotive Equipment Business Sector, Department for ….

19. Lee, T., et al., *Variability in operation-based NOx emission factors with different test routes, and its effects on the real-driving emissions of light diesel vehicles.* Science of the total environment, 2013. **461**: p. 377-385.

20. Schöneborn, M., et al., *Improved NOx Storage/Release Properties of Ceria-Based Lean NOx Trap Compositions with MnOx Modification.* Materials, 2019. **12**(13): p. 2127.

21. Maricq, M.M., *Chemical characterization of particulate emissions from diesel engines: A review.* Journal of Aerosol Science, 2007. **38**(11): p. 1079-1118.

22. Tighe, C., et al., *The kinetics of oxidation of diesel soots by NO2.* Combustion and flame, 2012. **159**(1): p. 77-90.

23. Burtscher, H., *Physical characterization of particulate emissions from diesel engines: a review.* Journal of Aerosol Science, 2005. **36**(7): p. 896-932.

24. O'Connor, J. and M. Musculus, *Post Injections for Soot Reduction in Diesel Engines: A Review of Current Understanding*. 2013, SAE International.

25. Sappok, A. and V. Wong, *Ash effects on diesel particulate filter pressure drop sensitivity to soot and implications for regeneration frequency and DPF control.* SAE International Journal of Fuels and Lubricants, 2010. **3**(1): p. 380-396.

26. Depcik, C., *ME 636: Chapter 6 - CI Engine Combustion*. 2018, University of Kansas.

27. Jorques Moreno, C., O. Stenlaas, and P. Tunestal, *Influence of Small Pilot on Main Injection in a Heavy-Duty Diesel Engine*. 2017, SAE International.

28. Gill, K., et al., *In-cylinder Studies of Multiple Diesel Fuel Injection in a Single Cylinder Optical Engine*. 2005, SAE International.

29. Hotta, Y., et al., *Achieving Lower Exhaust Emissions and Better Performance in an HSDI Diesel Engine with Multiple Injection*. 2005, SAE International.

30. Okude, K., et al., *Effects of Multiple Injections on Diesel Emission and Combustion Characteristics*. 2007, SAE International.

31. Lee, J., et al., *Effect of Multiple Injection Strategies on Emission and Combustion Characteristics in a Single Cylinder Direct-Injection Optical Engine*. 2009, SAE International.

32. Mingfa, Y., et al., *Experimental Study of Multiple Injections and Coupling Effects of Multi-Injection and EGR in a HD Diesel Engine*. 2009, SAE International.

33. Diwakar, R. and V. Domenech-Llopis, *Physics of Combustion Noise Reduction with Multiple Injections in a DI Diesel Engine - A Computational Study*. 2017, SAE International.

34. Park, C., S. Kook, and C. Bae, *Effects of Multiple Injections in a HSDI Diesel Engine Equipped with Common Rail Injection System*. 2004, SAE International.

35. Asad, U., et al., *Fuel Injection Strategies to Improve Emissions and Efficiency of High Compression Ratio Diesel Engines*. 2008, SAE International.

36. Koci, C.P., et al., *Multiple-Event Fuel Injection Investigations in a Highly-Dilute Diesel Low Temperature Combustion Regime*. 2009, SAE International.

37. Schulte, H., et al., *Preinjection—A Measure to Influence Exhaust Quality and Noise in Diesel Engines.* Journal of Engineering for Gas Turbines and Power, 1989. **111**(3): p. 445-450.

38. Dürnholz, M., H. Endres, and P. Frisse, *Preinjection A Measure to Optimize the Emission Behavior of DI-Diesel Engine*. 1994, SAE International.

39. Benajes, J., S. Molina, and J.M. García, *Influence of Pre- and Post-Injection on the Performance and Pollutant Emissions in a HD Diesel Engine*. 2001, SAE International.

40. Corcione, F.E., et al., *Potential of Multiple Injection Strategy for Low Emission Diesel Engines*. 2002, SAE International.

41. Mohan, B., et al., *Numerical investigation on the effects of injection rate shaping on combustion and emission characteristics of biodiesel fueled CI engine.* Applied Energy, 2015. **160**: p. 737-745.

42. Ehleskog, R., R.L. Ochoterena, and S. Andersson, *Effects of Multiple Injections on Engine-Out Emission Levels Including Particulate Mass from an HSDI Diesel Engine*. 2007, SAE International.

43. Chen, P., U. Ibrahim, and J. Wang, *Experimental investigation of diesel and biodiesel post injections during active diesel particulate filter regenerations.* Fuel, 2014. **130**: p. 286-295.

44. Mendez, S. and B. Thirouard, *Using Multiple Injection Strategies in Diesel Combustion: Potential to Improve Emissions, Noise and Fuel Economy Trade-Off in Low CR Engines*. 2008, SAE International.

45. Gao, J., et al., *Review of thermal management of catalytic converters to decrease engine emissions during cold start and warm up.* Applied Thermal Engineering, 2019. **147**: p. 177-187.

46. Neely, G.D., et al., *New Diesel Emission Control Strategy to Meet US Tier 2 Emissions Regulations*. 2005, SAE International.

47. Fang, T., et al., *Combustion and Soot Visualization of Low Temperature Combustion within an HSDI Diesel Engine Using Multiple Injection Strategy*. 2006, SAE International.

48. Najt, P.M. and D.E. Foster, *Compression-Ignited Homogeneous Charge Combustion*. 1983, SAE International.

49. Environmental Protection Agency. *EPA EMission Standards for Light-Duty Vehicles and Trucks*. 2016 [cited 2020 1/6/2020]; Available from: https://www.epa.gov/emission-standards-reference-guide/epa-emission-standards-light-duty-vehicles-and-trucks.

50. Nehmer, D.A. and R.D. Reitz, *Measurement of the Effect of Injection Rate and Split Injections on Diesel Engine Soot and NOx Emissions.* SAE Transactions, 1994. **103**: p. 1030-1041.

51. Mayer, K.P., *Fuel economy, emissions and noise of multi-spray light duty DI diesels–current status and development trends*. 1984, SAE International.

52. U. Augustin, V. Schwartz, *Low-Noise Combustion with Pilot Injection*, in *Truck Technology International*. 1991.

53. Hattori, H., et al., *Study on Performance Improvement of DI Diesel Engine with Pilot Injection Method*. 1991, Society of Automotive Engineers of Korea.

54. Shimada, T., T. Shoji, and Y. Takeda, *The Effect of Fuel injection Pressure on Diesel Engine Performance*. 1989, SAE International.

55. Aoyama, T., J.i. Mizuta, and Y. Oshima, *NOx Reduction by Injection Control*. 1990, SAE International.

56. Herdin, G., *Considerations on Low Load Smoke Emissions By Using Pilot and Modulated Injection*. 1990, Associazione Tecnica Dell'Automobile.

57. Shundoh, S., et al., *NOx Reduction from Diesel Combustion Using Pilot Injection with High Pressure Fuel Injection*. 1992, SAE International.

58. Needham, J.R. and A. Bouthenet, *Competitive Fuel Economy and Low Emissions Achieved Through Flexible Injection Control*. 1993, SAE International.

59. Bower, G.R. and D.E. Foster, *The Effect of Split Injection on Fuel Distribution in an Engine-Fed Combustion Chamber*. 1993, SAE International.

60. Tow, T.C., D.A. Pierpont, and R.D. Reitz, *Reducing Particulate and NOx Emissions by Using Multiple Injections in a Heavy Duty D.I. Diesel Engine*. 1994, SAE International.

61. Ishida, M., et al., *The Effect of Pilot Injection on Combustion in a Turbocharged D.I. Diesel Engine.* SAE Transactions, 1994. **103**: p. 1740-1749.

62. Yoshizu, F., Nakayama, M., *A Study of New Injector and Spray Concepts of Small DI Diesel Engine, 1st Report.* Trans.JSME, 1993(59-559(B)): p. 880-885.

63. Yamaki, Y., et al., *Application of Common Rail Fuel Injection System to a Heavy Duty Diesel Engine*. 1994, SAE International.

64. Ishiwata, H., et al., *A Feasibility Study of Pilot Injection in TICS (Timing and Injection Rate Control System)*. 1994, SAE International.

65. Nakakita, K., et al., *Optimization of Pilot Injection Pattern and Its Effect on Diesel Combustion with High-Pressure Injection.* JSME International Journal Series B, 1994. **37**(4): p. 966-973.

66. Minami, T., K. Takeuchi, and N. Shimazaki, *Reduction of Diesel Engine NOx Using Pilot Injection.* SAE Transactions, 1995. **104**: p. 1104-1111.

67. Pierpont, D.A., D.T. Montgomery, and R.D. Reitz, *Reducing Particulate and NOx Using Multiple Injections and EGR in a D.I. Diesel*. 1995, SAE International.

68. Han, Z., et al., *Mechanism of Soot and NOx Emission Reduction Using Multiple-injection in a Diesel Engine*. 1996, SAE International.

69. Yokota, H., et al., *A New Concept for Low Emission Diesel Combustion*. 1997, SAE International.

70. Payri, F., et al., *Contribution to the application of two-colour imaging to diesel combustion.* Measurement Science and Technology, 2007. **18**(8): p. 2579-2598.

71. Hampson, G.J. and R.D. Reitz, *Two-Color Imaging of In-Cylinder Soot Concentration and Temperature in a Heavy-Duty DI Diesel Engine with Comparison to Multidimensional Modeling for Single and Split Injections*. 1998, SAE International.

72. Bakenhus, M. and R.D. Reitz, *Two-Color Combustion Visualization of Single and Split Injections in a Single-Cylinder Heavy-Duty D.I. Diesel Engine Using an Endoscope-Based Imaging System*. 1999, SAE International.

73. Zhang, L., *A Study of Pilot Injection in a DI Diesel Engine*. 1999, SAE International.

74. transportpolicy.net. *US: Light-Duty: Emissions*. 2018 [cited 2020 January 10th]; Available from: https://www.transportpolicy.net/standard/us-light-duty-emissions/.

75. Chen, S.K., *Simultaneous Reduction of NOx and Particulate Emissions by Using Multiple Injections in a Small Diesel Engine*. 2000, SAE International.

76. Beatrice, C., et al., *Combustion Process Management in Common Rail DI Diesel Engines by Multiple Injection*. 2001, Consiglio Nazionale delle Ricerche.

77. Box, G.E. and N.R. Draper, *Empirical model-building and response surfaces*. Vol. 424. 1987: Wiley New York.

78. DieselNet. *European Stationary Cycle (ESC)*. 2020; Available from: https://dieselnet.com/standards/cycles/esc.php.

79. Badami, M., F. Millo, and D.D. D'Amato, *Experimental Investigation on Soot and NOx Formation in a DI Common Rail Diesel Engine with Pilot Injection.* SAE Transactions, 2001. **110**: p. 663-674.

80. Yamane, K. and Y. Shimamoto, *Combustion and Emission Characteristics of Direct-Injection Compression Ignition Engines by Means of Two-Stage Split and Early Fuel Injection.* Journal of Engineering for Gas Turbines and Power, 2002. **124**(3): p. 660-667.

81. Badami, M., et al., *Influence of Multiple Injection Strategies on Emissions, Combustion Noise and BSFC of a DI Common Rail Diesel Engine*. 2002, SAE International.

82. Mallamo, F., M. Badami, and F. Millo, *Analysis of Multiple Injection Strategies for the Reduction of Emissions, Noise and BSFC of a DI CR Small Displacement Non-Road Diesel Engine*. 2002, SAE International.

83. Payri, F., et al., *Influence of the Post-Injection Pattern on Performance, Soot and NOx Emissions in a HD Diesel Engine*. 2002, SAE International.

84. Beatrice, C., et al., *Downsizing of Common Rail D.I. Engines: Influence Of Different Injection Strategies on Combustion Evolution*. 2003, SAE International.

85. Carlucci, P., A. Ficarella, and D. Laforgia, *Effects of Pilot Injection Parameters on Combustion for Common Rail Diesel Engines.* SAE Transactions, 2003. **112**: p. 932-943.

86. Badami, M., et al., *Experimental investigation on the effect of multiple injection strategies on emissions, noise and brake specific fuel consumption of an automotive*

direct injection common-rail diesel engine. International Journal of Engine Research, 2003. **4**(4): p. 299-314.

87. Liu, Y. and R.D. Reitz, *Optimizing HSDI Diesel Combustion and Emissions Using Multiple Injection Strategies*. 2005, SAE International.

88. Carlucci, P., A. Ficarella, and D. Laforgia, *Effects on combustion and emissions of early and pilot fuel injections in diesel engines.* International Journal of Engine Research, 2005. **6**(1): p. 43-60.

89. Beatrice, C., et al., *Diesel Combustion control in common rail engines by new injection strategies.* International Journal of Engine Research, 2002. **3**(1): p. 23-36.

90. Ehleskog, R. and R.L. Ochoterena, *Soot Evolution in Multiple Injection Diesel Flames*. 2008, SAE International.

91. Vanegas, A., et al., *Experimental Investigation of the Effect of Multiple Injections on Pollutant Formation in a Common-Rail DI Diesel Engine*. 2008, SAE International.

92. Yang, S.Y. and S.H. Chung, *An experimental Study on the Effects of High-Pressure and Multiple Injection Strategies on DI Diesel Engine Emissions*. 2013, SAE International.

93. Barman, J., et al., *DOE Approach for Optimizing the Combustion Parameters with Multiple Injection Strategy in Light Duty Diesel Engine*. 2013, The Automotive Research Association of India.

94. Delphi. *Worldwide Emissions Standards*. 2020 [cited 2020 1/11]; Available from: https://www.delphi.com/sites/default/files/inline-files/delphi-worldwide-emissions-standards-passenger-cars-light-duty-2016-7.pdf.

95. Suh, H.K., *Study on the twin-pilot-injection strategies for the reduction in the exhaust emissions in a low-compression-ratio engine.* Proceedings of the Institution of Mechanical Engineers, Part D: Journal of Automobile Engineering, 2014. **228**(3): p. 335-343.

96. O'Connor, J. and M. Musculus, *In-Cylinder Mechanisms of Soot Reduction by Close-Coupled Post-Injections as Revealed by Imaging of Soot Luminosity and Planar Laser-Induced Soot Incandescence in a Heavy-Duty Diesel Engine*. 2014, SAE International.

97. Busch, S., et al., *Experimental and Numerical Investigations of Close-Coupled Pilot Injections to Reduce Combustion Noise in a Small-Bore Diesel Engine*. 2015, SAE International.

98. Biswas, S., et al., *Optimization of Multiple Injection Strategies to Improve BSFC Performance of a Common Rail Direct Injection Diesel Engine*. 2016, SAE International.

99. Sadafale, S.S., M. Mittal, and K. Inaba, *Phenomenological Modeling and Experiments to Investigate the Combined Effects of High Pressure and Multiple Injection Strategies with*

EGR on Combustion and Emission Characteristics of a CRDI Diesel Engine. 2019, SAE International.

100. Park, S.H., S.H. Yoon, and C.S. Lee, *Effects of multiple-injection strategies on overall spray behavior, combustion, and emissions reduction characteristics of biodiesel fuel.* Applied Energy, 2011. **88**(1): p. 88-98.

101. Choi, C.Y. and R.D. Reitz, *An experimental study on the effects of oxygenated fuel blends and multiple injection strategies on DI diesel engine emissions.* Fuel, 1999. **78**(11): p. 1303-1317.

102. Stringer, V.L., et al., *Combustion and Emissions of Biodiesel and Diesel Fuels in Direct Injection Compression Ignition Engines using Multiple Injection Strategies*. 2008, SAE International.

103. Mangus, M., et al., *Investigating the compression ignition combustion of multiple biodiesel/ULSD (ultra-low sulfur diesel) blends via common-rail injection.* Energy, 2015. **89**: p. 932-945.

104. Kim, M.Y., S.H. Yoon, and C.S. Lee, *Impact of Split Injection Strategy on the Exhaust Emissions and Soot Particulates from a Compression Ignition Engine Fueled with Neat Biodiesel.* Energy & Fuels, 2008. **22**(2): p. 1260-1265.

105. Fang, T. and C.-F.F. Lee, *Bio-diesel effects on combustion processes in an HSDI diesel engine using advanced injection strategies.* Proceedings of the Combustion Institute, 2009. **32**(2): p. 2785-2792.

106. Yehliu, K., A.L. Boehman, and O. Armas, *Emissions from different alternative diesel fuels operating with single and split fuel injection.* Fuel, 2010. **89**(2): p. 423-437.

107. Qi, D., et al., *Effect of EGR and injection timing on combustion and emission characteristics of split injection strategy DI-diesel engine fueled with biodiesel.* Fuel, 2011. **90**(5): p. 1884-1891.

108. Jeon, J. and S. Park, *Effects of pilot injection strategies on the flame temperature and soot distributions in an optical CI engine fueled with biodiesel and conventional diesel.* Applied Energy, 2015. **160**: p. 581-591.

109. Li, H., et al., *Assessment of the impact of post-injection on exhaust pollutants emitted from a diesel engine fueled with biodiesel.* Renewable Energy, 2017. **114**: p. 924-933.

110. Babu, D., R. Karvembu, and R. Anand, *Impact of split injection strategy on combustion, performance and emissions characteristics of biodiesel fuelled common rail direct injection assisted diesel engine.* Energy, 2018. **165**: p. 577-592.

111. Dhar, A. and A.K. Agarwal, *Effect of Multiple Injections on Particulate Size-Number Distributions in a Common Rail Direct Injection Engine Fueled with Karanja Biodiesel Blends*. 2013, SAE International.

112. Dhar, A. and A.K. Agarwal, *Experimental investigations of the effect of pilot injection on performance, emissions and combustion characteristics of Karanja biodiesel fuelled CRDI engine.* Energy Conversion and Management, 2015. **93**: p. 357-366.

113. How, H.G., et al., *Influence of injection timing and split injection strategies on performance, emissions, and combustion characteristics of diesel engine fueled with biodiesel blended fuels.* Fuel, 2018. **213**: p. 106-114.

114. Teoh, Y.H., et al., *Effect of two-stage injection dwell angle on engine combustion and performance characteristics of a common-rail diesel engine fueled with coconut oil methyl esters-diesel fuel blends.* Fuel, 2018. **234**: p. 227-237.

115. How, H.G., et al., *Impact of two-stage injection fuel quantity on engine-out responses of a common-rail diesel engine fueled with coconut oil methyl esters-diesel fuel blends.* Renewable Energy, 2019. **139**: p. 515-529.

116. Plamondon, E. and P. Seers, *Parametric study of pilot–main injection strategies on the performance of a light-duty diesel engine fueled with diesel or a WCO biodiesel–diesel blend.* Fuel, 2019. **236**: p. 1273-1281.

117. Mattson, J.M., M. Mangus, and C. Depcik, *Efficiency and emissions mapping for a single-cylinder, direct injected compression ignition engine*. 2014, SAE Technical Paper.

118. Mangus, M.D., *Implementation of Engine Control and Measurement Strategies for Biofuel Research in Compression-Ignition Engines*, in *Mechanical Engineering*. 2014, University of Kansas.

119. Langness, C.N., *Effects of Natural Gas Constituents on Engine Performance, Emissions, and Combustion in Compressed Natural Gas-Assisted Diesel Combustion*, in *Mechanical Engineering*. 2014, University of Kansas.

120. Srivatsa, C.V., J. Mattson, and C. Depcik, *Performance and Emission Analysis of Partially Premixed Charge Compression Ignition Combustion.* Journal of Engineering for Gas Turbines and Power, 2019. **141**(6).

121. Mattson, J.M. and C. Depcik, *Emissions–calibrated equilibrium heat release model for direct injection compression ignition engines.* Fuel, 2014. **117**: p. 1096-1110.

122. Heywood, J.B., *Combustion engine fundamentals.* 1ª Edição. Estados Unidos, 1988.

123. Depcik, C., et al., *Instructional Use of a Single-Zone, Premixed Charge, Spark-Ignition Engine Heat Release Simulation.* International Journal of Mechanical Engineering Education, 2007. **35**(1): p. 1-31.

124. Bahadori, A. and H. Vuthaluru, *Predicting emissivities of combustion gases.* Chemical engineering progress, 2009. **105**(6): p. 38-41.

125. Guezennec, Y.G. and W. Hamama, *Two-zone heat release analysis of combustion data and calibration of heat transfer correlation in an IC engine*. 1999, SAE Technical Paper.

126. Tamilporai, P., et al., *Simulation and analysis of combustion and heat transfer in low heat rejection diesel engine using two zone combustion model and different heat transfer models.* SAE transactions, 2003: p. 1185-1203.

127. Assanis, D.N., et al., *A methodology for cycle-by-cycle transient heat release analysis in a turbocharged direct injection diesel engine.* SAE transactions, 2000: p. 1327-1339.

128. Stiesch, G. and G.P. Merker, *A phenomenological model for accurate and time efficient prediction of heat release and exhaust emissions in direct-injection diesel engines*. 1999, SAE Technical Paper.

129. Nishida, K. and H. Hiroyasu, *Simplified three-dimensional modeling of mixture formation and combustion in a DI diesel engine.* SAE transactions, 1989: p. 276-293.

130. Shahlari, A.J., et al., *Comparison of compression ignition engine noise metrics in low-temperature combustion regimes.* SAE International Journal of Engines, 2013. **6**(1): p. 541-552.

131. Mattson, J.M. and C. Depcik, *Comparison of Engine Operational Modes with Respect to Compression Ignition Engine Knock*. 2018, SAE Technical Paper.

132. Russell, M., *Automotive diesel engine noise and its control.* SAE Transactions, 1973: p. 937-954.

133. Russell, M., D. Palmer, and C. Young, *Measuring diesel noise at source with a view to its control.* IMechE C142/84, 1984: p. 97-105.

134. AVL, *AVL 450 Combustion Noise Meter Instruction Manual*.

135. Bondioli, P., et al., *Evaluation of biodiesel storage stability using reference methods.* European journal of lipid science and technology, 2002. **104**(12): p. 777-784.

136. Christensen, E. and R.L. McCormick, *Long-term storage stability of biodiesel and biodiesel blends.* Fuel Processing Technology, 2014. **128**: p. 339-348.

137. Jose, T.K. and K. Anand, *Effects of biodiesel composition on its long term storage stability.* Fuel, 2016. **177**: p. 190-196.

138. Srivatsa, C.V.C., *Performance and Emissions Analysis of Pre-mixed and Partially Pre-mixed Charge Compression Ignition Combustion*, in *Mechanical Engineering*. 2017, University of Kansas.

139. Churkunti, P., J.M. Mattson, and C. Depcik, *Influence of Fuel Injection Pressure and Biodiesel upon NO x Emissions*. 2016, SAE Technical Paper.

140. Stone, R., *Introduction to Internal Combustion Engines, Fourth Edition*. 2012: Macmillan Press.

141. Phillips, C., *Material Safety Data Sheet for no. 2 Diesel Fuel*. 2007.

142. He, B., et al., *Moisture absorption in biodiesel and its petro-diesel blends.* Applied engineering in agriculture, 2007. **23**(1): p. 71-76.

143. E. Christensen, R.M., *Water Uptake and Weathering of Ethanol-Gasoline Blends in Humid Environments*. 2016, National Renewable Fuels Laboratory.

Appendix

Table A. 1: Euro 1-4 passenger car emissions regulations [94]

EURO 1-4 - PASSENGER CARS M (≤ 2,5T GVW, ≤ 6 SEATS)

Directive Text Number		Euro 1 (EC 93) [1]		Euro 2 (EC 96)		Euro 3 (EC 2000)		Euro 4 (EC 2005)	
		91/441/EEC or 93/59/EEC		94/12/EC or 96/69/EC		70/220/EEC, as amended by 98/69/EC and 2003/76/EC			
Application Date	month/year	TA: Jul 1992 FR: Jan 1993		TA: Jan 1996 FR: Jan 1997		TA: Jan 2000 FR: Jan 2001		TA: Jan 2005 FR: Jan 2006	
Test type	-	URBAN (40 sec idle) + EUDC		URBAN (40 sec idle) + EUDC		Rev. Urban (10 sec idle) + EUDC		Rev. Urban (10 sec idle) + EUDC	
Combustion Type		PI	CI	PI	CI [2]	PI	CI	PI	CI [4]
HC	g/km	-	-	-	-	0,20	-	0,10	-
NOx	g/km	-	-	-	-	0,15	0,5	0,08	0,25
HC+NOx	g/km	0,97 (1,13)	0,97 (1,13)	0,50	0,70	-	0,56	-	0,30
CO	g/km	2,72 (3,16)	2,72 (3,16)	2,20	1,00	2,30	0,64	1,00	0,50
PM	mg/km	-	140 (180)	-	80	-	50	-	25
Deteriation factors	-	CO, HC+NOx: 1,4	CO: 1,1 HC+NOx: 1,0 PM: 1,2	CO, HC+NOx: 1,5	CO: 1,1 HC+NOx: 1,0 PM: 1,3	CO, HC, NOx: 1,2	CO: 1,1 HC+NOx: 1,0 PM: 1,2	CO, HC, NOx: 1,2	CO: 1,1 HC+NOx: 1,0 PM: 1,2
Durability	km	80.000	80.000	80.000	80.000	80.000 or 5 years	80.000 or 5 years	100.000 or 5 years [3]	100.000 or 5 years [3]
EOBD	-	NO	NO	NO	NO	YES	YES	YES	YES

[1] In brackets: COP values [2] Limits for IDI Diesel. For DI Diesel until 30/09/1999: HC+NOx: 0,90 g/km, CO: 1,00 g/km, PM: 100 mg/km
[3] Newly required recording of in-use durability [4] Until 12/2002 Diesel cars with GVW > 2 t and - a) > 6 seats or - b) off road vehicles were considered as N1 vehicles

Table A. 2: Euro 1-4 large passenger cars and light duty trucks emissions regulations [94].

EURO 1-4 - LARGE PASSENGER CARS AND LIGHT DUTY TRUCKS N1 (> 2,5T GVW, 7-9 SEATS, LDT ≤ 3,5T)

Directive Text Number		Euro 1 (EC 93)			Euro 2 (EC 96)						Euro 3 (EC 2000)						Euro 4 (EC 2005)					
		93/59/EEC			96/44/EC or 94/12/EC and 93/116/EEC						70/220/EEC, as amended by 98/69/EC and 2003/76/EC						70/220/EEC, as amended by 98/69/EC and 2003/76/EC					
Vehicle Class		Class 1 ≤ 1250 kg [1]	Class 2 > 1250 kg ≤ 1700 kg [1]	Class 3 > 1700 kg [1]	Class 1 ≤ 1250 kg [1]		Class 2 > 1250 kg ≤ 1700 kg [1]		Class 3 > 1700 kg [1]		Class 1		Class 2		Class 3 [4]		Class 1		Class 2		Class 3 [4]	
Application Date	month /year	TA: Oct 1993 FR: Oct 1994			TA: Jan 1997 FR: Oct 1997		TA: Jan 1998 FR: Oct 1998		TA: Jan 1998 FR: Oct 1999		TA: Jan 2000 FR: Jan 2001		TA: Jan 2001 FR: Jan 2002		TA: Jan 2001 FR: Jan 2002		TA: Jan 2005 FR: Jan 2006		TA: Jan 2006 FR: Jan 2007		TA: Jan 2006 FR: Jan 2007	
Test type	-	URBAN (40 sec idle) + EUDC			URBAN (40 sec idle) + EUDC						Rev. Urban (10 sec idle) + EUDC						Rev. Urban (10 sec idle) + EUDC					
Combustion Type		Same limits for SI and CI engines			PI	CI	PI	CI	PI	CI	PI	CI	PI	CI	PI	CI	PI	CI	PI	CI	PI	CI
HC	g/km	-	-	-	-						0,20	-	0,25	-	0,29	-	0,10	-	0,13	-	0,16	-
NOx	g/km	-	-	-	-						0,15	0,5	0,18	0,65	0,21	0,78	0,08	0,25	0,1	0,33	0,11	0,39
HC+NOx	g/km	0,97 (1,13) [2]	1,4 (1,6) [2]	1,7 (2,0) [2]	0,5	0,7 (0,9) [2]	0,6	1,0 (1,3) [2]	0,7	1,2 (1,6) [2]	-	0,56	-	0,72	-	0,86	-	0,30	-	0,39	-	0,46
CO	g/km	2,72 (3,16) [2]	5,17 (6,0) [2]	6,9 (8,0) [2]	2,20	1,0	4,0	1,25	5,0	1,5	2,30	0,64	4,17	0,8	5,22	0,95	1,0	0,50	1,81	0,63	2,27	0,74
PM	mg/km	140 (180) [2][3]	190 (220) [2][3]	250 (290) [2][3]	-	80 (100) [2]		120 (140) [2]		170 (200) [2]	-	50	-	70	-	100	-	25	-	40	-	60
EOBD	-	NO			NO						YES [5]						YES [5]					

[1] Reference weight in running order plus 25 kg [2] in brackets: COP values [3] Limits Diesel [4] Included Large Passenger cars (> 2,5 t GVW)
[5] TA and FR application dates for EOBD differ from non OBD related dates: See EOBD section for more details

For Euro 2: COP =TA values (if not mentioned otherwise)

Table A. 3: Euro 5-6 spark ignition and compression ignition emissions regulations [94].

EURO 1-4 - LARGE PASSENGER CARS AND LIGHT DUTY TRUCKS N1 (> 2,5T GVW, 7-9 SEATS, LDT ≤ 3,5T)

Directive Text Number		Euro 1 (EC 93)			Euro 2 (EC 96)						Euro 3 (EC 2000)						Euro 4 (EC 2005)					
		93/59/EEC			96/44/EC or 94/12/EC and 93/116/EEC						70/220/EEC, as amended by 98/69/EC and 2003/76/EC						70/220/EEC, as amended by 98/69/EC and 2003/76/EC					
Vehicle Class		Class 1 ≤ 1250 kg [1]	Class 2 > 1250 kg ≤ 1700 kg [1]	Class 3 > 1700 kg [1]	Class 1 ≤ 1250 kg [1]		Class 2 > 1250 kg ≤ 1700 kg [1]		Class 3 > 1700 kg [1]		Class 1		Class 2		Class 3 [4]		Class 1		Class 2		Class 3 [4]	
Application Date	month /year	TA: Oct 1993 FR: Oct 1994			TA: Jan 1997 FR: Oct 1997		TA: Jan 1998 FR: Oct 1998		TA: Jan 1998 FR: Oct 1999		TA: Jan 2000 FR: Jan 2001		TA: Jan 2001 FR: Jan 2002		TA: Jan 2001 FR: Jan 2002		TA: Jan 2005 FR: Jan 2006		TA: Jan 2006 FR: Jan 2007		TA: Jan 2006 FR: Jan 2007	
Test type	-	URBAN (40 sec idle) + EUDC			URBAN (40 sec idle) + EUDC						Rev. Urban (10 sec idle) + EUDC						Rev. Urban (10 sec idle) + EUDC					
CombustionType		Same limits for SI and CI engines			PI	CI	PI	CI	PI	CI	PI	CI	PI	CI	PI	CI	PI	CI	PI	CI	PI	CI
HC	g/km	-	-	-	-						0,20	-	0,25	-	0,29	-	0,10	-	0,13	-	0,16	-
NOx	g/km	-	-	-	-						0,15	0,5	0,18	0,65	0,21	0,78	0,08	0,25	0,1	0,33	0,11	0,39
HC+NOx	g/km	0,97 (1,13) [2]	1,4 (1,6) [2]	1,7 (2,0) [2]	0,5	0,7 (0,9) [2]	0,6	1,0 (1,3) [2]	0,7	1,2 (1,6) [2]	-	0,56	-	0,72	-	0,86	-	0,30	-	0,39	-	0,46
CO	g/km	2,72 (3,16) [2]	5,17 (6,0) [2]	6,9 (8,0) [2]	2,20	1,0	4,0	1,25	5,0	1,5	2,30	0,64	4,17	0,8	5,22	0,95	1,0	0,50	1,81	0,63	2,27	0,74
PM	mg/km	140 (180) [2][3]	190 (220) [2][3]	250 (290) [2][3]	-	80 (100) [2]		120 (140) [2]		170 (200) [2]	-	50	-	70	-	100	-	25	-	40	-	60
EOBD	-	NO			NO						YES [5]						YES [5]					

[1] Reference weight in running order plus 25 kg [2] in brackets: COP values [3] Limits Diesel [4] Included Large Passenger cars (> 2,5 t GVW)
[5] TA and FR application dates for EOBD differ from non OBD related dates: See EOBD section for more details

For Euro 2: COP =TA values (if not mentioned otherwise)

Mode	Engine Speed	Load, %	Weight, %	Duration
1	Low idle	0	15	4 minutes
2	A	100	8	2 minutes
3	B	50	10	2 minutes
4	B	75	10	2 minutes
5	A	50	5	2 minutes
6	A	75	5	2 minutes
7	A	25	5	2 minutes
8	B	100	9	2 minutes
9	B	25	10	2 minutes
10	C	100	8	2 minutes
11	C	25	5	2 minutes
12	C	75	5	2 minutes
13	C	50	5	2 minutes

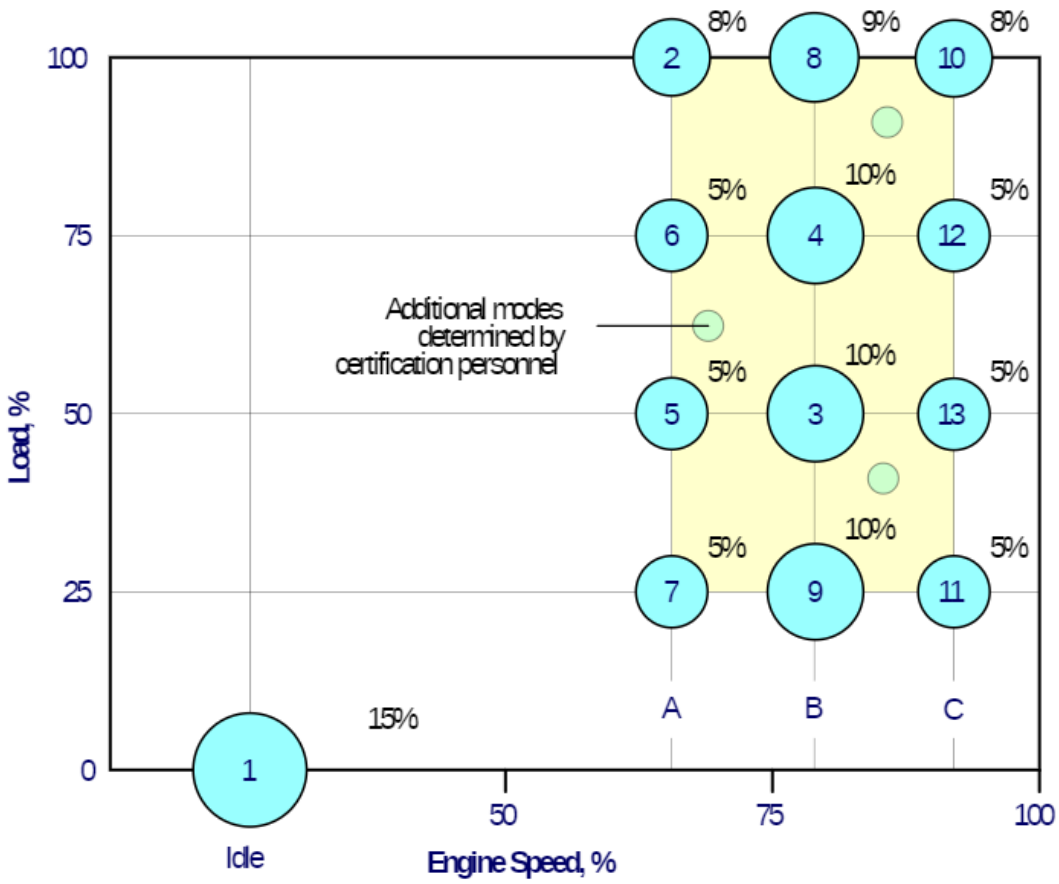

Figure A. 1: ESC test modes [78].

Table A. 4: Biodiesel fatty acid component mass fractions from Mangus et al [5].

component	palm	jatropha	soybean	beef tallow	chain length (pm)
C10:0	N/D	N/D	N/D	N/D	1525
C12:0	0.0017	N/D	N/D	N/D	1830
C14:0	0.0049	0.0003	0.0002	0.0288	2135
C15:0	N/D	N/D	N/D	0.0052	2288
C16:0	0.3219	0.1271	0.0904	0.2213	2440
C16:1	0.0013	0.0040	N/D	0.0275	2421
C17:0	0.0002	0.0003	0.0003	0.0249	2593
C18:0	0.0396	0.0740	0.0481	0.1746	2745
C18:1	0.4940	0.4559	0.2542	0.4844	2726
C18:2	0.1320	0.3365	0.5250	0.0332	2707
C18:3	0.0019	0.0010	0.0758	N/D	2687
C20:0	0.0026	0.0009	0.0029	N/D	3050
C22:0	N/D	N/D	0.0026	N/D	3355
C22:1	N/D	N/D	N/D	N/D	3336
C24:0	N/D	N/D	0.0006	N/D	3660
unsaturation degree	0.76	1.14	1.53	0.58	
% unsat	62.91%	79.74%	85.50%	54.51%	
% polyunsat	13.39%	33.76%	60.08%	3.32%	

Table A. 5: Coefficients used in noise filter curve-fit [130].

i	a_i	b_i
0	-1.594243E+02	-1.065899E+02
1	2.029175415E-01	1.896910E-02
2	-2.981767797E-04	-7.393291000E-06
3	2.494291193E-07	1.266005000E-09
4	-1.166026273E-10	-1.278282000E-13
5	2.820300100E-14	7.033316000E-18
6	-2.747693353E-18	-1.621458000E-22